EXPERIMENTAL INVESTIGATION OF SOME CONDUCTING CROSSED GRATINGS

by

LI-HE CAI

B.A.Sc., Tsinghua University (China), 1970

A THESIS SUBMITTED IN PARTIAL FULFILMENT OF

THE REQUIREMENTS FOR THE DEGREE OF

MASTER OF APPLIED SCIENCE

in

THE FACULTY OF GRADUATE STUDIES

ELECTRICAL ENGINEERING

We accept this thesis as conforming

to the required standard

THE UNIVERSITY OF BRITISH COLUMBIA

January 1985

In presenting this thesis in partial fulfilment of the requirements for an advanced degree at the University of British Columbia, I agree that the Library shall make it freely available for reference and study. I further agree that permission for extensive copying of this thesis for scholarly purposes may be granted by the head of my department or by his or her representatives. It is understood that copying or publication of this thesis for financial gain shall not be allowed without my written permission.

Department of Electrical Engineering

The University of British Columbia
1956 Main Mall
Vancouver, Canada
V6T 1Y3

Date March 4, 1985

ABSTRACT

The properties of a crossed grating of square pyramids and a crossed grating with hemispherical cavities to eliminate specular reflection from a conducting surface are studied experimentally. Measurements were made in the microwave range of 35 GHz. The best performance is that 99.94% of the power of a TM-polarized incident wave can be scattered into a single spectral order by a pyramidal crossed grating, while for TE polarization the reduction in specular reflection can be as high as 98%. Anti-reflection properties of a crossed grating with hemispherical cavities near normal incidence are also observed. Comparison between the behavior of triangular and pyramidal gratings of the same profile is made. Effects of the profile parameters are investigated. Basically the experimental results agree with the theoretical predictions. This investigation provides a set of experimental data to assist further numerical study.

Table of Contents

ABSTRACT ii

TABLE OF CONTENTS iii

LIST OF ILLUSTRATIONS v

ACKNOWLEDGEMENTS ix

1. INTRODUCTION 1

2. SCATTERING BY CROSSED GRATINGS 9

2.1 Formulation of the Problem 9

2.2 The Rayleigh Expansion for the Diffracted Field .11

2.3 Determination of the Directions of Propagation of the Diffracted Waves 15

2.3.1 Grating with Period Smaller than Half of Wavelength 16

2.3.2 Grating with Period between a Half Wavelength and One Wavelength 17

2.3.2.1 Under Non-oblique Incidence (ψ_i=0) 17

2.3.2.2 Under Oblique Incidence 18

2.3.3 Grating with Period Greater than Wavelength 19

2.4 Determination of the Angular Region Where a Diffracted Order Exists 21

2.5 A Product Formula Linking Crossed and Classical Gratings 23

3. EXPERIMENTAL ARRANGEMENT AND PROCEDURE 25

4. EXPERIMENTAL RESULTS OF PYRAMIDAL CROSSED GRATINGS ..31

4.1 Introduction 31

4.2 Plate B9 ---- In Comparison with its Single-periodic Equivalent 35

4.3 Plate C4 ---- A Deeply-grooved Plate in Comparison with its Singly-periodic Equivalent ..47

4.4 Plate A4 ---- an Essentially Perfect Blazed Crossed Grating Surface for TM polarization 58

4.5 Plate A9 ---- Influence of the Ratio λ/d 70

4.6 Plate B6 ---- Influence of Apex Angle α 78

4.7 Plate A6 ---- a Blazed Crossed Grating Surface for TE Polarization 85

5. EXPERIMENTAL RESULTS OF CROSSED GRATINGS WITH HEMISPHERICAL CAVITIES 91

5.1 Introduction 91

5.2 Plate R4 93

5.3 Plate R6 101

6. ERROR ANALYSIS 106

7. CONCLUSIONS 111

APPENDIX: NUMERICAL RESULTS FOR PERFECTLY CONDUCTING STRIPS OF SIX SYMMETRICAL TRIANGULAR CORRUGATIONS ...115

REFERENCES 122

LIST OF ILLUSTRATIONS

Fig. 2.1. The specification of the incident field $\bar{E}^i$ and of the diffracted wave vectors $\bar{k}_{pq}$ in the (Oxyz) system 9

Fig. 2.2. The directions of the diffracted wave vectors scattered by a crossed grating with $\lambda/d=0.66$ in normal incidence 20

Fig. 3.1. Photograph of experimental set-up 26

Fig. 3.2. Experimental arrangement 27

Fig. 4.1. Photograph of a pyramidal crossed grating plate (plate C4) 32

Fig. 4.2. A classical triangular (echelette) grating and a pyramidal crossed grating with the same profile, and dimensions for all pyramidal plates 33

Fig. 4.3a. Relative reflected power (or ϵ_0) vs. angle of incidence for the singly periodic equivalent of plate B9 at f=35 GHz, $\psi_i=0$ 36

Fig. 4.3b. Relative reflected power (or ϵ_{00}) vs. angle of incidence for plate B9 at f=35 GHz, $\psi_i=0$ 37

Fig. 4.4. Reflected power vs. angle of rotation for plate B9 at f=35 GHz, $\theta_i=43.5°$ 43

Fig. 4.5. Diagram of azimuthal angular regions in which spectral orders exist for a crossed grating at $\lambda/d=1.37$, $\theta_i=43.5°$ 44

Fig. 4.6. Reflected power vs. frequency for plate B9 at $\theta_i=43.5°$, $\psi_i=0$ 46

Fig. 4.7. Relative reflected power (or ϵ_0) vs. angle of incidence for the singly periodic equivalent of plate C4 at f=35 GHz, $\psi_i=0$ 48

Fig. 4.8. Reflected power vs. frequency for the singly periodic equivalent of plate C4 at $\theta_i=38°$, $\psi_i=0$ 49

Fig. 4.9. Relative reflected power (or ϵ_0) vs. angle of incidence for the singly periodic equivalent of plate C4 at f=33.75 GHz, $\psi_i=0$ 50

Fig. 4.10. Relative reflected power (or ϵ_{00}) vs. angle of incidence for plate C4 at f=33.75 GHz, $\psi_i=0$ ..52

Fig. 4.11. Reflected power vs. angle of incidence for

plate C4: a. at f=33.75 GHz
b. at f=35 GHz 53

Fig. 4.12. Reflected power vs. frequency for plate C4 at θ_i=38°, ψ_i=0 54

Fig. 4.13. Reflected power vs. angle of rotation for plate C4 at f=35 GHz, θ_i=38° 56

Fig. 4.14. Diagram of azimuthal angular regions in which spectral orders exist for a crossed grating at λ/d=1.24, θ_i=38° 57

Fig. 4.15. Relative reflected power (or ϵ_0) vs. angle of incidence for the singly periodic equivalent of plate A4 at f=35 GHz, ψ_i=0 59

Fig. 4.16. Reflected power vs. angle of incidence for plate A4 at: a. f=35 GHz, ψ_i=0
b. f=33 GHz, ψ_i=0 60

Fig. 4.17. Reflected power vs. frequency for plate A4 at θ_i=46°, ψ_i=0 61

Fig. 4.18. Reflected power vs. angle of incidence for plate A4 at f=37.5 GHz, ψ_i=0 63

Fig. 4.19. Reflected power vs. angle of rotation for plate A4 at f=37.5 GHz, θ_i=46° 65

Fig. 4.20. Diagram of azimuthal angular regions in which spectral orders exist for a crossed grating at λ/d=1.00, θ_i=46° 66

Fig. 4.21. Reflected power vs. angle of rotation for plate A4 at f=35 GHz, θ_i=32.5° 67

Fig. 4.22. Diagram of azimuthal angular regions in which spectral orders exist for a crossed grating at λ/d=1.07, θ_i=32.5° 68

Fig. 4.23. Reflected power vs. angle of incidence for plate A9: a. at f=37.5 GHz (λ/d=1.00)
b. at f=35 GHz (λ/d=1.07) 71

Fig. 4.24. Reflected power vs. angle of incidence for
a. plate A9 at f=33 GHz (λ/d=1.14)
b. plate B9 at f=35 GHz (λ/d=1.37) 72

Fig. 4.25. Reflected power vs. frequency for plate A9 at θ_i=32.5°, ψ_i=0 74

Fig. 4.26. Reflected power vs. angle of rotation for plate A9 at θ_i=35°, f=35 GHz 75

Fig. 4.27. Diagram of azimuthal angular regions in which spectral orders exist for a crossed grating at $\lambda/d=1.07$, $\theta_i=35°$ 76

Fig. 4.28. Relative reflected power (or ϵ_0) vs. angle of incidence for the singly periodic equivalent of plate B6 at f=35 GHz, $\psi_i=0$ 79

Fig. 4.29. Relative reflected power (or ϵ_{00}) vs. angle of incidence for plate B6 at f=35 GHz, $\psi_i=0$ 80

Fig. 4.30. Reflected power vs. frequency for plate B6 at $\theta_i=43.5°$, $\psi_i=0$ 82

Fig. 4.31. Reflected power vs. angle of rotation for plate B6 at f=35 GHz, $\theta_i=43.5°$ 83

Fig. 4.32. Reflected power vs. angle of incidence for plate A6: a. at f=37.5 GHz ($\lambda/d=1.00$) b. at f=35 GHz ($\lambda/d=1.07$) 86

Fig. 4.33. Reflected power vs. angle of incidence a. for plate A6, at f=33 GHz ($\lambda/d=1.14$) b. for plate B6, at f=35 GHz ($\lambda/d=1.37$) 87

Fig. 4.34. Reflected power vs. angle of rotation for plate A6 at f=35 GHz, $\theta_i=35°$ 89

Fig. 5.1. The profile of a crossed grating with hemispherical cavities, and dimensions for such two plates investigated 92

Fig. 5.2. Measured reflected power vs. θ_i for plate R4 at f=35 GHz, $\psi_i=0$ 94

Fig. 5.3 Measured reflected power vs. θ_i for plate R4 at f=33 GHz, $\psi_i=0$ 96

Fig. 5.4. Measured reflected power vs. ψ_i for plate R4 at f=35 GHz, $\theta_i=10°$ 98

Fig. 5.5. Measured reflected power vs. ψ_i for plate R4 at f=35 GHz, $\theta_i=30°$ 100

Fig. 5.6. Measured reflected power vs. θ_i for plate R6 at f=35 GHz, $\psi_i=0$ 102

Fig. 5.7. Measured reflected power vs. θ_i for plate R6 at f=33 GHz, $\psi_i=0$ 103

Fig. 5.8. Measured reflected power vs. ψ_i for plate R6 at $\theta_i=10°$, f=35 GHz 105

Fig. 6.1. Relative power of TM component of the reflected wave when a TE-polarized wave is

incident on plate C4 109

Fig. A.1. Comparison between numerical results for perfectly conducting strips of six symmetrical triangular corrugations and experimental results for the corresponding triangular grating plates of 30-39 grooves with the same profile 116

Fig. A.2. Calculated power patterns for strip A4 at θ_i=32.4° and f=35 GHz 117

Fig. A.3. Calculated power patterns for strip B6 at θ_i=43.5° and f=35 GHz 118

Fig. A.4. Calculated power patterns for strip B9 at θ_i=43.5° and f=35 GHz 119

Fig. A.5. Calculated power patterns for strip C4 at θ_i=38.1° and f=35 GHz 120

Fig. A.6. Calculated power patterns for strip C4 at θ_i=40.0° and f=33.75 GHz 121

ACKNOWLEDGEMENTS

I wish to express sincere thanks to my supervisor Dr. E. V. Jull for his patience, guidance and encouragement during the research work of this thesis.

Special thanks are due to Dr. R. Deleuil (Université de Provence, France) for the helpful advice and suggestions that he gave me during his two visits to Vancouver.

I would like to thank Mr. Derek Daines for his spending many hours milling the plates. Two plates with hemispherical cavities were made by Laboratoire de Radioélectricité, Université de Provence, France.

Financial support, a research assistantship from the Natural Sciences and Engineering Research Council of Canada and a teaching assistantship from the Department of Electrical Engineering, U.B.C., is grateful acknowledged.

Chapter 1

INTRODUCTION

During the past fifteen years the study of diffraction gratings has made great progress. Rigorous electromagnetic theories [20] have been developed to explain the behavior of singly-periodic, or classical gratings with a period in the range of the incident wavelength, and they seem capable of dealing with all structures of practical importance.

In the last decade interest has grown in the properties of doubly-periodic gratings, or crossed gratings, which have regular two-dimensional structure (pyramids, bisinusoidal bumps, hemispherical cavities, etc.) distributed periodically on a plane. In a series of recent publications, it has been shown that such structures have great potential in useful applcations, particularly in connection with selective absorption of solar radiation [5,19,24], non-absorptive reflection reduction [24], and microwave filtering [15]. Thus, it is very important to have accurate theoretical models of crossed grating behavior and to confirm these models with careful experimental measurements.

Theoretical studies of the diffraction by crossed gratings are still developing. Their commencement had to wait until the study of classical gratings reached a highly-developed stage. However, the progress has been slow, which is due mainly to the fact that in going from classical to crossed gratings, the size of the associated numerical problem is more than squared, and so rigorous techniques

valuable for the former become, when generalized, impracticable for the latter (given the capabilities of present computers). For example, such techniques would require the inversion of complex matrices having more than a million elements[20].

Several different formalisms have been proposed for the diffraction of electromagnetic radiation by crossed gratings. The earlier formalisms (for example those of Chen [3] for the case of a conducting screen perforated periodically with either circular or rectangular holes) rely upon the availability of a complete set of modal functions which can be superposed to specify the field in the aperture region. These modal functions must satisfy the wave equation and the boundary conditions on the aperture walls, and are only known analytically for a small number of perfectly conducting geometries [20]. Recently Toro and Deleuil [21,22] implemented a rigorous modal theory for the study of electromagnetic diffraction from a perfectly conducting crossed grating with hemispherical cavities. The theoretical study was realized for any incidence and direction of polarization, but the first numerical results were only for the simpler case of normal incidence.

Wirgin's formalism [25] is also restricted to the case of a perfectly-conducting crossed grating. This extremely simple method is based on an approximation that the diffracted field above the surface can be expressed as the Rayleigh plane wave expansion. Hence, it can only be applied

to very shallowly-grooved (h/d, groove depth over period of grating, in the range of 0.1) conducting surfaces. A few numerical results were obtained by this method for a perfectly conducting crossed grating of a sinusoidal profile with h/d=0.14 under normal incidence.

Maystre and Neviére [17], as well as Vincent [23] worked out differential formalisms valid for crossed gratings whose surface conductivity is not very high and whose depth is not very large compared with the wavelength. They obtained a few numerical results for a pyramidal grating with finite conductivity and h/d=0.25.

Derrick et al. [5,19] elaborated a formalism which is quite different from others. They used a coordinate transformation technique which flattens the crossed grating profile, combined with an iterative method for resolution of the very large system of complex equations expressing the boundary and outgoing wave conditions for the diffraction problem of crossed gratings. They presented in [19] some numerical results for the sinusoidally-grooved crossed gratings and a few examples for pyramidal crossed gratings with finite conductivity. In a private communication [16], they gave some calculated curves for pyramidal crossed gratings with infinite conductivity.

Among all existing formalisms, the last one is the most versatile and powerful, since it can work throughout the whole range of values of surface conductivity, including infinite conductivity. Much work had been devoted to this

formalism in order to extend its range of applicability. Recently it was reported [19] that a practical limit had been reached: the theory could not be extended to deeper crossed gratings in which h/d is greater than one, and further significant progress required a completely new method.

In comparison with theoretical investigations, experimental research on the diffraction by crossed gratings has been very limited. Wilson and Hutley [24] investigated experimentally the optical properties of artificial 'moth eye' antireflection surfaces which can be regarded as some kind of irregular sinusoidally-grooved crossed gratings. They found that metal moth eyes can selectively absorb visible radiation and reject infrared re-emission and this made them promising selective solar absorbers. Because of the difficulty of measuring accurately the shape of the structure (noting the spacing of less than 1 μm), they did not give a comparison of theory and experiment.

Bliek and Deleuil [1] undertook an extensive experimental study on classical gratings in the microwave range, and they also began an investigation of two kinds of crossed gratings, a conducting grid with circular holes and a conducting pyramidal grating. Their experimental setup was very powerful for diffraction measurements which were made with less than 3% relative error. Unfortunately they were not able to complete the investigation due to the loss of the experimental facility.

Here is given an experimental investigation of a metal crossed grating with square pyramids and a metal crossed grating with hemispherical cavities in the microwave region. The reasons that we chose these two kinds of crossed gratings are as follows:

- These two structures are expected to be efficient solar absorbing surfaces [19,20].
- Numerical analysis is still impossible for a deeply-grooved pyramidal crossed grating. Experimental investigation of it would be very useful.
- The behavior of a triangular groove grating , which is the singly-periodic equivalent of the corresponding pyramidal crossed grating, is well-known [9]. This provides the opportunity for a comparison between the behavior of triangular and pyramidal gratings of the same profile.
- A modal theory [22] was recently developed for a crossed grating with hemispherical cavities. Experimental verification of it would be valuable.

The reason that the deep pyramidal groove grating cannot be analyzed rigorously is that ,on one hand, the coordinate transformation method can only analyze crossed gratings which is not very deep (h/d less than one); on the other hand, a rigorous modal expansion for the fields between the pyramids cannot be written. The sides of the pyramids do not constitute a set of orthogonal surfaces, and a spherical coordinate system does not fit the boundaries of

the pyramids as it does the surfaces of a hemisphere.

Experimental study in the microwave region has an important advantage in that all grating dimensions are large enough to be milled accurately and thus a valid comparison between theory and experiment is possible.

With measurements made in the range of 35 GHz, Jull, Ebbeson, Heath, Beaulieu and Hui have sucessfully compared their theoretical results concerning three types of singly periodic conducting gratings: comb grating [10], rectangular grating [8,11] and triangular grating [9]. They attempted to find a perfectly blazed grating which completely converts specular reflection from a conducting surface to backscatter, and they showed numerically and experimentally that this blaze effect can be achieved by a rectangular grating or a triangular grating with adequately chosen dimensions. They also proposed applications to multipath interference reduction and radar target design.

The experimental study of crossed gratings given here represents a natural extension of the previous work on the blaze effect of some classical gratings. Crossed reflection gratings with square symmetry are also interesting possibilities for the suppression of specular reflection from conducting surfaces when the direction of incidence is arbitrary. The objectives of this experimental study are:

- to exploit the possibility of a pyramidal reflection grating to scatter all incident energy into a single spectral order,

- to investigate experimentally the predicted capability of a crossed grating with hemispherical cavities to eliminate specular reflection around normal incidence,
- to study the relation between the behavior of singly-periodic and its corresponding doubly-periodic gratings,
- to observe the effects of profile parameters, incident angles, period of grating and incident wavelength on the reflection behavior of these gratings,
- to compare the measured results with a few numerical predictions,
- to provide a set of experimental data for deeply-grooved pyramidal gratings and obtain some behavior curves of crossed grating with hemispherical cavities under non-normal incidence, which will assist further numerical investigations.

In chapter 2, through a derivation of the Rayleigh expansion for the diffracted field, the crossed grating equation and the Rayleigh wavelength equation are obtained. These play an important part in explaining the shape of the measured behavior curves of gratings. Methods to determine the propagating direction and the existing angular region of a diffracted wave by use of these two equations are discussed.

Chapter 3 describes the experimental arrangement and measuring procedure.

Experimental results of six pyramidal crossed gratings and two crossed grating with hemispherical cavities, and discussions on them are presented in Chapters 4 and 5 respectively. Basically the experimental data verify the theoretical and numerical predictions. Comparison between the behavior of triangular and pyramidal gratings of the same profile is made. The effects of varying grating and measuring parameters are observed by comparing measured curves.

Chapter 6 lists the sources of errors and discusses the effects of them. Finally, conclusions from this investigation are presented in Chapter 7.

Chapter 2

SCATTERING BY CROSSED GRATINGS

2.1 FORMULATION OF THE PROBLEM

Consider the diffraction problem in which a linearly polarized harmonic electromagnetic plane wave with wavelength λ is incident upon a doubly-periodic surface, having orthogonal periodicity axes and separating free space from a perfectly conducting metallic medium. Set up a rectangular coordinate system Oxyz, and let the Oy axis be

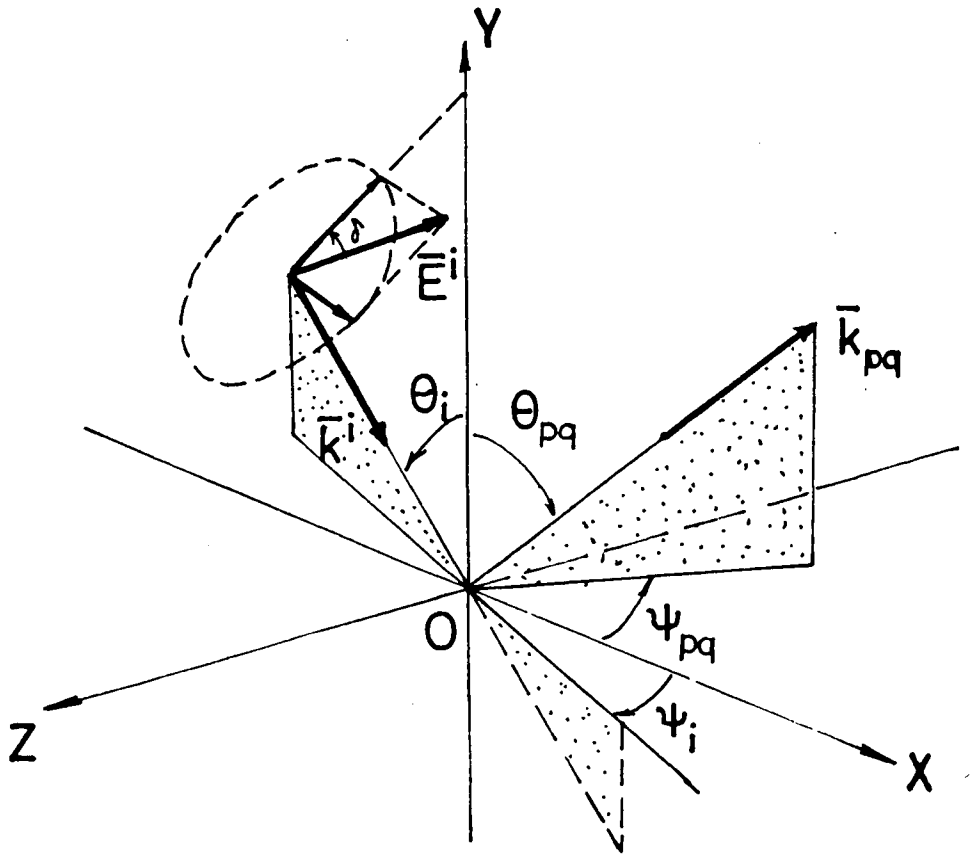

Fig. 2.1. The specification of the incident field $\bar{E}^i$ and of the diffracted wave vectors $\bar{k}_{pq}$ in the (Oxyz) system

perpendicular to the plane of the grating and Ox axis to be aligned with one of the axes of periodicity. The two periodicities of the crossed grating are defined by d_1, the period along Ox, and d_2, the period along Oz.

As shown in Fig. 2.1, the direction of the incoming plane wave is specified by the polar angles ψ_i and θ_i, and is represented by the wave vector $\bar{k}^i$. The polarization is specified by the angle δ between the electric field vector $\bar{E}^i$ and the intersection of the plane of incidence with the plane perpendicular to $\bar{k}^i$. If δ equals $\pi/2$, the incident electric field is parallel to the surface plane and we say that the incident wave is transverse electric-polarized, or TE-polarized. If δ equals zero, the incident magnetic field is parallel to the surface and we say that the incident wave is transverse magnetic-polarized, or TM-polarized. TE and TM polarizations are two fundamental polarization cases, since an arbitrarily polarized incident plane wave can be resolved into TE and TM components which scatter essentially independently from highly conducting classical grating surfaces, but not, in general, for crossed gratings.

Let the grating surface have the equation $y=f(x,z)$, and we have

$$f(x+d_1,z+d_2)=f(x,z), \tag{2.1}$$

since the grating is periodic along Ox and Oz.

In the region of $y<f(x,z)$, the fields are null because the medium is assumed perfectly conducting. Above the surface, because of its double-periodicity, the crossed

grating gives rise to a discrete spectrum of diffracted waves in the various orders, (p,q), the directions of which are represented by the wave vectors $\bar{k}_{pq}$. We will show in next section that the diffracted field above the surface plane (i.e. the region y>max[f(x,z)]) may be written as a superposition of plane waves (i.e. Rayleigh expansion). The derivation is similar to that in [21].

2.2 THE RAYLEIGH EXPANSION FOR THE DIFFRACTED FIELD

The incident plane wave fields are given by:

$$\bar{E}^i=\bar{E}^i_o\exp[j(-\bar{k}^i\cdot\bar{r}+\omega t)],$$

$$\bar{H}^i=\bar{H}^i_o\exp[j(-\bar{k}^i\cdot\bar{r}+\omega t)],$$

where $\bar{k}^i=\alpha_o\hat{x}-\beta_o\hat{y}+\gamma_o\hat{z}$, $\bar{r}=x\hat{x}+y\hat{y}+z\hat{z}$, ($\hat{x}$, $\hat{y}$, and $\hat{z}$ are unit vectors along the x, y and z axes respectively)
with: $\alpha_o=k\sin\theta_i\cos\psi_i$, $\beta_o=k\cos\theta_i$, $\gamma_o=k\sin\theta_i\sin\psi_i$, where $k=2\pi/\lambda$ is the wave number of the incident wave.
then,

$$\bar{E}^i=\bar{E}^i_o\exp[-j(\alpha_o x-\beta_o y+\gamma_o z)]\exp(j\omega t).$$

In what follows we will suppress the time dependence $\exp(j\omega t)$ for all fields.

Let $\bar{E}^d$ and $\bar{E}^t$ be the diffracted electric field and the total electric field respectively. Then $\bar{E}^t=\bar{E}^i+\bar{E}^d$.

To determine the diffracted field $\bar{E}^d$, we seek a vector function $\bar{E}^d(x,y,z)$ which satisfies:

1. the vector Helmholz equation for y>f(x,z): $(\nabla^2+k^2)\bar{E}^d=0$, where $\nabla^2=\partial^2/\partial x^2+\partial^2/\partial y^2+\partial^2/\partial z^2$
2. the boundary conditions at the grating surface:

$\bar{E}^d x\bar{n}=-\bar{E}^i x\bar{n}$, and $\nabla x\bar{E}^d\cdot\bar{n}=-\nabla x\bar{E}^i\cdot\bar{n}$, where $\bar{n}$ is the normal unit vector of the surface

3. the outgoing wave condition.

The solution of this problem should exist for physical reasons, and it should be unique according to the uniqueness theorem. Let us show that the function

$$\bar{F}(x,y,z)=\bar{E}^d(x,y,z)\exp[j(a_0x+\gamma_0z)] \tag{2.2}$$

is periodic along the directions Ox and Oz with the periods d_1 and d_2 respectively.

First, we show $\bar{F}(x,y,z+d_2)=\bar{F}(x,y,z)$.

Obviously, the total field $\bar{E}^t$ is periodic along Oz, that is,

$$\bar{E}^t(x,y,z+d_2)=\bar{E}^t(x,y,z) .$$

Considering $\bar{E}^t=\bar{E}^i+\bar{E}^d$, we have

$$\bar{E}^i(x,y,z+d_2)+\bar{E}^d(x,y,z+d_2)=\bar{E}^i(x,y,z)+\bar{E}^d(x,y,z) .$$

But since

$$\begin{aligned}\bar{E}^i(x,y,z+d_2)&=\bar{E}^i_0\exp\{-j[a_0x-\beta_0y+\gamma_0(z+d_2)]\}\\&=\bar{E}^i_0\exp\{-j[a_0x-\beta_0y+\gamma_0]\}\exp(-jd_2\gamma_0)\\&=\bar{E}^i(x,y,z)\exp(-jd_2\gamma_0),\end{aligned}$$

then

$$\begin{aligned}\bar{E}^d(x,y,z+d_2)&=\bar{E}^d(x,y,z)\exp(-jd_2\gamma_0) \qquad (2.4)\\&=\bar{E}^d(x,y,z)\exp[j(a_0x-\beta_0+\gamma_0z)]\exp\{-j[a_0x-\beta_0y+\gamma_0(z+d_2)]\}\end{aligned}$$

We can write

$$\bar{E}^d(x,y,z+d_2)\exp\{j[a_0x-\beta_0y+\gamma_0(z+d_2)]\}=\bar{E}^d(x,y,z)\exp[j(a_0x-\beta_0y+\gamma_0z)] \tag{2.5}$$

Recalling the definition of $\bar{F}(x,y,z)$, the above is

$$\bar{F}(x,y,z+d_2)=\bar{F}(x,y,z),$$

and we have demonstrated that $\bar{F}(x,y,z)$ is periodic along the Oz direction with the period d_2. Similarly we can demonstrate that $\bar{F}(x,y,z)$ is also periodic along the Ox direction with the period d_1.

Since the function $\bar{F}$ is doubly-periodic along Ox and Oz with periods d_1 and d_2, we can now expand it in a double Fourier series:

$$\bar{F}(x,y,z)=\sum_{p=-\infty}^{+\infty}\sum_{q=-\infty}^{+\infty}\bar{F}_{pq}(y)\exp[-j(pK_1\hat{x}+qK_2z)]$$

where $\bar{F}_{pq}(y)$ is a function of y only,

$K_1=2\pi/d_1$, $K_2=2\pi/d_2$,

$p=0,\pm1,\pm2,\cdots$, $q=0,\pm1,\pm2,\cdots$.

From the definition $\bar{F}(x,y,z)=\bar{E}^d(x,y,z)\exp[j(a_0x+\gamma_0z)]$, we have

$$\bar{E}^d(x,y,z)=\sum_{p=-\infty}^{+\infty}\sum_{q=-\infty}^{+\infty}\bar{F}_{pq}(y)\exp[-j(a_px+\gamma_qz)]$$

where $a_p=a_0+p\cdot2\pi/d_1$, $\gamma_q=\gamma_0+q\cdot2\pi/d_2$.

We can introduce this expansion for $\bar{E}^d$ in the Helmholtz equation $(\nabla^2+k^2)\bar{E}^d=0$ and get

$$d^2\bar{F}_{pq}(y)/dy^2+(k^2-a_p^2-\gamma_q^2)\bar{F}_{pq}(y)=0.$$

We obtain

$$\bar{F}_{pq}(y)=\bar{E}^d_{pq}\exp(-j\beta_{pq}y)$$

where

$$\beta_{pq}=\begin{cases}\sqrt{k^2-a_p^2-\gamma_q^2}, & \text{if } k^2-a_p^2-\gamma_q^2\geq0\\ -j\sqrt{a_p^2+\gamma_q^2-k^2}, & \text{otherwise.}\end{cases}$$

Therefore, at any point of the half-space $y>\max[f(x,z)]$, the field diffracted by a crossed grating can be expressed as a double sum of plane waves, the so-called Rayleigh expansion:

$$\bar{E}^d(x,y,z)=\sum_{p=-\infty}^{+\infty}\sum_{q=-\infty}^{+\infty}\bar{E}^d_{pq}\exp(-j\bar{k}_{pq}\cdot\bar{r}) \tag{2.6}$$

where

$$\bar{k}_{pq}=a_p\hat{x}+\beta_{pq}\hat{y}+\gamma_q\hat{z},$$

$$a_p=a_0+p\cdot 2\pi/d_1, \tag{2.7}$$

$$\beta_{pq}=\sqrt{k^2-a_p^2-\gamma_q^2}, \tag{2.8}$$

$$\gamma_q=\gamma_0+q\cdot 2\pi/d_2. \tag{2.9}$$

Equation (2.8) is called the crossed grating equation. We can see that the orders of diffraction formed by a crossed grating are specified by a pair of integers (p,q) rather than the single integer adequate in the case of singly periodic gratings. If β_{pq} is real, the order (p,q) is refered to as being a propagating order , since it can carry energy to infinity away from the grating surface. If β_{pq} is imaginary, the order (p,q) is said to be evanescent and carries no energy away from the grating surface. Important physical phenomena called the Wood anomalies arise in the vicinity of the transition point $\beta_{pq}=0$. If the incidence parameters θ_i and ψ_i are fixed, β_{pq} vanishes at the Rayleigh wavelength

$$\lambda_r(p,q)=(-B+\sqrt{B^2+A\cos^2\theta_i})/A \tag{2.10}$$

where

$$A=p^2/d_1^2+q^2/d_2^2,$$

$$B=\sin\theta_i(\cos\psi_i\cdot p/d_1+\sin\psi_i\cdot q/d_2).$$

We define the efficiency of a grating in a given order (p,q) to be the ratio between the power P(p,q) diffracted into this order and the incident power P(i). It is easy to show that

$$\epsilon_{pq}=|\bar{E}^d_{pq}|^2\beta_{pq}/(|\bar{E}^i_0|^2\beta_0). \tag{2.11}$$

Because of the conservation of energy and because of the assumption of perfectly-conducting surface, we have

$$|\bar{E}^i_0|^2\beta_0=\sum_{p=-\infty}^{+\infty}\sum_{q=-\infty}^{+\infty}|\bar{E}^d_{pq}|^2\beta_{pq}$$

which is reduced to

$$\sum_{p=-\infty}^{+\infty}\sum_{q=-\infty}^{+\infty}\epsilon_{pq}=1. \tag{2.12}$$

This equality, which means that the sum of the efficiencies is equal to unity, is generally called the energy balance criterion and can be used to check the numerical results.

2.3 DETERMINATION OF THE DIRECTIONS OF PROPAGATION OF THE DIFFRACTED WAVES

A plane wave incident on a crossed grating excites a discrete, rather than continuous, spectrum of diffracted plane waves. The wave vector $\bar{k}_{pq}$ of the diffracted wave of the (p,q) order can be specified by

$$\bar{k}_{pq}=\alpha_p\hat{x}+\beta_{pq}\hat{y}+\gamma_q\hat{z}.$$

It is easy to show that

$\alpha_p=k\sin\theta_{pq}\cos\psi_{pq}$, $\beta_{pq}=k\cos\theta_{pq}$, and $\gamma_q=k\sin\theta_{pq}\sin\psi_{pq}$. Thus, from (2.7) and (2.9), we obtain

$$k\sin\theta_{pq}\cos\psi_{pq}=\alpha_0+p\cdot 2\pi/d_1=k\sin\theta_i\cos\psi_i+p\cdot 2\pi/d_1,$$

and

$$k\sin\theta_{pq}\sin\psi_{pq}=\gamma_0+q\cdot 2\pi/d_2=k\sin\theta_i\sin\psi_i+q\cdot 2\pi/d_2,$$

which can be reduced to

$$\sin\theta_{pq}\cos\psi_{pq}=\sin\theta_i\cos\psi_i+p\cdot\lambda/d_1, \tag{2.13}$$

$$\sin\theta_{pq}\sin\psi_{pq}=\sin\theta_i\sin\psi_i+q\cdot\lambda/d_2. \tag{2.14}$$

Dividing (2.13) into (2.14), we get

$$\tan\psi_{pq}=(\sin\theta_i\sin\psi_i+q\cdot\lambda/d_2)/(\sin\theta_i\cos\psi_i+p\cdot\lambda/d_1). \tag{2.15}$$

These three equations can be used to determine the directions of the diffracted waves in the various orders.

In the following discussion, we assume $d_1=d_2=d$ for simplicity.

2.3.1 GRATING WITH PERIOD SMALLER THAN HALF OF WAVELENGTH

Since now $\lambda/d>2$, this requires $p=0$ and $q=0$ in (2.13) and (2.14). Then we have the set

$$\sin\theta_{pq}\cos\psi_{pq}=\sin\theta_i\cos\psi_i$$

$$\sin\theta_{pq}\sin\psi_{pq}=\sin\theta_i\sin\psi_i$$

which leads to $\psi_{pq}=\psi_i$ and $\theta_{pq}=\theta_i$. This is the only real solution for $d<\lambda/2$. Therefore, for a crossed grating with the period $d<\lambda/2$, only the (0,0) order wave (i.e., the specularly reflected wave) propagates, carrying all the incident energy, and the surface behaves as a plane conductor no matter what kind of profile the grating

has. For large periods specular reflection is reduced by scatter into other spectral orders.

2.3.2 GRATING WITH PERIOD BETWEEN A HALF WAVELENGTH AND ONE WAVELENGTH

2.3.2.1 Under Non-oblique Incidence ($\psi_i=0$)

We often study the case in non-oblique incidence, i.e., the case when $\psi_i=0$, the incident beam is perpendicular to one of the axes of the grating periodicity. Then we get

$$\sin\theta_{pq}\cos\psi_{pq}=\sin\theta_i+p\cdot\lambda/d \tag{2.16}$$

$$\sin\theta_{pq}\sin\psi_{pq}=q\cdot\lambda/d \tag{2.17}$$

Since now $1\le\lambda/d\le2$, from (2.17), we can conclude that $q=0$, which requires $\theta_{pq}=0$ or $\psi_{pq}=0$.

If $\theta_{pq}=0$, it is easy to derive from (2.16) that $p=0$ and $\theta_i=0$, which is the normally incident case.

Otherwise, $\psi_{pq}=0$. From (2.16), we have

$$\sin\theta_{p,0}=\sin\theta_i+p\cdot\lambda/d \tag{2.18}$$

which is of the same form as the classical linear grating formula. Thus we can see that the three-dimensional grating problem where $\lambda/2\le d\le\lambda$ and $\psi_i=0$ is reduced to the two-dimensional grating problem, some discussion[11] of which can be used for this special crossed grating case.

In some applications, it is desired to reduce reflection from a surface. This can be done by increasing backscatter. Maximum constructive

interference in the direction of backscatter, or back in the direction of incidence, occurs for $kd\sin\theta_i = m\pi$ or

$$\sin\theta_i = m\lambda/(2d), \quad m=1,2,\cdots. \tag{2.19}$$

It is easier to blaze a surface when the number of propagating orders are few; i.e., when the period d is small,but greater than half of wavelength. This is true in (2.19) when m=1 or

$$d=\lambda/(2\sin\theta_i) \tag{2.20}$$

which is called the Bragg condition. Combining the above equation with (2.19), we get

$$\sin\theta_{p,0} = (p+1/2)\lambda/d, \quad p=0,\pm1,\pm2,\cdots \tag{2.21}$$

and for periods in the range $\lambda/2 \le d \le \lambda$ the only real solutions to (2.21) are $\theta_{0,0}$ and $\theta_{-1,0}$, and from (2.20) and (2.21), $\theta_{-1,0} = -\theta_i$. Therefore only specular reflection (the order (0,0)) and backscatter (the order (-1,0)) exist. By adjusting other parameters of the grating, we can get a increase in backscatter and a corresponding decrease in specular reflection.

2.3.2.2 Under Oblique Incidence

We now consider oblique incidence when $\psi_i \neq 0$. Assume $0<\theta_i<\pi/2$ and $0<\psi_i<\pi/2$ without losing generality. Since $1 \le \lambda/d \le 2$, we can conclude from Eq. 2.13 and Eq. 2.14 that only p=0,-1 and q=0,-1 are possible solutions, so there are four possible orders of diffracted waves: (0,0), (0,-1), (-1,0) and (-1,-1).

For example, in the case of $\lambda/d=1.24$, $\theta_i=38°$ and $\psi_i=30°$, which is one of the experimental cases, after

some calculation using Eq. 2.13 and Eq. 2.14, we find that in this case of oblique incidence, besides the order (0,0), only the order (-1,0) occurs, the direction of which can be determined by finding $\theta_{-1,0}$ =50.5° and $\psi_{-1,0}$=156.5°.

2.3.3 GRATING WITH PERIOD GREATER THAN WAVELENGTH

We consider the cases of non-oblique incidence (ψ_i=0). Again we have Eq. 2.16 and Eq. 2.17, from which we can see that q=±1 and possible higher orders are excited since now $\lambda/d<1$.

For instance, we can calculate the directions of all the diffracted waves scattered by a crossed grating with hemispherical cavities which we have investigated. The case is in normal incidence, and λ=8.57 mm, d=13 mm. Since θ_i=0, we get

$$\sin\theta_{pq}\cos\psi_{pq}=p\cdot\lambda/d, \tag{2.22}$$

and

$$\sin\theta_{pq}\sin\psi_{pq}=q\cdot\lambda/d. \tag{2.23}$$

Now that λ/d=0.66, p and q can only take values of 0,1 or -1, and we obtain nine sets of equations from the above two equations. Solving them, the directions of nine orders of the diffracted waves can be found as follows:

order (0,0): specular reflection, $\theta_{0,0}$ =0;

order (0,1): $\psi_{0,1}$=90°, $\theta_{0,1}$ =41.3°;

order (0,-1): $\psi_{0,-1}=270°$, $\theta_{0,-1}=41.3°$;

order (1,0): $\psi_{1,0}=0°$, $\theta_{1,0}=41.3°$;

order (-1,0): $\psi_{-1,0}=180°$, $\theta_{-1,0}=41.3°$;

order (1,1): $\psi_{1,1}=45°$, $\theta_{1,1}=69°$;

order (1,-1): $\psi_{1,-1}=315°$, $\theta_{1,-1}=69°$;

order (-1,1): $\psi_{-1,1}=135°$, $\theta_{-1,1}=69°$;

order (-1,-1): $\psi_{-1,-1}=225°$, $\theta_{-1,-1}=69°$.

From the above results, it turns out that except for the order (0,0), which is back in the direction of incidence, the diffracted wave vectors lie on two cones

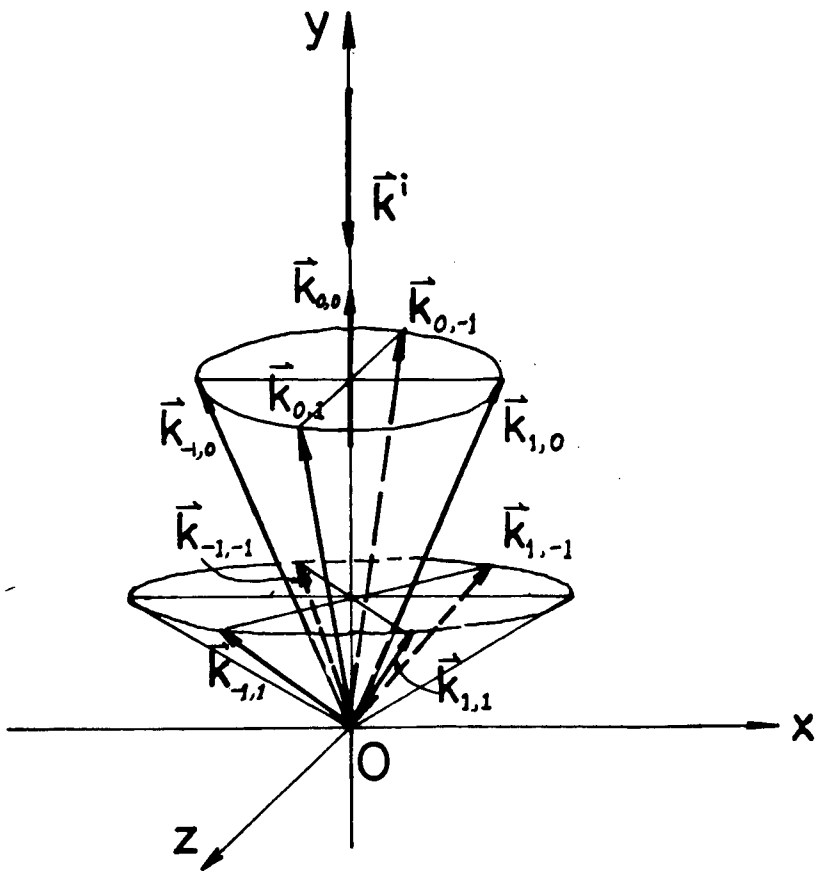

Fig. 2.2. The directions of the diffracted wave vectors scattered by a crossed grating with $\lambda/d=0.66$ in normal incidence

whose axes are superposed on the incident wave vector and whose half-angles are 41.3° and 69° respectively (see Fig. 2.2).

2.4 DETERMINATION OF THE ANGULAR REGION WHERE A DIFFRACTED ORDER EXISTS

In general, we can use the Rayleigh wavelength equation (2.10) as a guide to find the region of the azimuthal angle ψ_i where the diffracted order (p,q) exists: for fixed incident angles θ_i and ψ_i, if the actual wavelength λ is not greater than the Rayleigh wavelength $\lambda_r(p,q)$ given by (2.10), the diffracted order (p,q) can exist at this position. Let us consider the range $0 \le \psi_i \le 90°$ and a crossed grating with $\lambda/2 \le d \le \lambda$.

For the order (-1,0), we have from (2.10)

$$\lambda_r(0,-1)/d = \sin\theta_i \cos\psi_i + \sqrt{\sin^2\theta_i \cos^2\psi_i + \cos^2\theta_i} \qquad (2.24)$$

which is a decreasing function of θ_i in the range $0 \le \psi_i \le 90°$, and

$$(\sin\theta_i + 1)\Big|_{\psi_i=0} \le \lambda_r(-1,0)/d \le \cos\theta_i\Big|_{\psi_i=90°} \qquad (2.25)$$

If we now assume $\theta_i \le \sin^{-1}(\lambda/d - 1)$ which is the necessary condition that the order (-1,0) exists at $\psi_i = 0$, and increase ψ_i from zero while holding θ_i at that constant value, we can see that the diffracted order (-1,0) will remain existing until ψ_i reaches a certain value which makes the right side of (2.24) equal to the actual value of λ/d. This is the transition point where the (-1,0) Wood anomaly occurs and the order (-1,0) ceases to propagate.

For the spectral order (0,-1), we obtain from (2.10)

$$\lambda_r(0,-1)/d=\sin\theta_i\sin\psi_i+\sqrt{\sin^2\theta_i\sin^2\psi_i+\cos^2\theta_i} \qquad (2.26)$$

which is an increasing function of ψ_i in the range $0\le\psi_i\le 90°$, and

$$\cos\theta_i\Big|_{\psi_i=0} \le \lambda_r(0,-1)/d \le (1+\sin\theta_i)\Big|_{\psi_i=90°} \qquad (2.27)$$

At $\psi_i=0$, the order (0,-1) does not exist since we have assumed $1\le\lambda/d\le 2$. As ψ_i becomes large enough while θ_i is fixed, the diffracted order (0,-1) appears. It begins to propagate at the point where the actual value of λ/d is equal to the right side of (2.26), and the (0,-1) Wood anomaly happens.

For the diffracted order (-1,-1), the normalized Rayleigh wavelength can be expressed as

$$\lambda_r(-1,-1)/d=\{\sqrt{2}\sin\theta_i\cos(\psi_i-45°)+\sqrt{\sin^2\theta_i(\sin 2\psi_i-1)+2}\}/2. \qquad (2.28)$$

When $\psi_i=0$ or 90°, we get

$$\lambda_r(-1,-1)/d=(\sin\theta_i+\sqrt{2-\sin^2\theta_i})/2 \qquad (2.29)$$

which is always less than one when $0\le\theta_i\le 90°$. Thus, in the case of $1\le\lambda/d\le 2$, the order (-1,-1) does not exist around $\psi_i=0$ or 90°, this agrees with the previous discussion.

The maximum value of $\lambda_r(-1,-1)/d$ can be easily found from (2.28) as

$$\max[\lambda_r(-1,-1)/d]=(1+\sin\theta_i)/\sqrt{2}, \qquad \text{at } \psi_i=45°. \qquad (2.30)$$

If θ_i is large enough, the order (-1,-1) can exist around $\psi_i=45°$, and two (-1,-1) Wood anomalies, located symmetrically about $\psi_i=45°$, defines the region where the order (-1,-1) exists.

In this way, we can find out the range of ψ_i where a diffracted order (p,q) can propagate. We will apply this method when discussing experimental results from the cases of oblique incidence. For the case of non-oblique incidence (ψ_i=0 fixed), the range of θ_i where a diffracted order (p,q) can exist will be similarly determined.

2.5 A PRODUCT FORMULA LINKING CROSSED AND CLASSICAL GRATINGS

It is interesting to investigate any simple relation between the behavior of singly periodic grating and doubly periodic grating having the same profile and use it as a guide to the design of crossed grating surfaces since the theories for the diffraction by classical grating are now capable of dealing with all structures of practical importance. Here we introduce an empirical equivalence formula linking crossed and classical gratings which was suggested by Derrick et al. [5].

Let us suppose that the crossed grating is of the form y=f(x,z)=u(x)+v(z). The equivalence formula indicates that the efficiency ϵ_{mn} of the crossed grating in the order (m,n) is given by

$$\epsilon_{mn}=\eta_m^1\cdot\eta_n^2/R, \tag{2.31}$$

where η_m^1 and η_n^2 are the efficiencies of the classical gratings with profile equations y=u(x) and y=v(z) in orders m and n respectively, under the same conditions of incidence and polarization as for the crossed grating , and R is the Fresnel reflectance of a plane surface with the same

conditions of incidence.

This formula in the case of the order (0,0) can be derived roughly by use of Taylor series for sufficiently shallow crossed gratings under normally incident radiation [20]. Indeed, comparisons [5,19] between the rigorous theoretical results and those obtained using the equivalence formula showed that this product formula gave to a good accuracy the efficiency ϵ_{00} of some sinusoidally-modulated crossed gratings under normally incident radiation at optical frequencies. It is worth while pointing out that the agreement is still very good for a crossed grating with h/d=1 [19, Fig. 1] although the product formula is supposed to be valid for very shallow crossed gratings.

We are mostly concerned about investigating the reflection free property of a crossed grating and if this product formula were always true, a crossed grating would have the reflection free property when its singly-periodic equivalent grating can backscatter all the incident energy (i.e., $\epsilon_{00}=0$ if η_0^1 or η_0^2 equals to zero). This would be a simple way to find a reflection-free crossed grating since it is possible now to design a blazed classical grating by numerical methods. We will investigate this possibility experimentally.

Chapter 3

EXPERIMENTAL ARRANGEMENT AND PROCEDURE

For our experimental investigation, six metal crossed gratings of square pyramids and two metal crossed gratings with hemispherical cavities were made in all. The details of dimensions of these plates will be given in the following two chapters. Each of these surfaces consisted of a matrix of more than 15x15 identical elements with the period d, the value of which is in the range of the wavelength of radiation used.

The experimental arrangement was similar to that used in [8]. A photograph of the experimental set up is shown in Fig. 3.1 and a diagram of the experimental arrangement is shown in Fig. 3.2. Reflection measurements were made in a microwave anechoic area. Transmitting and receiving antennas were two identical pyramidal horns with 24.7 dB gain and E-plane 3 dB beamwidth of 9°, the orientation of which can be changed to have TE or TM polarization of the incident wave and to analyze the polarization of the diffracted wave. Microwave absorbers suspended between the horns prevented direct transmission, while absorbers were positioned around the plate to eliminate reflection from any surface except the top of the grating plate investigated. Absorbers were also placed at the end of the grating to reduce transmission under the plate. The incident angle θ_i could be varied from approximately 5° to 90°, but it was difficult to eliminate coupling of two antennas near the 5° limit and direct

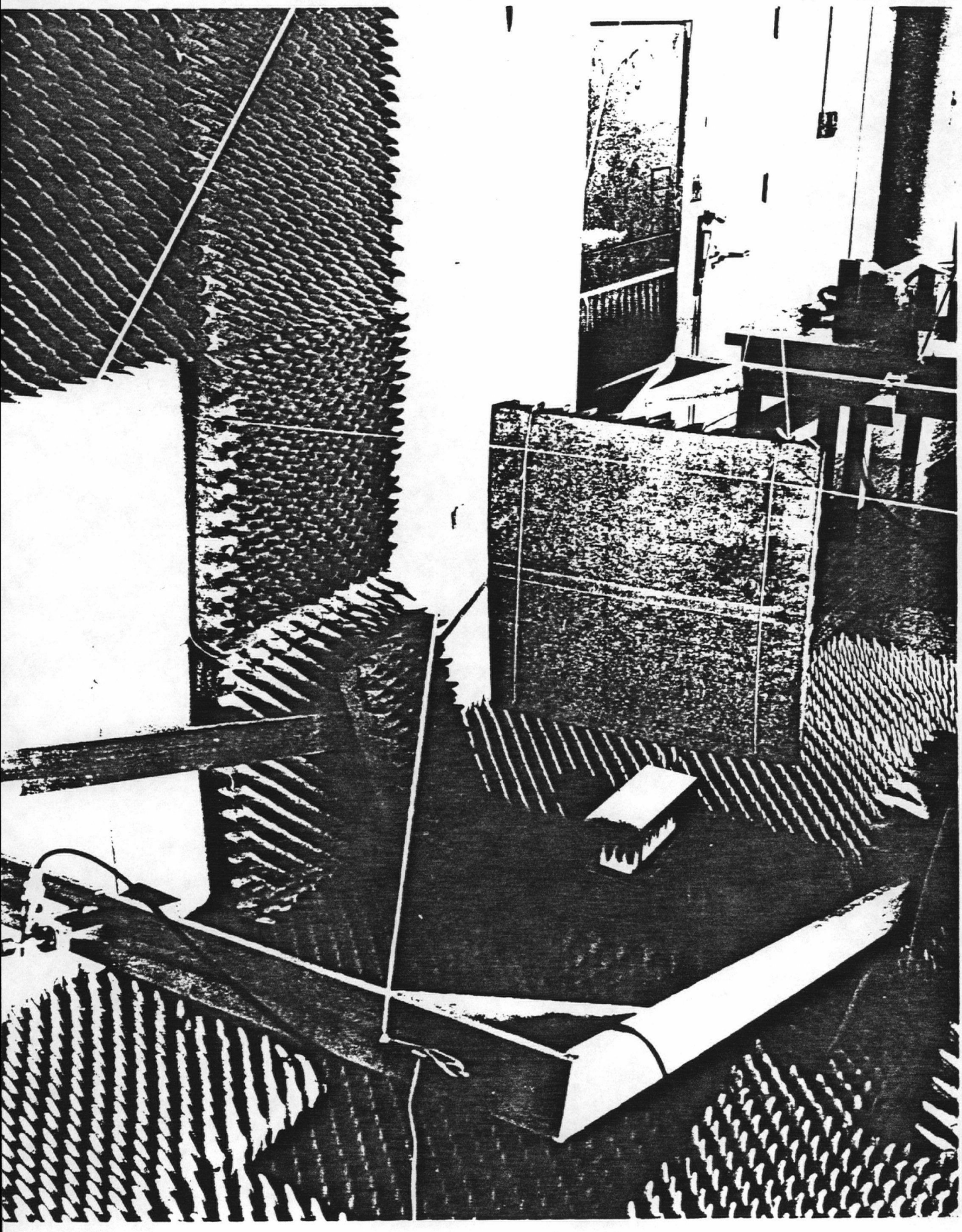

Fig. 3.1. Photograph of experimental set-up, receiving horn in foreground

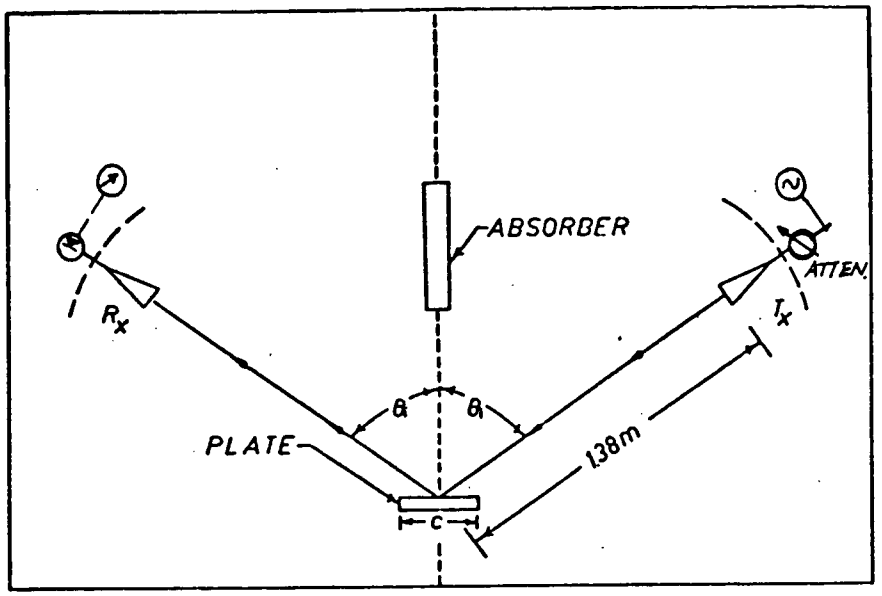

(a)

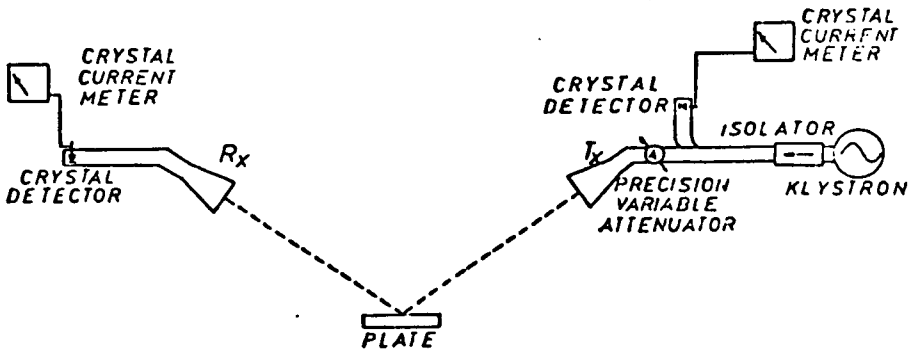

(b)

Fig. 3.2. Experimental arrangement

a. Range
b. Circuit

transmission between the antennas near the 90° limit. Therefore, our measurements were usually taken in the range of incident angles from 10° to 80° or less, with an reading accuracy of about 1°. The distance from the grating surface to either of the antennas was 1.38 m. This non-plane wave illumination, as reported by Jull and Ebbeson [10] and Heath [8], has very little effect on the grating performances, and the results, as far as reflection reduction is concerned, could only be better under plane wave illumination.

A diagram of the experimental circuit is shown schematically in Fig. 3.2(a). With the corrugated surface exposed, the crystal current reading of the receivng antenna was noted. When the grating was covered by a flat and thin (1 mm thickness) conducting plate of the same area as the grating surface, the crystal current reading increased but was restored by adjusting a precision variable attenuator. The power reduction in surface reflection due to the grating is the difference between the former and latter precision variable attenuation readings, accurate to about ±0.2 dB. The tuning range of the millimeter reflex klystron is 33 GHz to 37.5 GHz (or the wavelength λ is from 9.09 mm to 8.00 mm), and the klystron output was monitored continuously to detect output level changes during the measurements.

To investigate the effects of oblique illumination, the grating surfaces were mounted on a platform which could be rotated around the vertical axis by an azimuthal angle ψ_i. After each rotation, the grating surface was re-leveled by

adjusting three screws which were mounted on the platform, thus increasing the accuracy of the θ_i measurements.

Although the emphasis of our investigation was upon measuring the relative reflected power by a grating plate under non-oblique incidence, we also measured the other two kinds of responses of each grating: azimuthal angular response and frequency response in reflected power. Normally, the measurement procedure was as follows:

1. With the incident beam perpendicular to one of the axes of the grating periodicity, the relative reflected power was measured by varying the incident angle from 10° to 80° with increments of 2.5°. More measurement points were taken near a reduction peak to increase the accuracy of the position and the value of the maximum reduction of reflected power.
2. With a fixed incident angle which was usually the angle where the maximum reflection reduction occured or was the Bragg angle ($\theta_i=\sin^{-1}(\lambda/(2a))$, an azimuthal angular response was recorded by rotating the plate horizontally from $\psi_i=-45°$ to $\psi_i=45°$. Since the crossed gratings investigated were square symmetric, the full ψ_i response between 0° to 360° could be derived from the measurements taken between 0° and 45°. Nevertheless, we also measured the response from -45° to 0° in order to check the symmetry of the response curve .
3. With the same incident angle θ_i and $\psi_i=0°$ (non-oblique incidence), the frequcncy response was obtained by

varying the incident wave frequency from 33.0 GHz to 37.5 GHz (the tuning range of the klystron). Whenever a more satisfactory result was found at a new frequency, measurements in steps 1 and 2 were repeated at that frequency.

In all the measurements, the performance for TM polarization and for TE polarization was recorded individually by changing the orientation of the antenna horns.

The experimental values for TM polarization were plotted as small circles which were joined by straight lines, while those for TE polarization as small crosses connected by broken lines.

Normally we drew curves of variation of the reflected power level in terms of dB by using the measured data directly. Sometimes for convenience we also plotted curves of the efficiency in the order (0,0); i.e., the relative reflected power.

Chapter 4

EXPERIMENTAL RESULTS OF PYRAMIDAL CROSSED GRATINGS

4.1 INTRODUCTION

In this chapter measurements of the power reflected by a pyramidal crossed grating are presented. Fig. 4.1 shows a photograph of one of the pyramidal crossed grating plates studied experimentally, which is composed of conducting pyramids with a square base. The pyramids were constructed by ruling consecutively, in orthogonal directions, two symmetrical triangular groove grating having the same groove spacing d and the same apex angle α. Fig. 4.2 shows a classical triangular groove grating (echelette grating) and a pyramidal crossed grating with the same profile, and lists the plate dimensions (period d and pyramid height h), apex angle α, the depth-to-period ratio h/d and the numbers of pyramids for all pyramidal grating plates investigated experimentally. These were milled within ±0.03 mm (±0.001 in.) of the given dimensions. The grating periods were designed for an incident wave at a frequency of 35 GHz (λ=8.57 mm) to satisfy the relation of $\lambda/2<d\leq\lambda$, and hence only specular reflection (the order (0,0)) and the diffracted order (-1,0) existed under non-oblique incidence according to the discussion in Section 2.3.

Since in general it is only possible to obtain by using current theories numerical results for a crossed grating whose depth is less than its period (also depending on

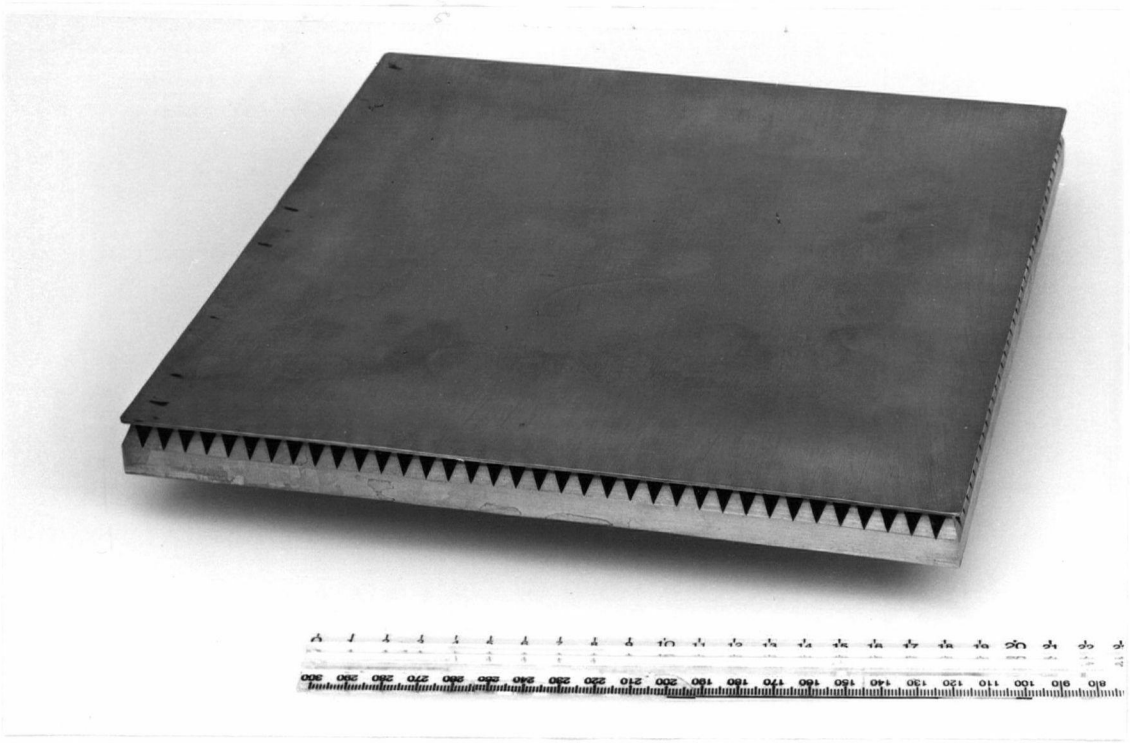

a.

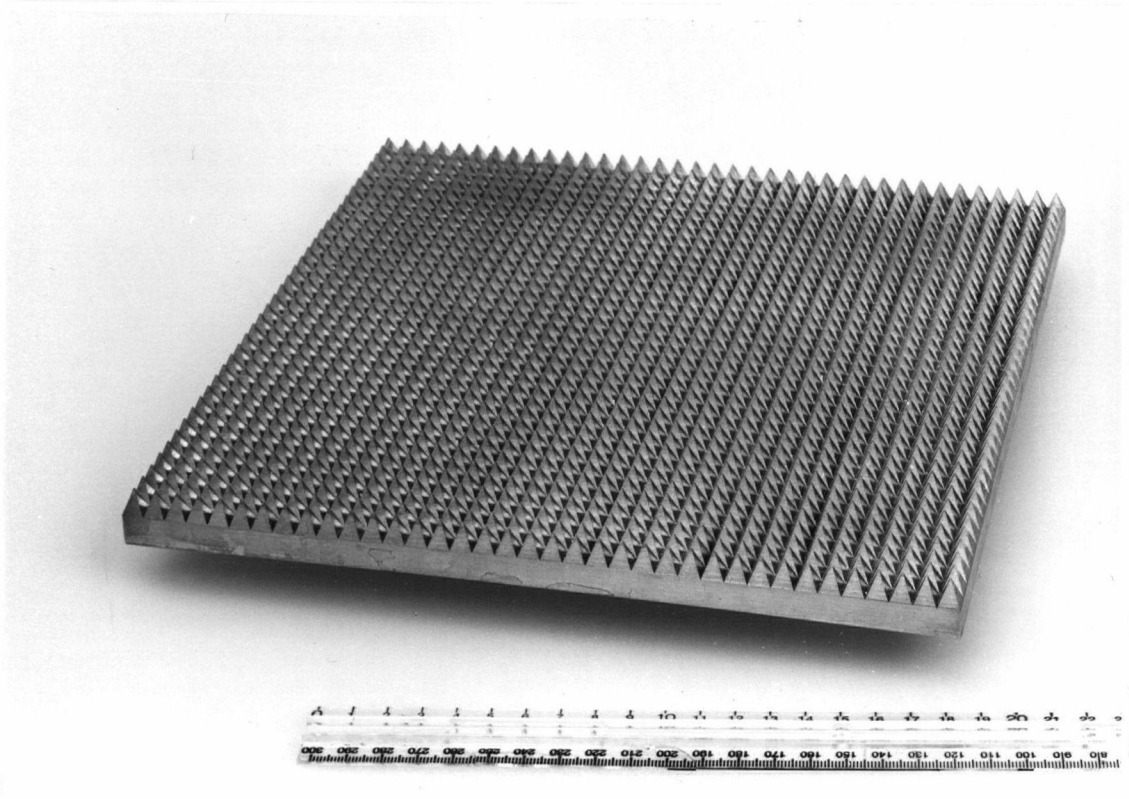

b.

Fig. 4.1. Photograph of a pyramidal crossed grating plate (plate C4)
a. covered with a flat conducting plate
b. crossed grating exposed

REFLECTION GRATINGS

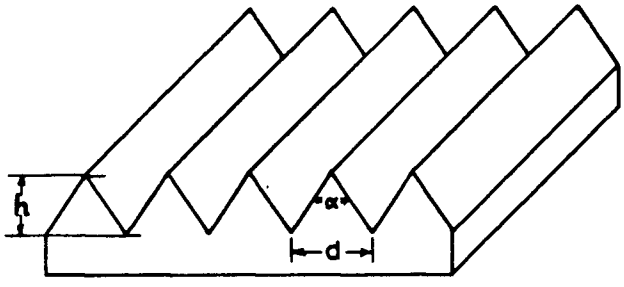

ECHELETTE

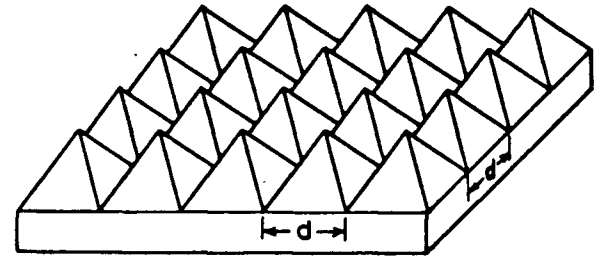

CROSSED PYRAMIDAL

PLATE	APEX ANGLE (degrees)	DIMENSIONS d(mm)	h(mm)	h/d	PYRAMIDS
A4	45	8.00	9.66	1.21	30x30
A6	60	8.00	6.93	0.87	30x30
A9	90	8.00	4.00	0.50	30x30
B6	60	6.23	5.40	0.87	39x39
B9	90	6.23	3.12	0.50	39x39
C4	44	6.95	8.60	1.24	37x37

Fig. 4.2. A classical triangular (echelette) grating and a pyramidal crossed grating with the same profile, and dimensions for all pyramidal plates

wavelength) [19], it is interesting to get experimentally diffraction patterns for crossed gratings which are deeply-grooved. Therefore, each grating depth which we chose was equal to or greater than half of the period, or, in other words, the apex angle α of each grating was equal to or less than 90°.

The surfaces of the first set (set A) consisted of a matrix of 30x30 identical pyramids with base dimension d=8.00 mm and apex angles α=90°, 60° and 45°. These were machined on 240x240 mm brass plates whose thickness was about 20 mm. A second set (set B) consisted of 39x39 pyramids with d=6.23 mm. Plate B9 with apex angle of 60° is made of brass while Plate B6 with apex angle of 60° is made of aluminium, but no problem in the measurements should arise from using these two different materials because both can be treated as essentially perfectly conducting in the microwave region. Two plates of set B were chosen for comparison with earlier work [16] for which some numerical results are available. There was only one brass grating plate with d=6.95 mm and α=44° in set C, which was specially designed to observe how well the reflection free properties of a singly-periodic surface carry over to its doubly-periodic equivalent.

Unlike previous experiments on classical gratings where numerical data were used to design the gratings, we had little suitable theoretical results on pyramidal crossed gratings with infinite conductivity available for predicting

our investigation. Therefore, in order to search for the best operating point where the maximum reflection reduction occured, we tried to change between limits the parameters which could be changed, i.e., the parameters of the grating (period d, and apex angle α (or height h)) and the parameters of the measurement (incident angle θ_i, azimuthal incident angle ψ_i, and frequency of the incident wave).

4.2 PLATE B9 ---- IN COMPARISON WITH ITS SINGLE-PERIODIC EQUIVALENT

In our departmental workshop, a symmetrical triangular groove grating was first milled across the brass plate in making a square pyramidal crossed grating of the same profile. One such comparison is shown in Fig. 4.3 for 39 symmetrical triangle grooves with apex angle of 90° (Fig. 4.3a) and the corresponding plate B9 (Fig. 4.3b) of 39x39 square pyramids at the frequency of 35 GHz ($\lambda/d=1.37$). The experimental results have already been presented in [12].

For TM polarization, the triangular grooves are essentially perfectly blazed to the n=-1 spectral order at the Bragg angle $\theta_i=\sin^{-1}(\lambda/(2d))=43.5°$ where a reduction in the reflected power is about 47 dB ($\epsilon_0=0.00002$) or 99.998% of the incident energy is reflected back in the direction of incidence. Over a wide angular range of $30°\leq\theta_i\leq70°$, the zero order efficiency is below 0.01 and specular reflection is almost eliminated. TE polarized reflection is approximately halved ($\epsilon_0=0.45$ at $\theta_i=43.5°$) by the grooves for Bragg angle

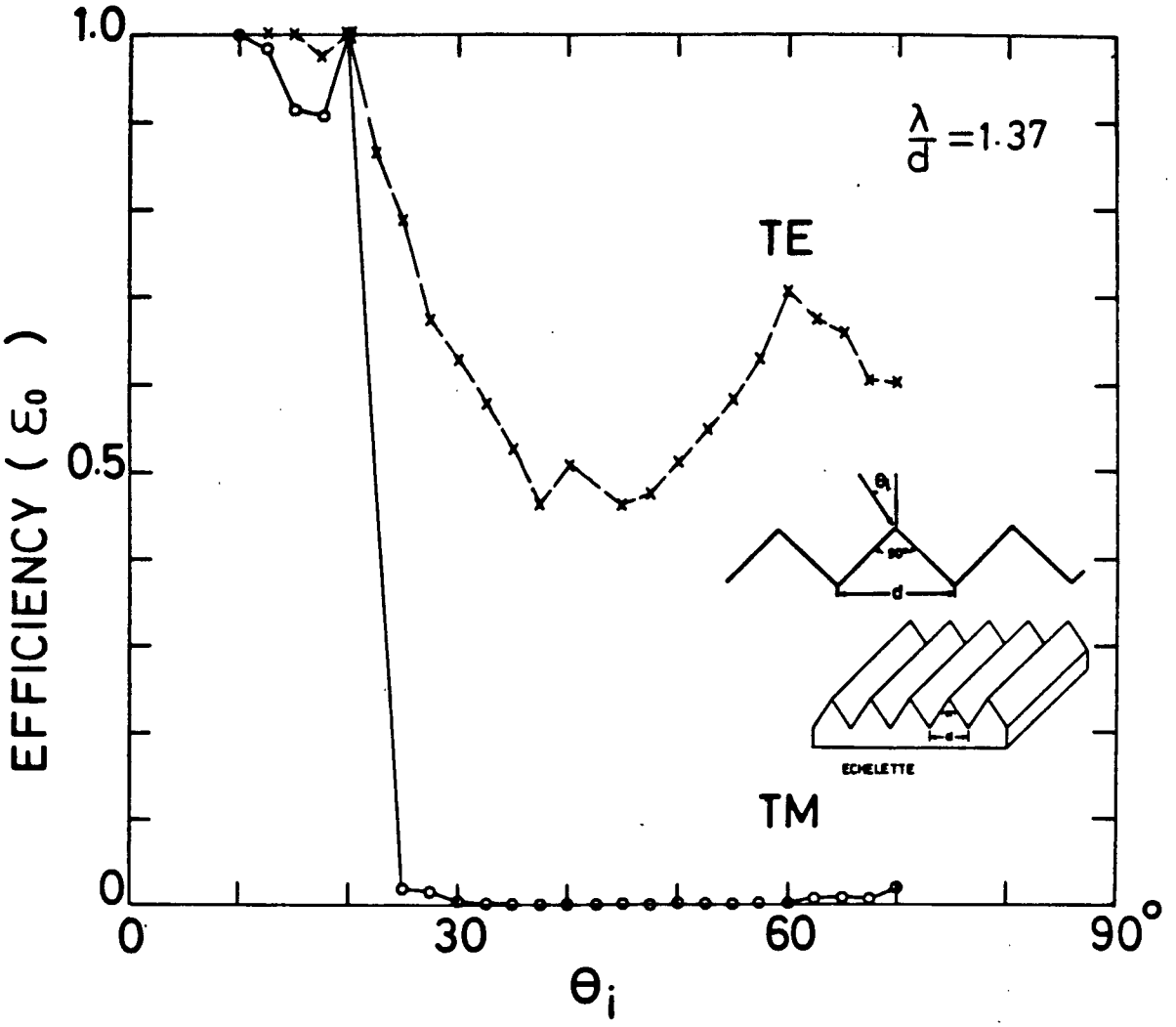

Fig. 4.3a. Relative reflected power (or ϵ_0) vs. angle of incidence for the singly periodic equivalent of plate B9 at f=35 GHz, ψ_i=0

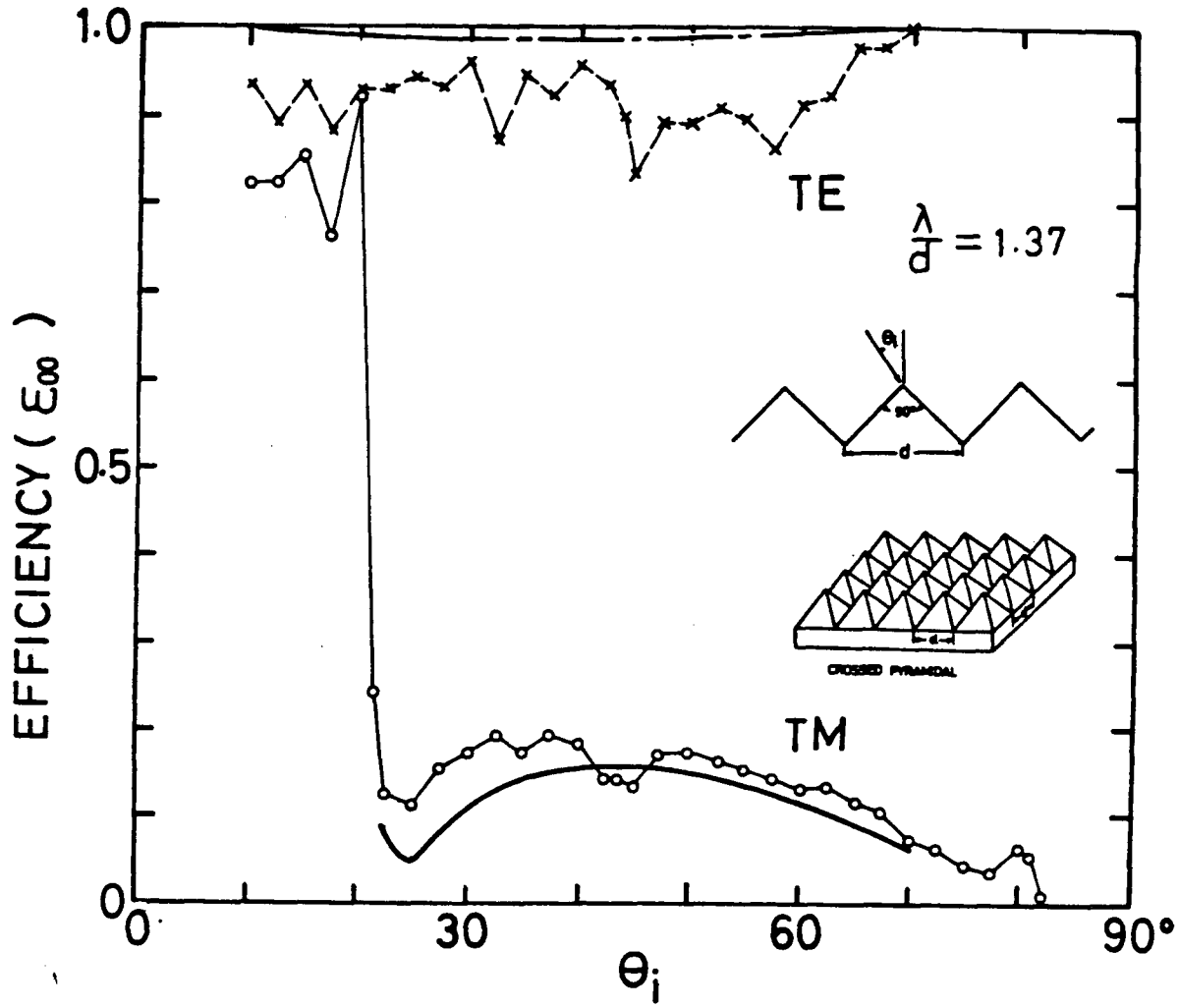

Fig. 4.3b. Relative reflected power (or ϵ_{00}) vs. angle of incidence for plate B9 at f=35 GHz, ψ_i=0.

Predicted for infinite surfaces:
——·—— TE case, ——— TM case

incidence. We also obtained from a computer program by Facq [17] two numerical results of ϵ_0=0.04 for TM polarization and ϵ_0=0.64 for TE polarization at θ_i=43.5° and f=35 GHz for a perfectly conducting strip of six symmetrical triangular grooves with the same period and apex angle. The calculated power patterns were also obtained (see Fig. A.2, Appendix). After taking into account the effect of the larger size (39 grooves) of the experimental grating, the correspondence between the calculated and measured values is good.

With the corresponding pyramidal grating Fig. 4.3b shows that TM polarized specular reflection is still substantially reduced over a wide range of incident angles where at least 80% of incident energy is diffracted into the order (-1,0). At this point, it seems that the TM polarized reflection free property of the corresponding singly-periodic surface carries over in a certain extent to crossed grating plate B9. TE polarized reflection is only slightly affected by the surface.

Fig. 4.3b also shows that the experimental results for both TM and TE cases agree with predicted results [16] indicated by bold solid (TM) and broken (TE) curves. A slightly upward shift of the experimental TM curve with respect to the calculated TM curve is probably due to the site reflections. P. Blick and R. Deleuil had reported their experimental results [10, Fig. 12] obtained from the same kind of pyramidal crossed grating with the same apex angle of 90° under the same incident conditions. These are the

only pair of experimental curves available for comparison with our work. Their results almost coincided with the numerical curves presented here. Our measuring arrangement is much simpler and incapable of the same precision (their relative accuracy of the grating efficiency measurement was better than 3% as reported), but still has provided adequate experimental accuracy to verify theoretical predictions for millimeter-wave reflection gratings, as proved in the previous work on classical gratings [9-12].

For classical gratings maximum reflection reduction always occurs at the Bragg angle, which can also be seen in Fig. 4.3a. However, from Fig. 4.3b, it seems that basically there is no Bragg angle effect for crossed grating plate B9.

It is also noted that the experimental points are in good agreement with the theoretical predictions concerning the so-called Wood anomaly, which occurs at any wavelength where a diffracted order ceases to propagate, that is, at the Rayleigh wavelength introduced in Section 2.2. Using (2.10), the Rayleigh wavelength λ_r of the order (p=-1,q=0) under non-oblique incidence (ψ_i=0) can be found as

$$\lambda_r(-1,0)=(1+\sin\theta_i)d,$$

from which we deduce that when the incident angle θ_i is less than

$$\theta_i=\sin^{-1}(\lambda/d-1), \qquad (4.1)$$

the diffracted order(-1,0) ceases to propagate and only the specular reflection exists.

In the case of classical gratings, by applying the grating equation

$$\sin\theta_n=\sin\theta_i+n\lambda/d, \quad (n=0,\pm1,\pm2,...)$$

where θ_n is the diffraction angle from the surface normal, and considering that when $\theta_n=-\pi/2$, the n=-1 spectral order will cease to propagate, we can get easily the value of incident angle where the n=-1 Wood anomaly occurs which is also

$$\theta_i=\sin^{-1}(\lambda/d-1),$$

the same as (4.1).

Therefore, the (-1,0) Wood anomaly for plate B9 and the n=-1 Wood anomaly for its singly-periodic equivalent at 35 GHz should both occur at

$$\theta_i=\sin^{-1}(1.375-1)=22^\circ.$$

Back to the experimental results presented in Fig. 4.3a or 4.3b, we can see that there is indeed an abrupt drop at about $\theta_i=22^\circ$ in the relative reflected power curve for TM polarization, which is due to a rapid exchange of power between specularly reflected and diffracted modes – in a change of only 2° in θ_i, 80% of the incident energy switches from the order (0,0) (or the n=0 order for classical grating) to the order (-1,0) (or the n=-1 order for classical grating) which can only exist when $\theta_i>22^\circ$. Thus, the agreement between theory and experiment is very good. In the case of TE polarization, the Wood anomaly is still evident for the classical grating, but is not clear for the crossed grating.

Let us concentrate our study on the crossed grating. For angles of incidence less than the limit value 22°, only the order (0,0) propagates and the efficiency ϵ_{00} in the two polarizations TM and TE should be identical and equal to unity. The fact that ϵ_{00} is only near unity when $\theta_i<22°$ in Fig. 4.3b is due to experimental error. The effect of polarization becomes apparent rapidly as soon as the incident angle is greater than 20°. ϵ_{00} for TM polarization falls rapidly to about 0.1 and stays below 0.2,while ϵ_{00} for TE polarization remains close to one. Thus, this structure behaves like a polarizer,because it can diffracted most of the TM component of an arbitrarily polarized incident wave into a single order (-1,0) and reflect specularly most of the TE component.

Fig. 4.3b also shows that when the incident angle is greater than 65°, the relative reflected power is below 0.1 and even reach as low as 0.007 at $\theta_i=82°$. Measurements for $\theta_i>80°$ are difficult due to direct transmission between transmitting and receiving horns, but it has been established that ϵ_{00} at $\theta_i=82°$ is at most 0.007 or less (since the effect of direct transmission is to make the measured value of ϵ_{00} larger than its true value). Also, this near-zero value of ϵ_{00} agrees with the tendency of both the calculated and the experimental curves for TM polarization in Fig. 4.3b when the incident angle is greater than 50°. It seems that ϵ_{00} would approach zero and almost total cancellation of specular reflection would occur over a

wide range of θ_i for near-grazing incidence, which is a desirable property for some applications (for example, multipath interference suppression,since most multipath interference occurs for near-grazing incidence). Thus this kind of crossed grating appears to be a promising structure for those applications.

The experimental plot of the relative reflected power as a function of the angle of rotation (ψ_i) for plate B9 at an angle of incidence θ_i =43.5° is exhibited in Fig. 4.4. The measurements were taken at 35 GHz. The curves for TE and TM cases are essentially symmetrical about ψ_i=0, which is expected from the square symmetry of this crossed grating and will be found to be true basically for all plates investigated. Hence we will consider mainly the region $0 \le \psi_i \le 45°$ when we discuss the cases of oblique incidence for all plates. As shown in Fig. 4.4, in a broad range $-42° \le \psi_i \le 42°$,the reduction in TM polarized specular reflection is at least 7.3 dB, while the reduction in TE polarized specular reflection is less 1 dB. Thus the behavior of a polarizer is conserved over the full range of ψ_i except for a narrow range of about six degrees centered by ψ_i=45°. This exception is caused by the (-1,0) and (0,-1) Wood anomalies. By applying the method of Rayleigh wavelength equation discussed in Section 2.4, we can determine which diffracted order can exist and where it can exist in the full range of ψ_i. Fig. 4.5 shows schematically the results of calculation which is corresponding to Fig.

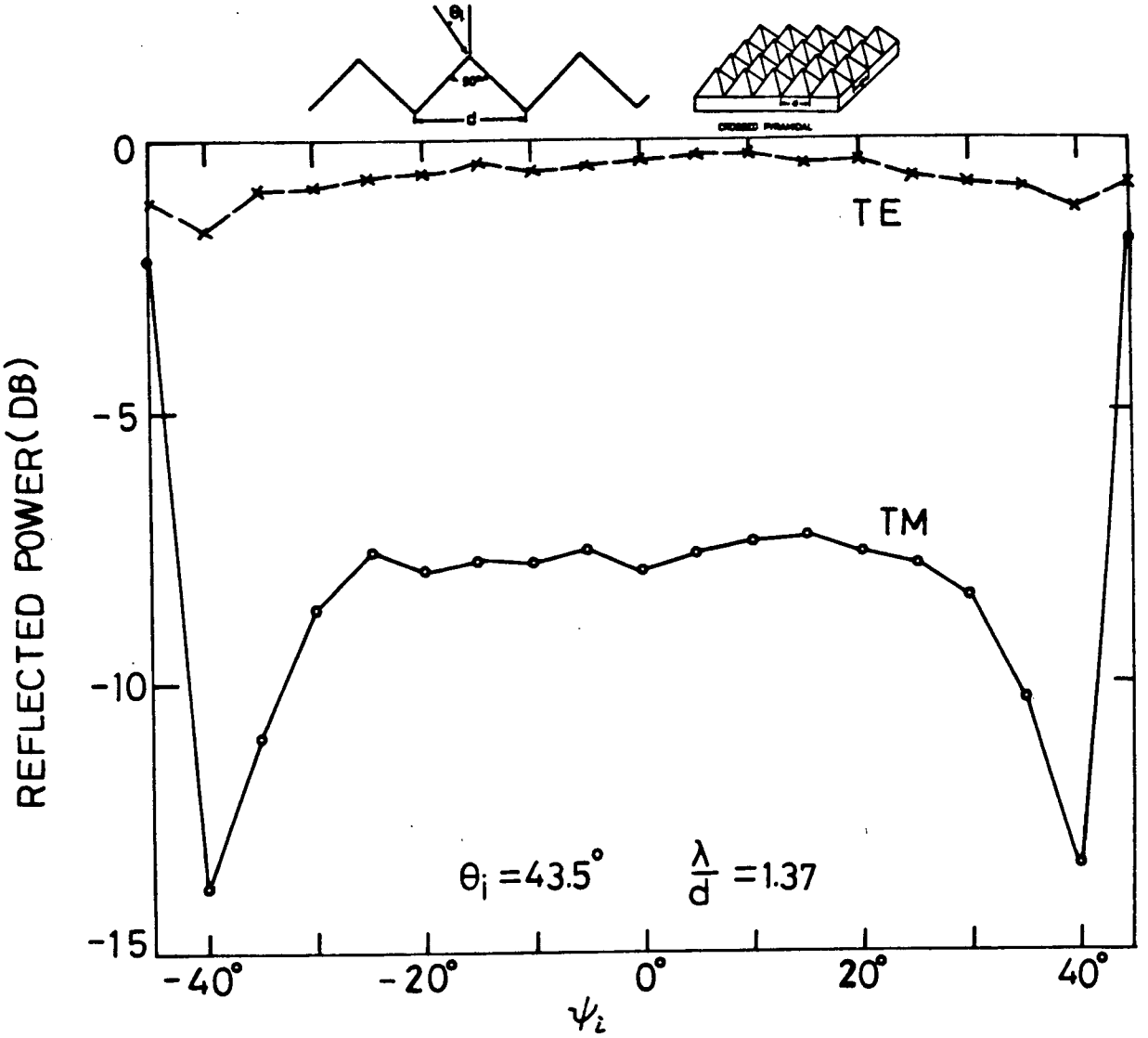

Fig. 4.4. Reflected power vs. angle of rotation for plate B9 at f=35 GHz, θ_i=43.5°

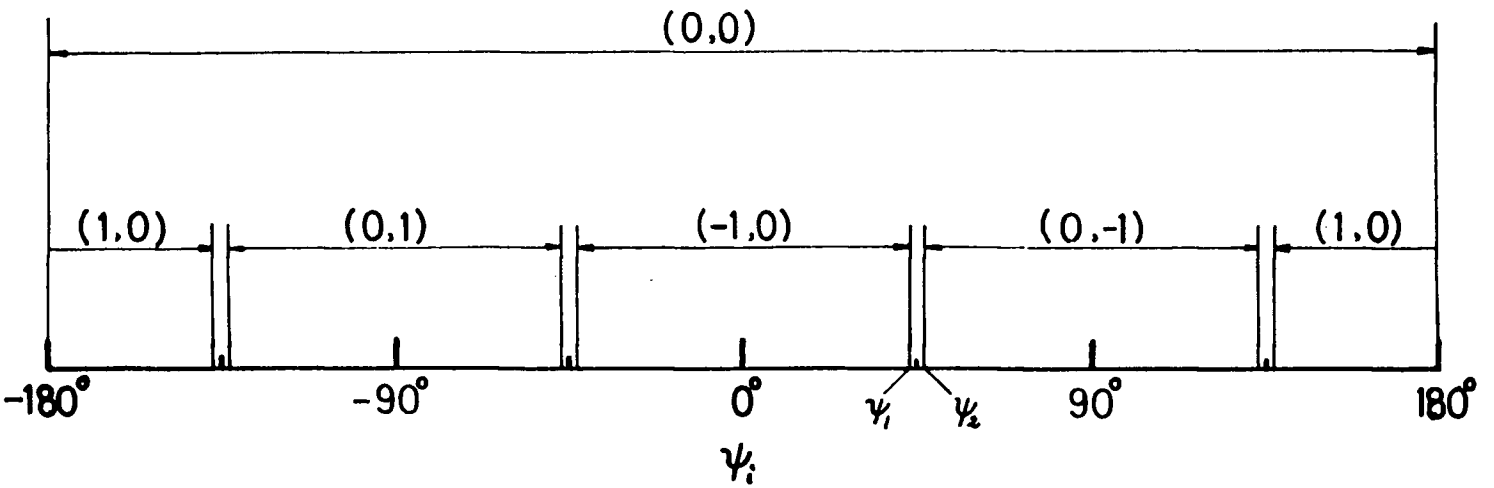

Fig. 4.5. Diagram of azimuthal angular regions in which spectral orders exist for a crossed grating at $\lambda/d=1.37$, $\theta_i=43.5°$

region boundaries: $\psi_1=43.9°$, $\psi_2=46.1°$

4.4 and can be applied to a crossed grating having any type of square-symmetrical profile with the incident conditions of $\lambda/d=1.37$ and $\theta_i=43.5°$. Since the pyramidal surface is square-symmetrical, the regions for the orders (-1,0),(0,-1),(0,1) and (1,0) have the same width and are symmetrical about 0°, 90°, -90° and 180° respectively, as indicated in Fig. 4.5. For $\theta_i=43.5°$ fixed, at any value of ψ_i, there is at most one more diffracted order which can exist besides the order (0,0). According to the calculation, the order (-1,0) ceases to propagate at $\psi_i=43.9°$ where the (-1,0) Wood anomaly occurs, and the order (0,-1) begins to propagate at $\psi_i=46.1°$ where the (0,-1) Wood anomaly exists. Thus there is only specular reflection in a very narrow azimuthal range of about two degrees around $\psi_i=45°$. This explains the abrupt rise of TM polarized power from 40° to 45° in Fig. 4.4: the energy in the order (-1,0) switches totally to the order (0,0). Ideally the relative reflected power at $\psi_i=45°$ should be one in this case. The experimental discrepancy is attributed to positioning the plate.

The measured frequency response curves of plate B9 at $\theta_i=43.5°$ under non-oblique incidence are shown in Fig. 4.6. The broad band nature of this polarizer-like plate is readily seen. Within the tuning range of the klystron, the reduction in TM polarized specular reflection remains about 8dB,or 84% of the TM-polarized incident power is scattered, while the TE-polarized incident wave is almost completely reflected.

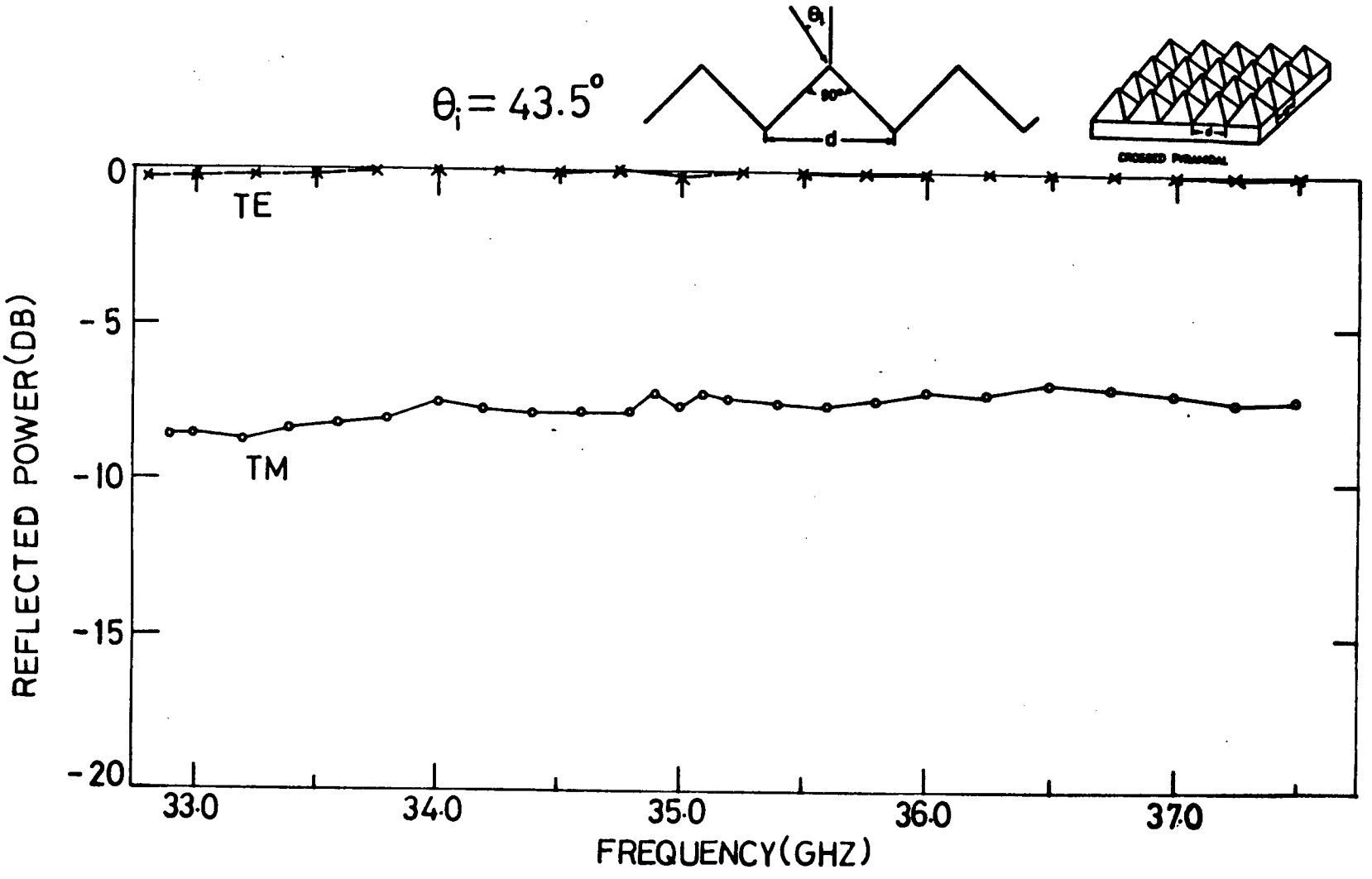

Fig. 4.6. Reflected power vs. frequency for plate B9 at θ_i=43.5°, ψ_i=0

4.3 PLATE C4 ---- A DEEPLY-GROOVED PLATE IN COMPARISON WITH ITS SINGLY-PERIODIC EQUIVALENT

It is interesting to investigate experimentally deeper groove surfaces which cannot be handled theoretically at present while seem most likely to be effective in some applications [20]. It had been reported that essentially perfect blazing to the n=-1 spectral order for arbitrary polarization should occur for symmetrical triangular groove reflection gratings when the apex angle is 44° and the angle of incidence is θ_i=38.1° [4,9]. Such a surface was first milled in making its doubly-periodic equivalent plate C4. The experimental values in Fig. 4.7, which were obtained from this classical grating at f=35 GHz, show that although essentially perfect blazing occurs for TM polarization at the Bragg angle θ_i=38° where ϵ_0=0.00003 or the reduction is 45 dB, the result for TE polarization (ϵ_0=0.039 or the reduction is 14 dB) is less satisfied. Fig. 4.8 shows the measured frequency response of this grating at θ_i=38° under non-oblique incidence. The intersection of the TM and TE curves proves the same effect for arbitrary polarization, and the corresponding frequency is 33.75 GHz where the reduction is about 23 dB, or the diffraction efficiency to the n=-1 order for both polarizations is about 99.5%. The angular response of this triangular grating at the new frequency 33.75 GHz in Fig. 4.9 shows that at the new Bragg angle θ_i=40°, near-perfect dual blazing is achieved, a good improvement over that obtained at f=35 GHz. Numerical

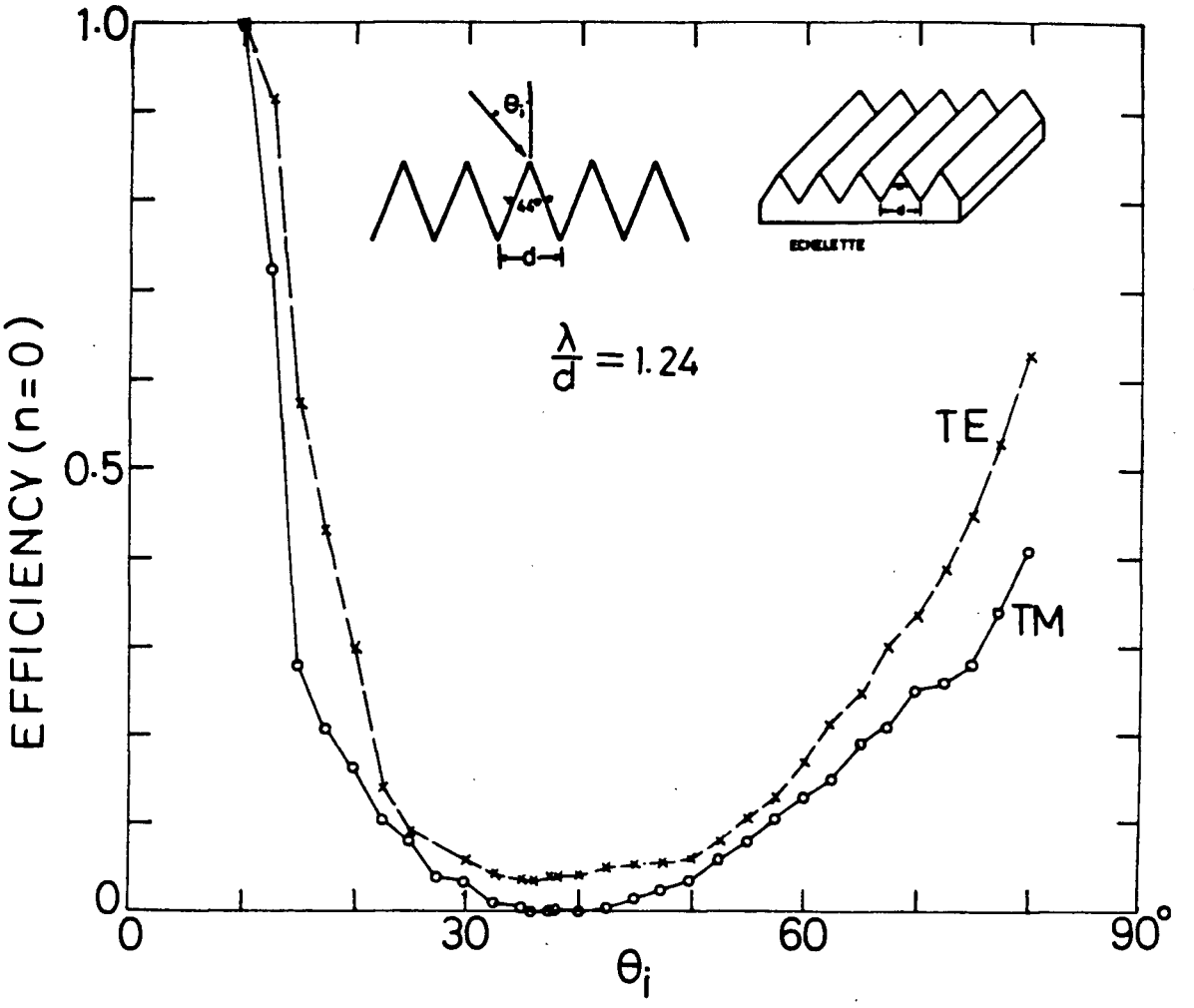

Fig. 4.7. Relative reflected power (or ϵ_0) vs. angle of incidence for the singly periodic equivalent of plate C4 at f=35 GHz, ψ_i=0

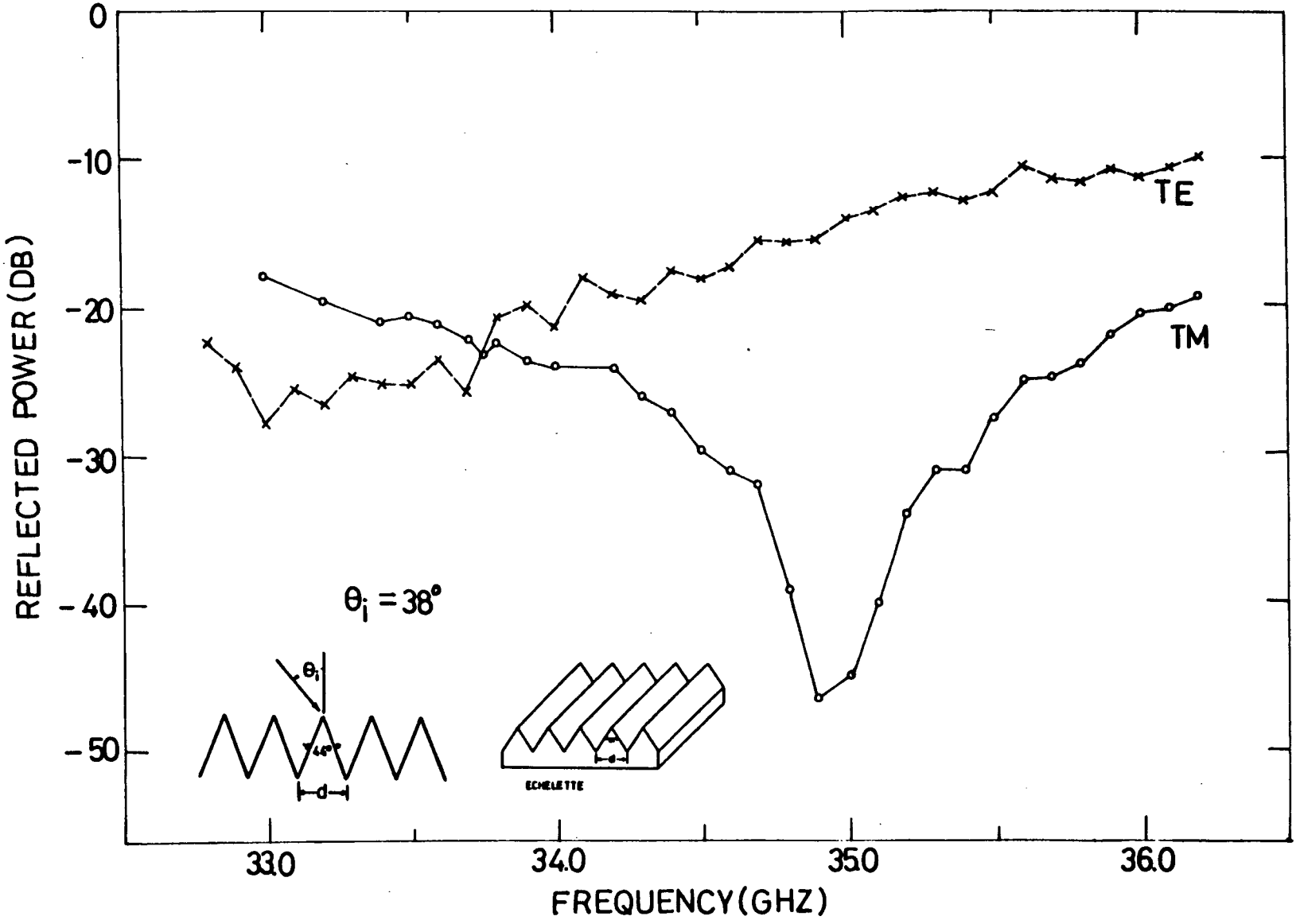

Fig. 4.8. Reflected power vs. frequency for the singly periodic equivalent of plate C4 at θ_i=38°, ψ_i=0

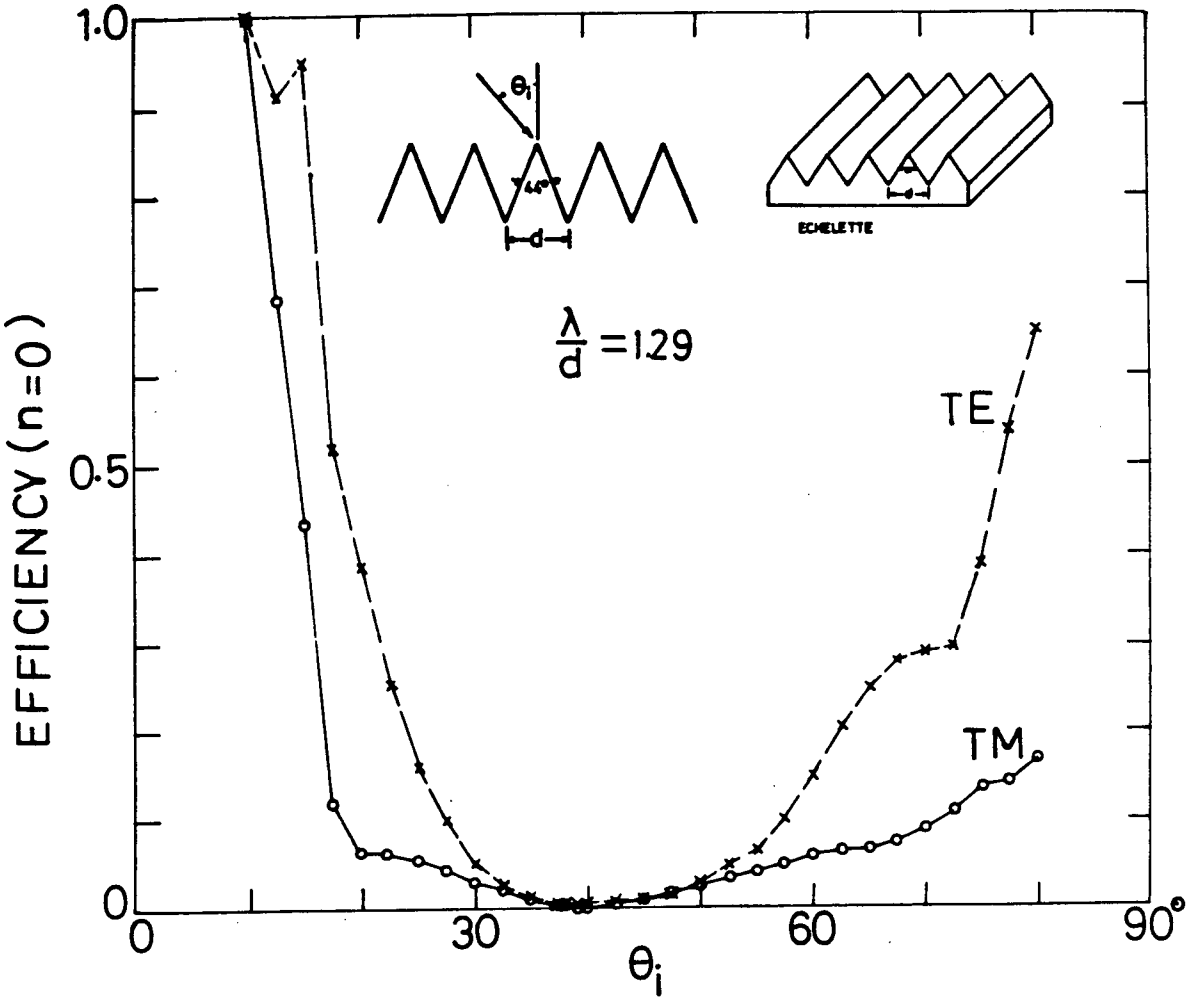

Fig. 4.9. Relative reflected power (or ϵ_0) vs. angle of incidence for the singly periodic equivalent of plate C4 at f=33.75 GHz, ψ_i=0

results from Facq's program agree with these experimental results (see Appendix).

Fig. 4.10 shows the measured relative reflected power as a function of the incident angle for the corresponding pyramidal grating plate C4. Both TM and TE polarized reflections near the Bragg angle θ_i=40° are only halved by the crossed grating. Apparently, the reflection free properties of the singly-periodic surface are lost for its doubly-periodic equivalent . Therefore, we can conclude from this example of plate C4 that the product formula (2.31) linking shallow crossed and classical gratings cannot in general be applied to deeper gratings under non-normal incidence.

In Fig. 4.10, the (-1,0) Wood anomaly occurred around $\theta_i=\sin^{-1}(\lambda/d-1)$=17° is evident only as a change in the gradient of the TE and TM curves, while for the classical grating, Fig. 4.9 shows the corresponding n=-1 Wood anomaly around the same incident angle as being an abrupt energy transfer from the specular reflection to the n=-1 order.

The measured angular response at f=35 GHz is represented in Fig. 4.11, along with the response at f=33.75 GHz which is the same as that in Fig. 4.10 except that now it is plotted in terms of dB for easy comparison. At both frequencies, the behavior for TM polarization is similar to that for TE case, and no maximum reduction is observed around the Bragg angle. The experimental frequency response at θ_i=38° shown in Fig. 4.12 confirms further the

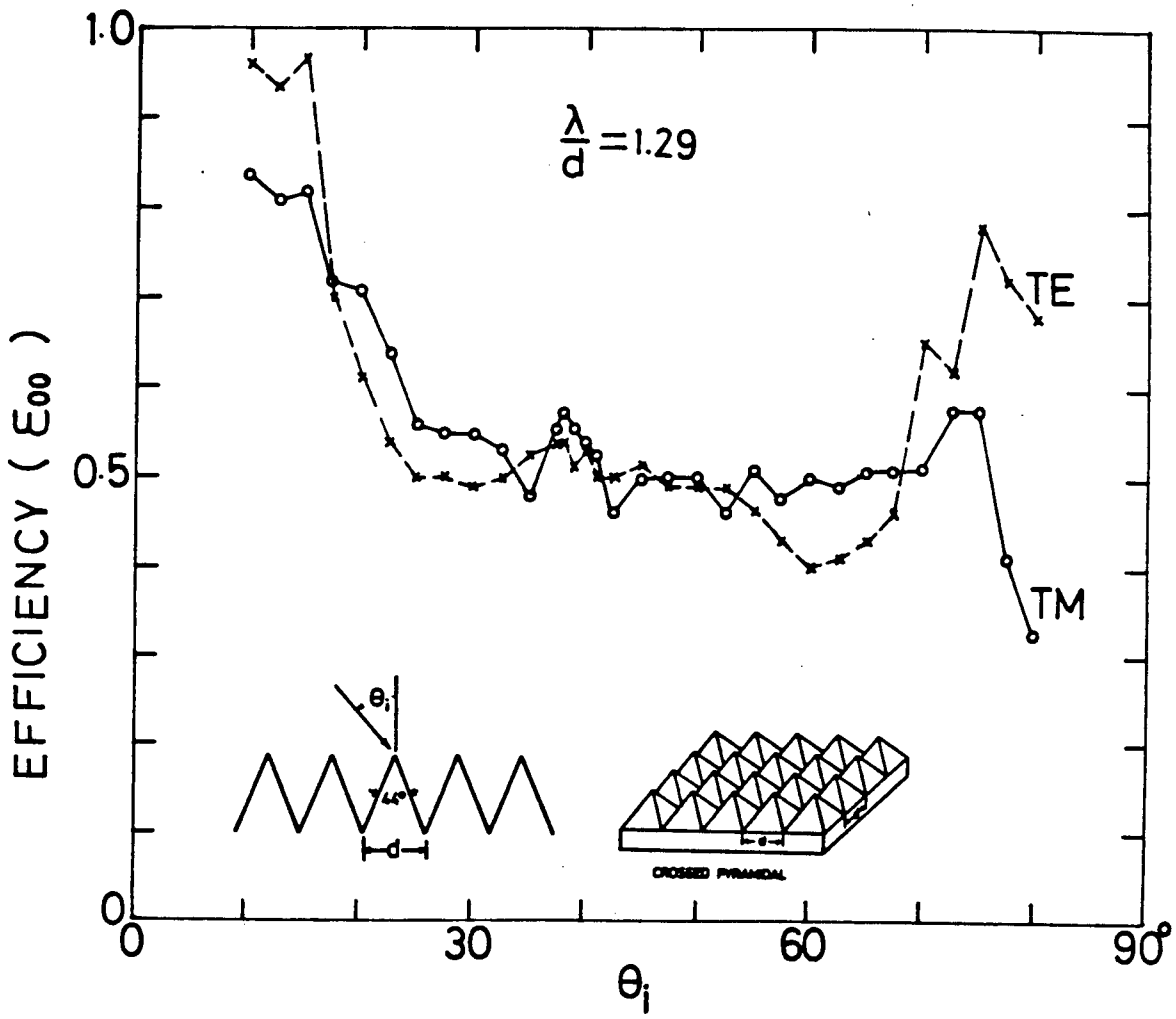

Fig. 4.10. Relative reflected power (or ϵ_{00}) vs. angle of incidence for plate C4 at f=33.75 GHz, ψ_i=0

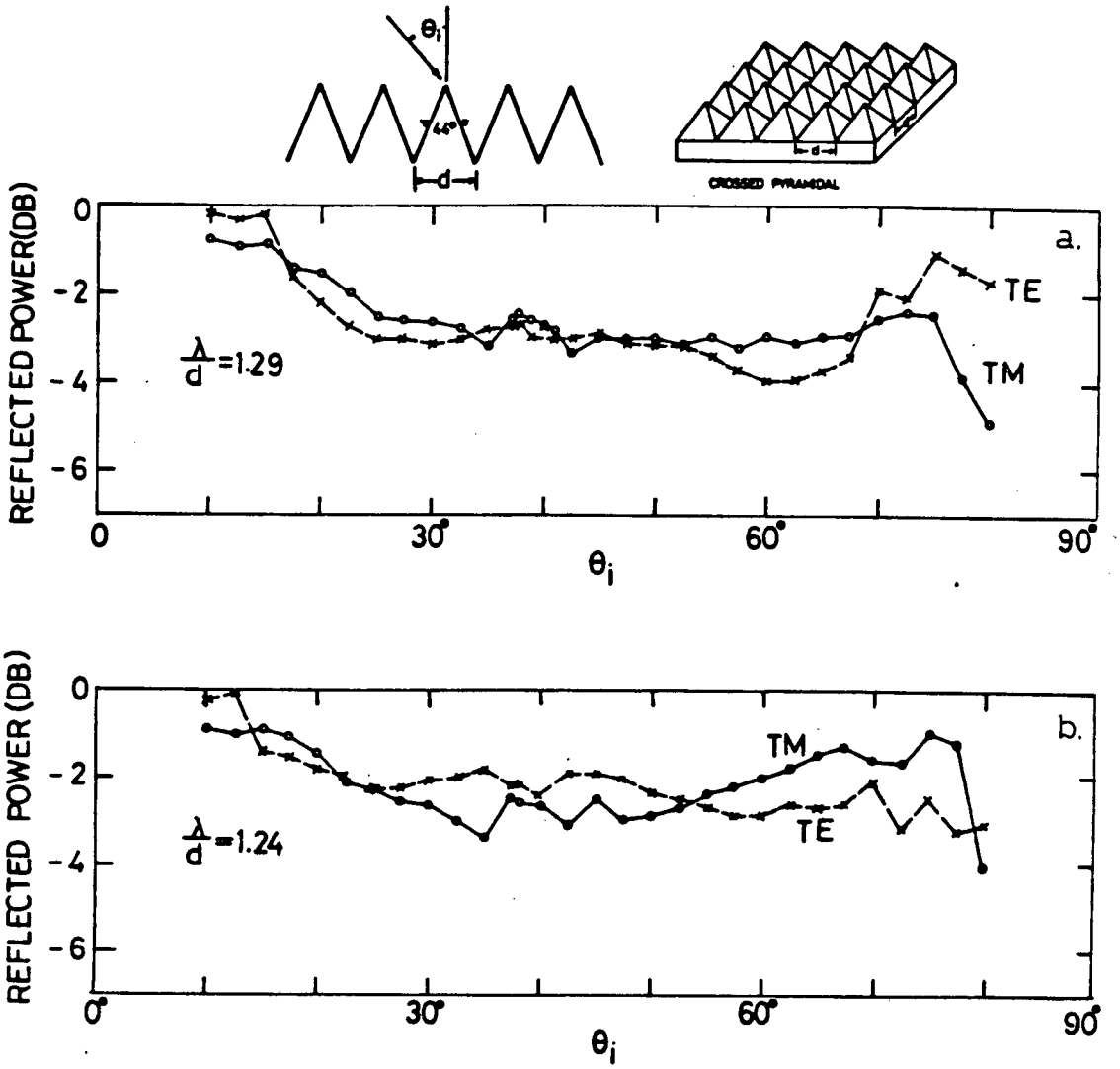

Fig. 4.11. Reflected power vs. angle of incidence for plate C4: a. at f=33.75 GHz
b. at f=35 GHz

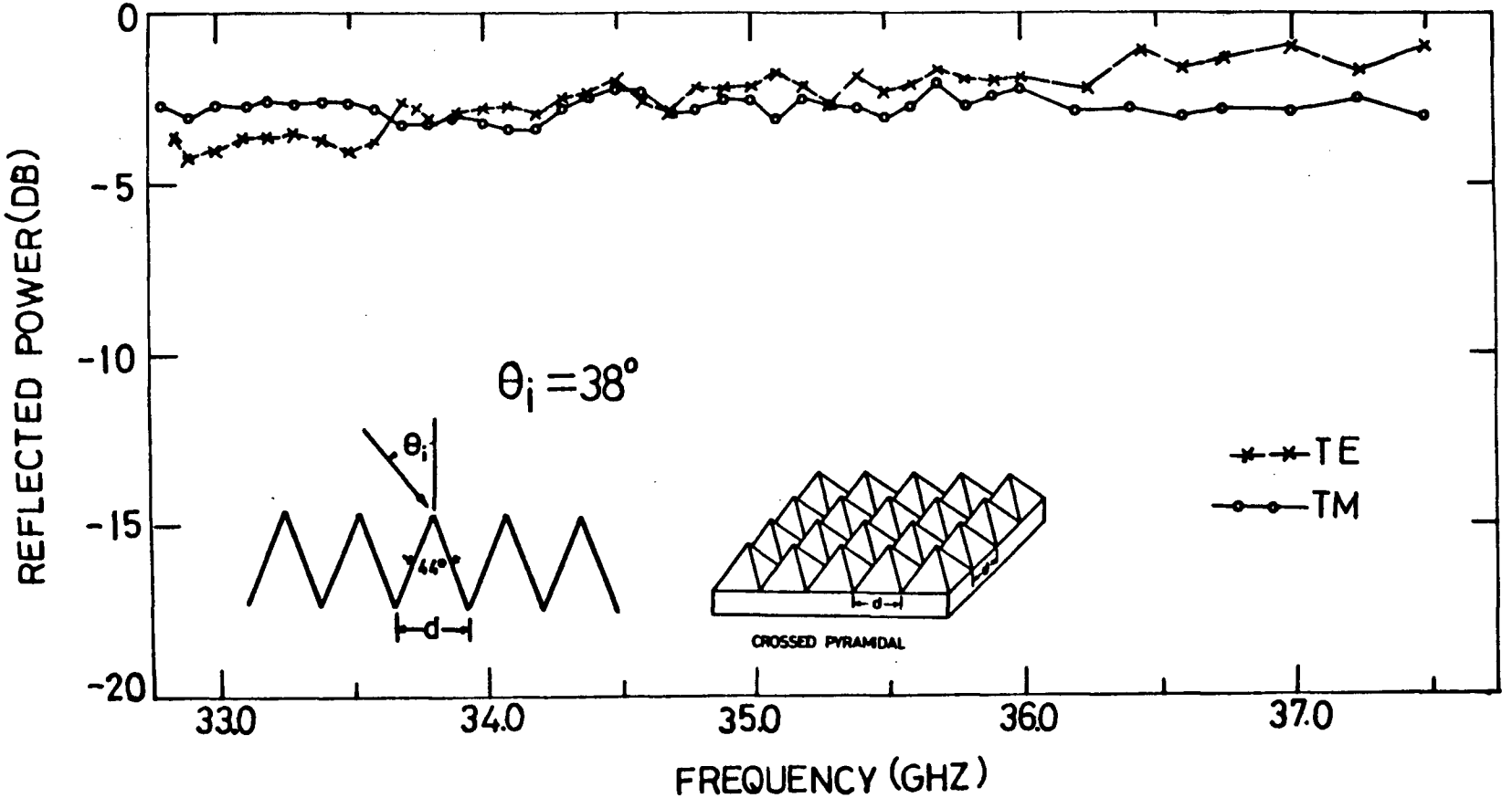

Fig. 4.12. Reflected power vs. frequency for plate C4 at θ_i=38°, ψ_i=0

insensitivity of this crossed grating to frequency changes around 35 GHz. Increasing or decreasing by 2 GHz from 35 GHz does not affect the diffraction efficiency of plate C4 very much and the reduction of reflected power is always below 5 dB.

Fig. 4.13 shows the measured reflected power as a function of rotation angle ψ_i for plate C4 at f=35 GHz and θ_i=38°. Again, the curves are basically symmetrical about ψ_i=0°. Although the diffraction efficiency of the grating is insensitive to polarization under non-oblique incidence, the effect of polarization become apparent in a remarkably rapid manner as the plate is rotated apart from the ψ_i=0° position. For TM polarization, the reduction gets larger and reaches its maximum 13 dB at about ψ_i=35°, while the reduction in TE polarized specular reflection remains under 2 dB. The calculated region diagram for all spectral orders diffracted by plate C4 with λ/d=1.24 and θ_i=38° is shown in Fig. 4.14. We can see that only two spectral orders (0,0) and (-1,0) exist between ψ_i=-37° and ψ_i=37°, and hence from Fig. 4.13, 95% of the incident energy is diffracted into the order (-1,0) at θ_i=35°, the direction of which can be determined by (2.13) and (2.14). The results of calculation in Fig. 4.14 predict that the regions of orders (-1,0) and (0,-1) are overlapped around ψ_i=45° and the (0,-1) Wood anomaly should occur at ψ_i=37° where the (0,-1) order starts to propagate. This Wood anomaly causes a re-distribution of incident power among three orders (0,0), (-1,0) and (0,-1)

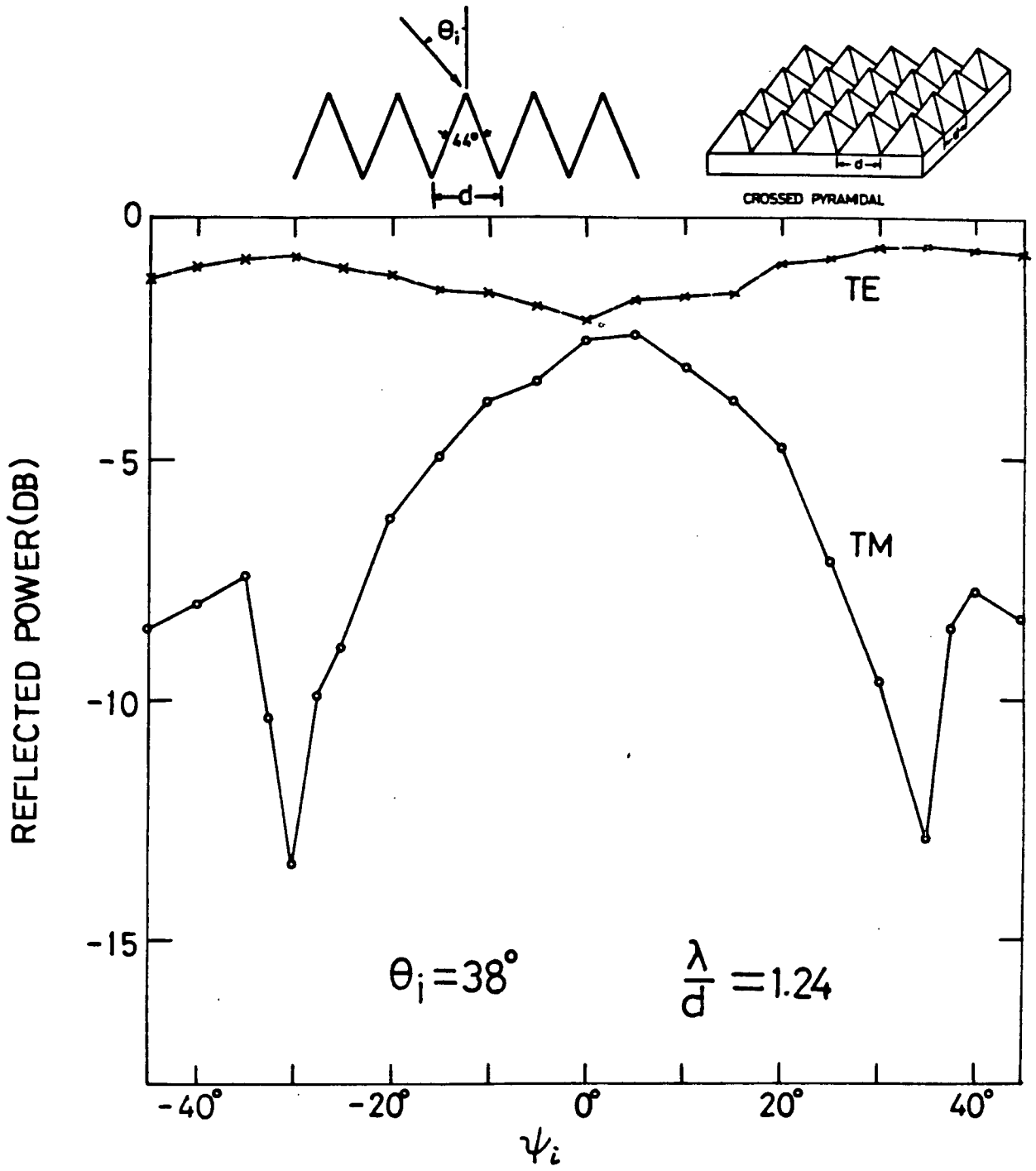

Fig. 4.13. Reflected power vs. angle of rotation for plate C4 at f=35 GHz, θ_i=38°

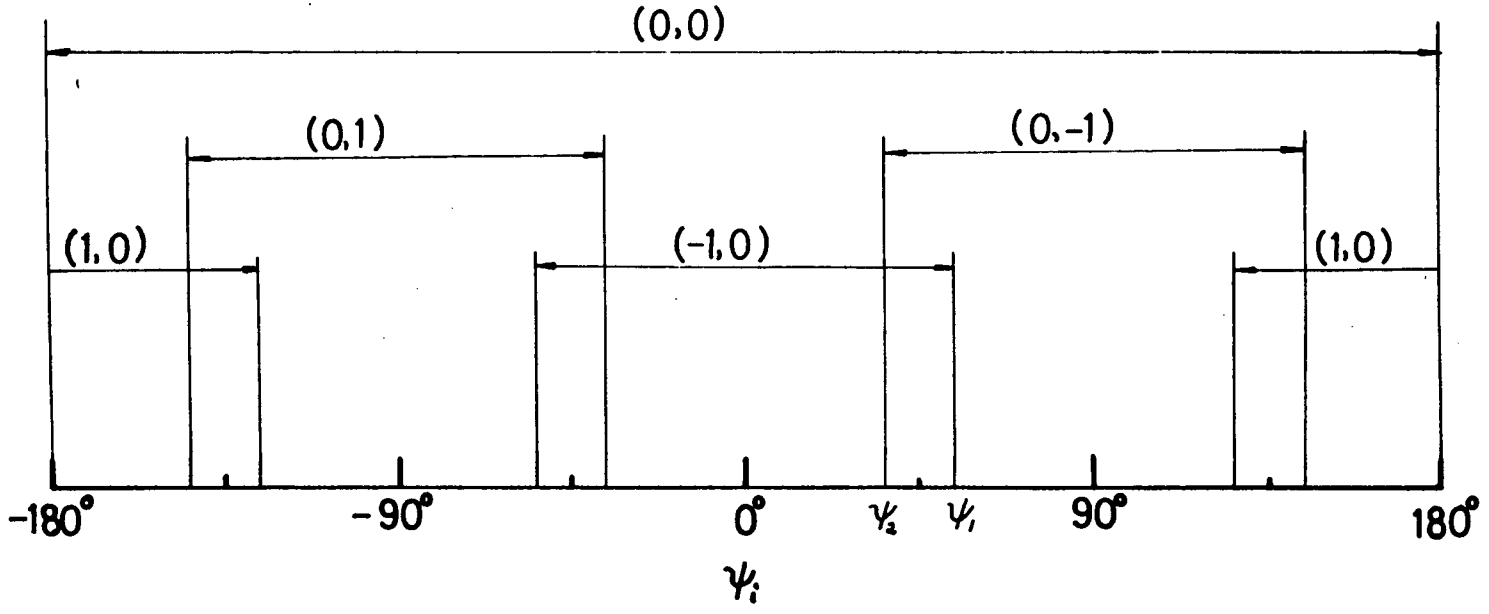

Fig. 4.14. Diagram of azimuthal angular regions in which spectral orders exist for a crossed grating at $\lambda/d=1.24$, $\theta_i=38°$

region boundaries: $\psi_1=53°$, $\psi_2=37°$

when ψ_i>37°. This explains the rise of the experimental TM curve from 35° to 40°.

4.4 PLATE A4 ---- AN ESSENTIALLY PERFECT BLAZED CROSSED GRATING SURFACE FOR TM POLARIZATION

Plate A4 is also a deeply-grooved surface with the period d=8 mm and the apex angle α=45°. Fig. 4.15 shows experimental values of the reduction in specular reflection by the singly-periodic equivalent of plate A4, with 30 triangular grooves at f=35 GHz. The maximum reduction 16.1 dB for TM polarization occurs almost exactly at the Bragg angle $\theta_i=\sin^{-1}(\lambda/(2d))=32.4°$, where the diffraction efficiency (ϵ_{-1}) of this classical grating is 97.5%, whereas for TE polarization there is no maximum reduction observed at the Bragg angle.

The behavior of the corresponding crossed grating plate A4 at the same frequency of 35 GHz is exhibited in Fig. 4.16a. The Bragg angle effect for TM case now becomes not evident and the reduction in the specular reflection for both TM and TE polarizations is always below 4 dB. The experimental results of plate A4 measured at f=33 GHz is shown in Fig. 4.16b, which shows a decrease by about 6% in frequency does not change the behavior of this surface very much.

Measured frequency variation of TE and TM polarized reflection from plate C4 at θ_i=46° under non-oblique incidence is shown in Fig. 4.17. For TE polarization, the

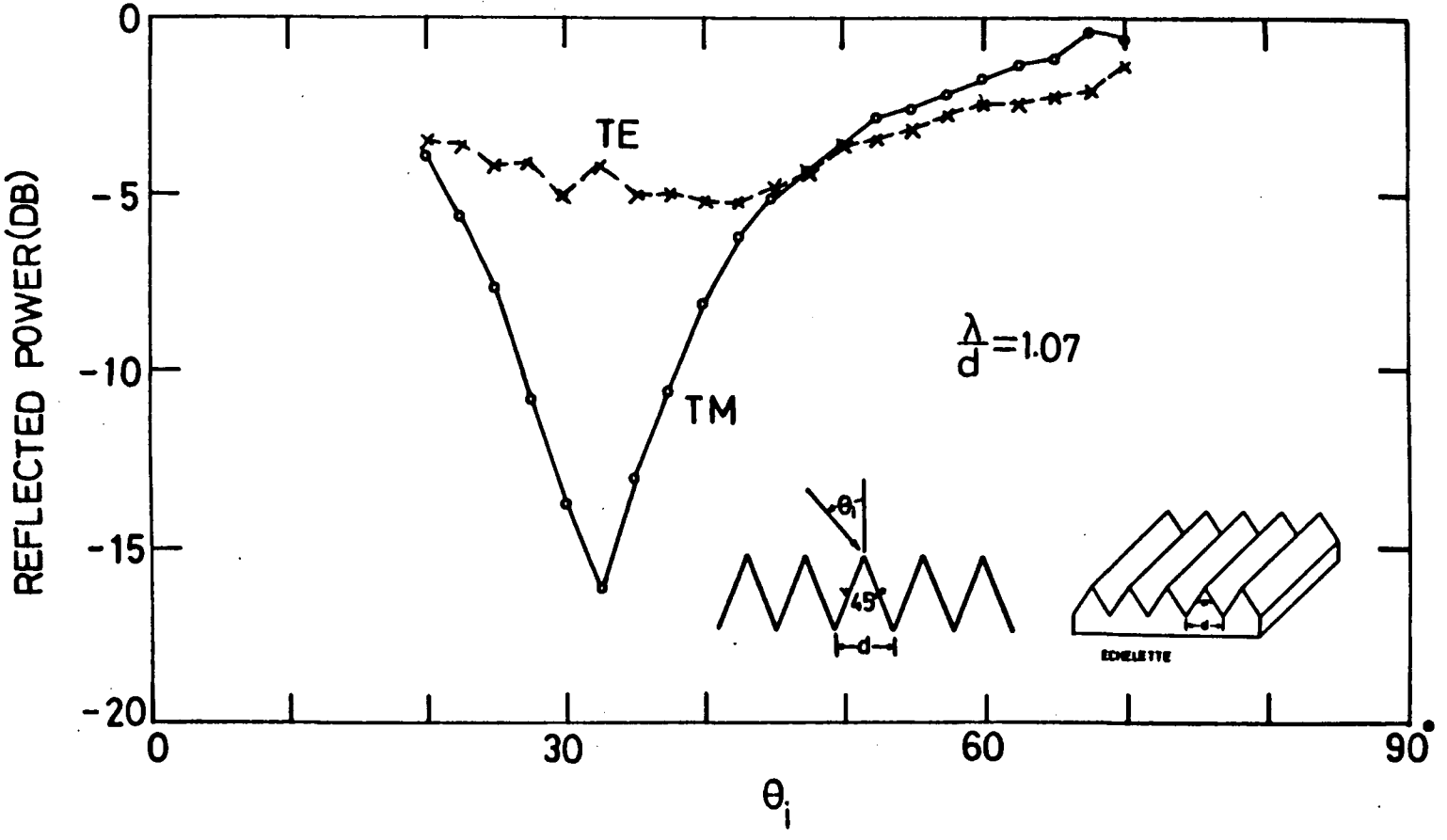

Fig. 4.15. Relative reflected power (or ϵ_0) vs. angle of incidence for the singly periodic equivalent of plate A4 at f=35 GHz, ψ_i=0

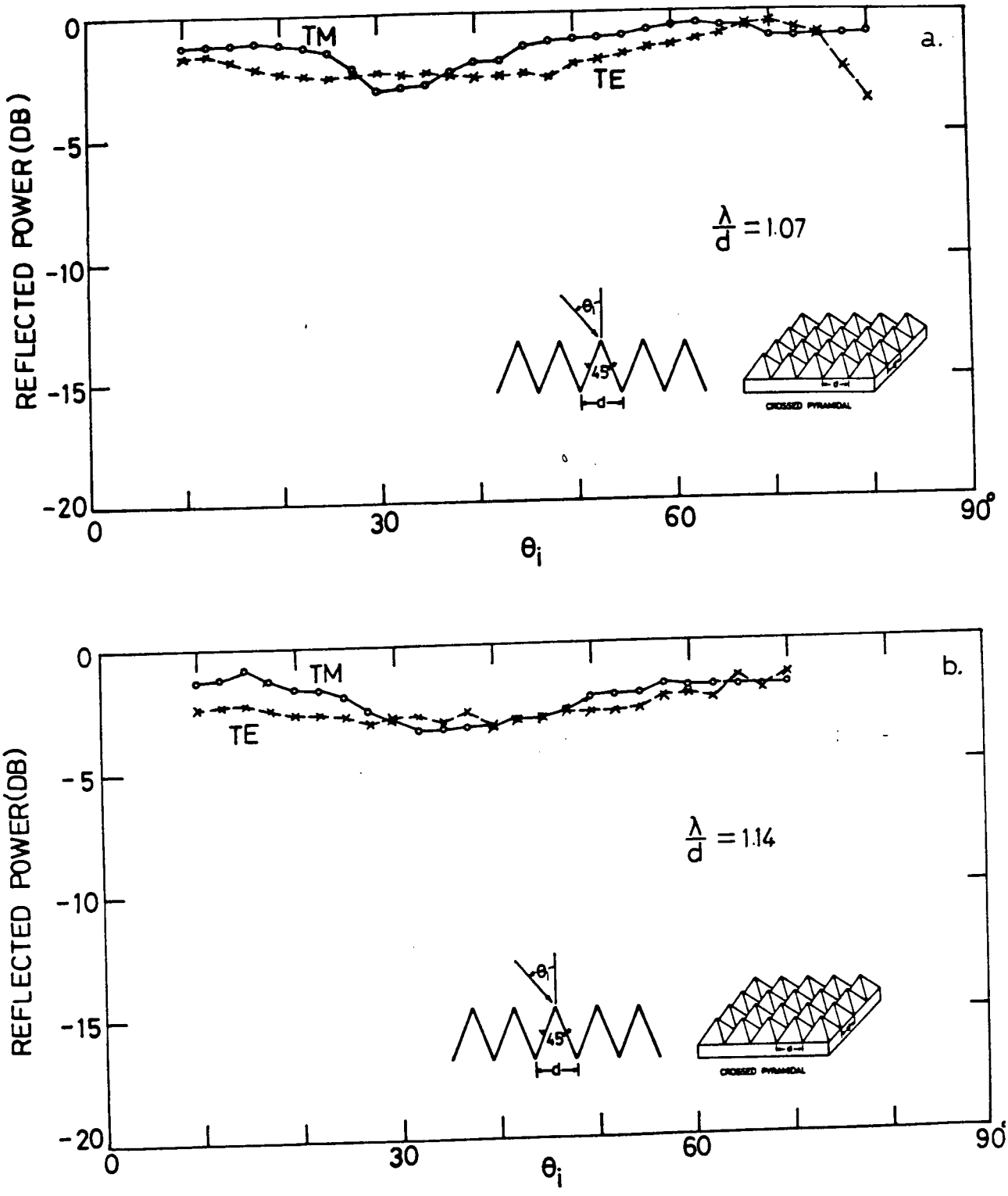

Fig. 4.16. Reflected power vs. angle of incidence for plate A4 at: a. f=35 GHz, $\psi_i=0$
b. f=33 GHz, $\psi_i=0$

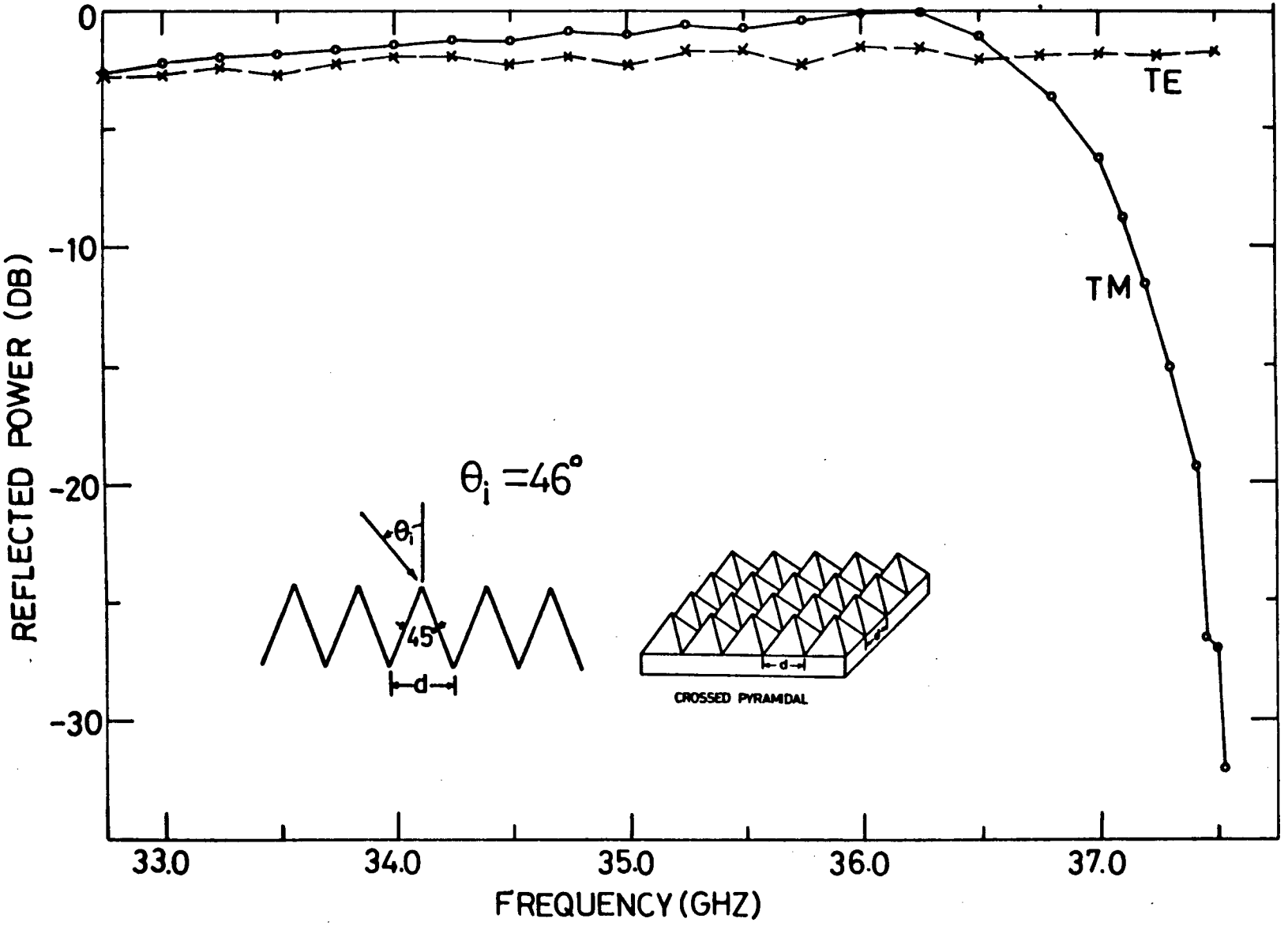

Fig. 4.17. Reflected power vs. frequency for plate A4 at θ_i=46°, ψ_i=0

reduction is below 3 dB and the curve is quite flat within the full frequency range. The reduction for TM polarization from f=32.75 GHz to f=36.5 GHz is a little less than that for TE polarization. However, when the frequency becomes larger than 36.5 GHz, TM curve descends steeply and the reduction reaches as large as 32 dB at f=37.52 GHz which is the highest attainable frequency of the klystron. Here, for TM polarization, a increase by about 3% in frequency completely changes the properties of this crossed grating from reflecting specularly 100% of the incident power at f=36.25 GHz to diffracting essentially totall (99.94%) of the incident power into the (-1,0) order at f=37.52 GHz. This is the best result that we got from all plates investigated, as far as total cancellation of specular reflection is concerned. Therefore, we demonstrated experimentally near perfect blazing of the pyramidal crossed grating for TM polarization.

Fig. 4.18 shows the measured relative reflected power as a function of θ_i under non-oblique incidence at f=37.5 GHz. Very interesting behavior of plate A4 is observed when the incident wavelength is equal to the period. There are two remarkable reduction peaks for TM polarization. The larger one occurs at θ_i=46° where the reduction is 27 dB, or 99.8% of the incident power is diffracted to the order (-1,0), the direction of which can be found as $\theta_{-1,0}$ =16.3° and $\psi_{-1,0}$=180° by using (2.13) and (2.14). Over a narrow angular range of about 3°, the reduction is greater than 20

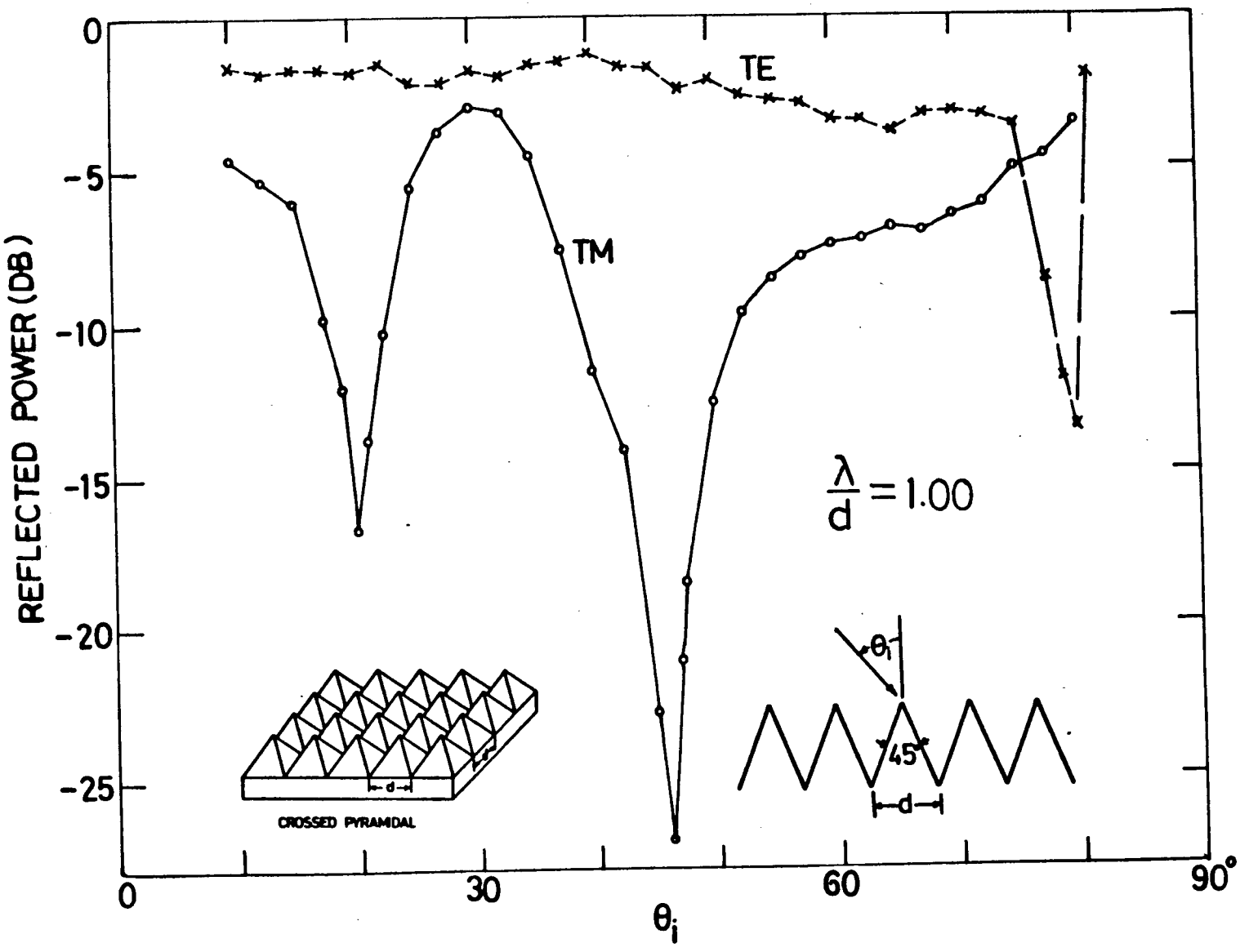

Fig. 4.18. Reflected power vs. angle of incidence for plate A4 at f=37.5 GHz, $\psi_i=0$

dB or 99%, and the specular reflection is essentially eliminated. The smaller peak is at θ_i=20° where the reduction for TM polarization is 16.7 dB. It is surprising that at the Bragg angle $\theta_i=\sin^{-1}(\lambda/(2d))$=30°, a local minimum reduction is observed, instead of a maximum reduction of specular reduction. This behavior is quite different from that of classical gratings. The reduction in TE polarized specular reflection is much less than that for TM polarization and is below 4 dB, except for a peak at θ_i=80° where the reduction is 13.1 dB or 95.1%.

Holding the frequency at 37.5 GHz and the incident angle at 46° where maximum reduction for TM polarization occurs under non-oblique incidence, we recorded reflected power as a function of angle of rotation by rotating plate A4 horizontally (see Fig. 4.19). Both TM and TE curves look somewhat complicated in this case where the ratio of wavelength over period is one. For TM polarization, the plate could be rotated up to about three degrees in both directions and still give about 20 dB or 99% reduction. Within this narrow azimuthal angular range, the surface is blazed to the spectral order (-1,0). Fig. 4.20 shows the corresponding diagram of azimuthal angular regions where spectral orders exist, which is the results of calculation by applying Rayleigh wavelength equation. Theory predicts that the (-1,-1) Wood anomaly occurs at ψ_i=3.2° where the diffracted order (-1,-1) begins to propagate. This prediction corresponds to the sudden rise of the

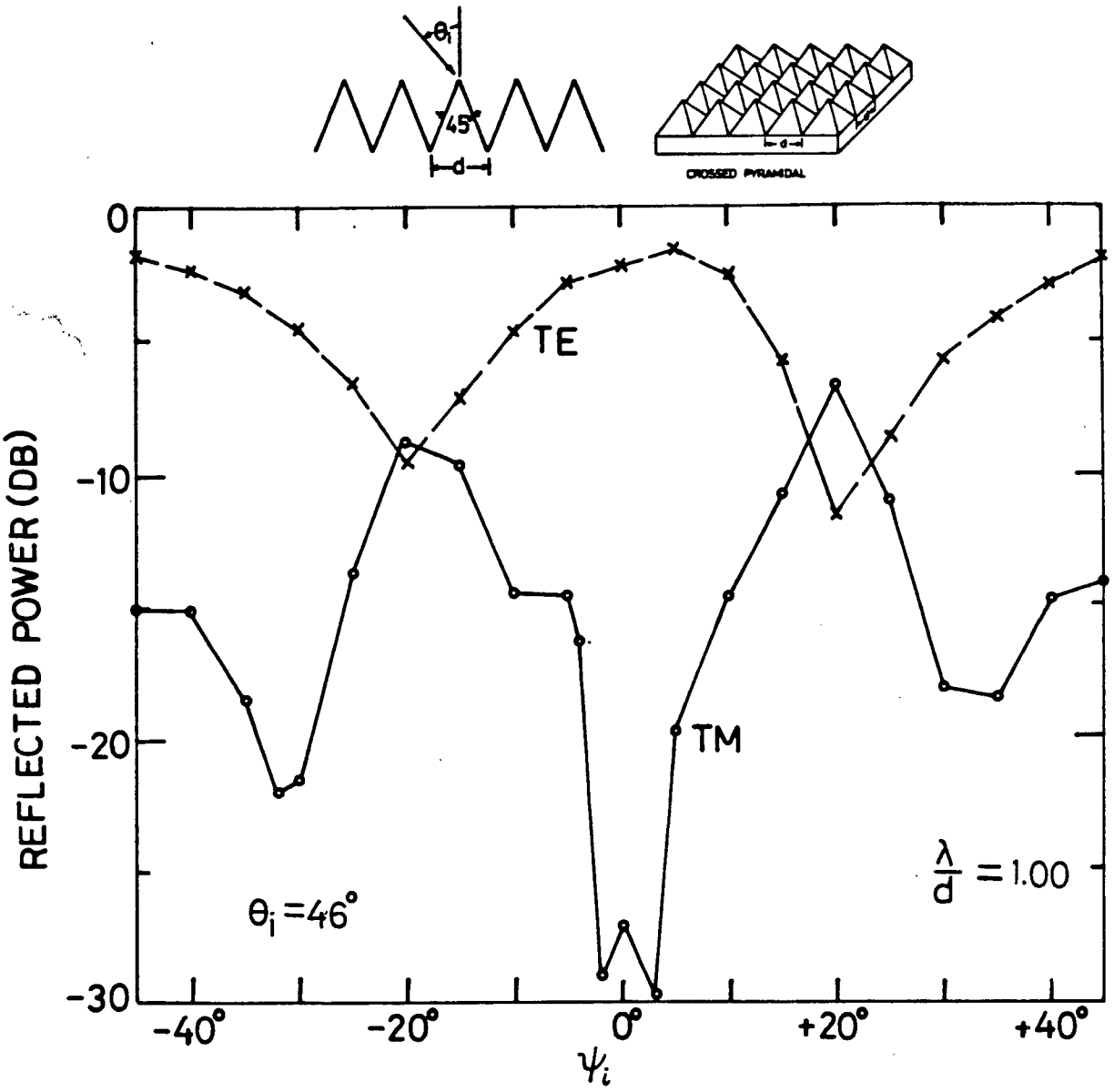

Fig. 4.19. Reflected power vs. angle of rotation for plate A4 at f=37.5 GHz, θ_i=46°

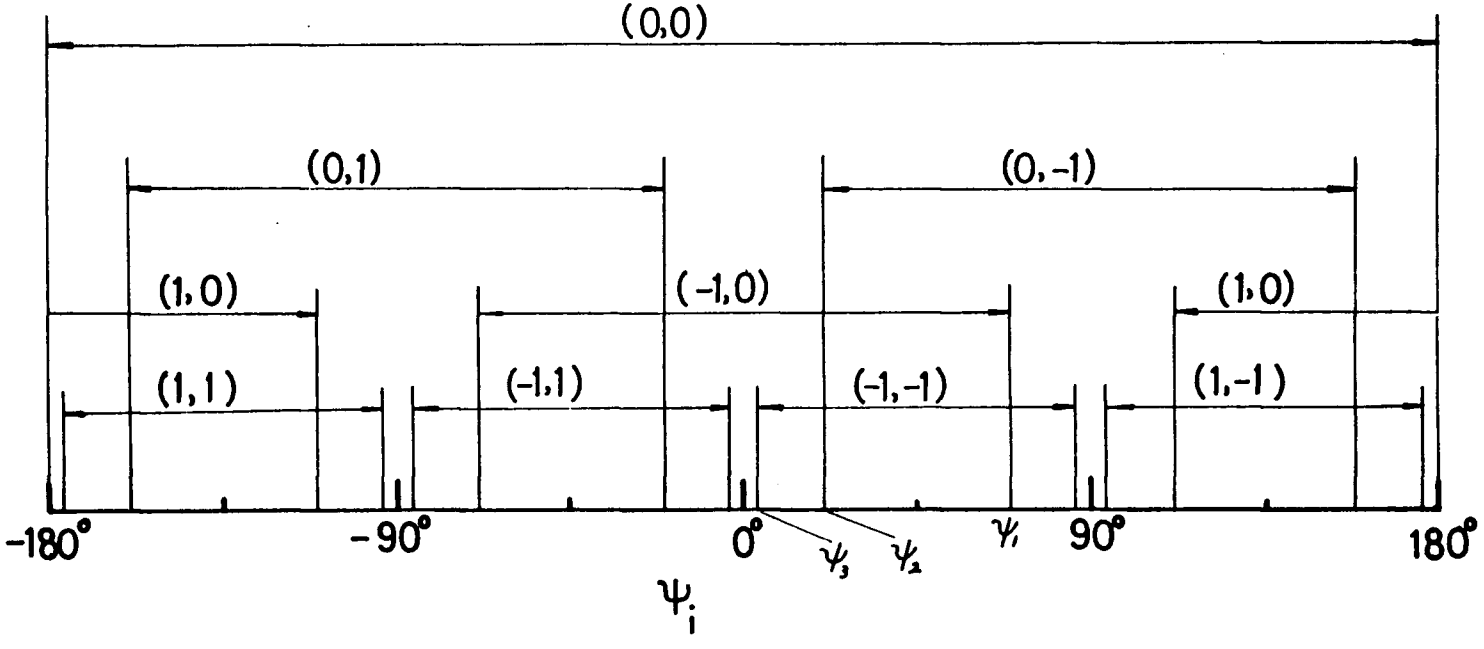

Fig. 4.20. Diagram of azimuthal angular regions in which spectral orders exist for a crossed grating at $\lambda/d=1.00$, $\theta_i=46°$

region boundaries: $\psi_1=68.9$, $\psi_2=21.1°$, $\psi_3=3.2°$

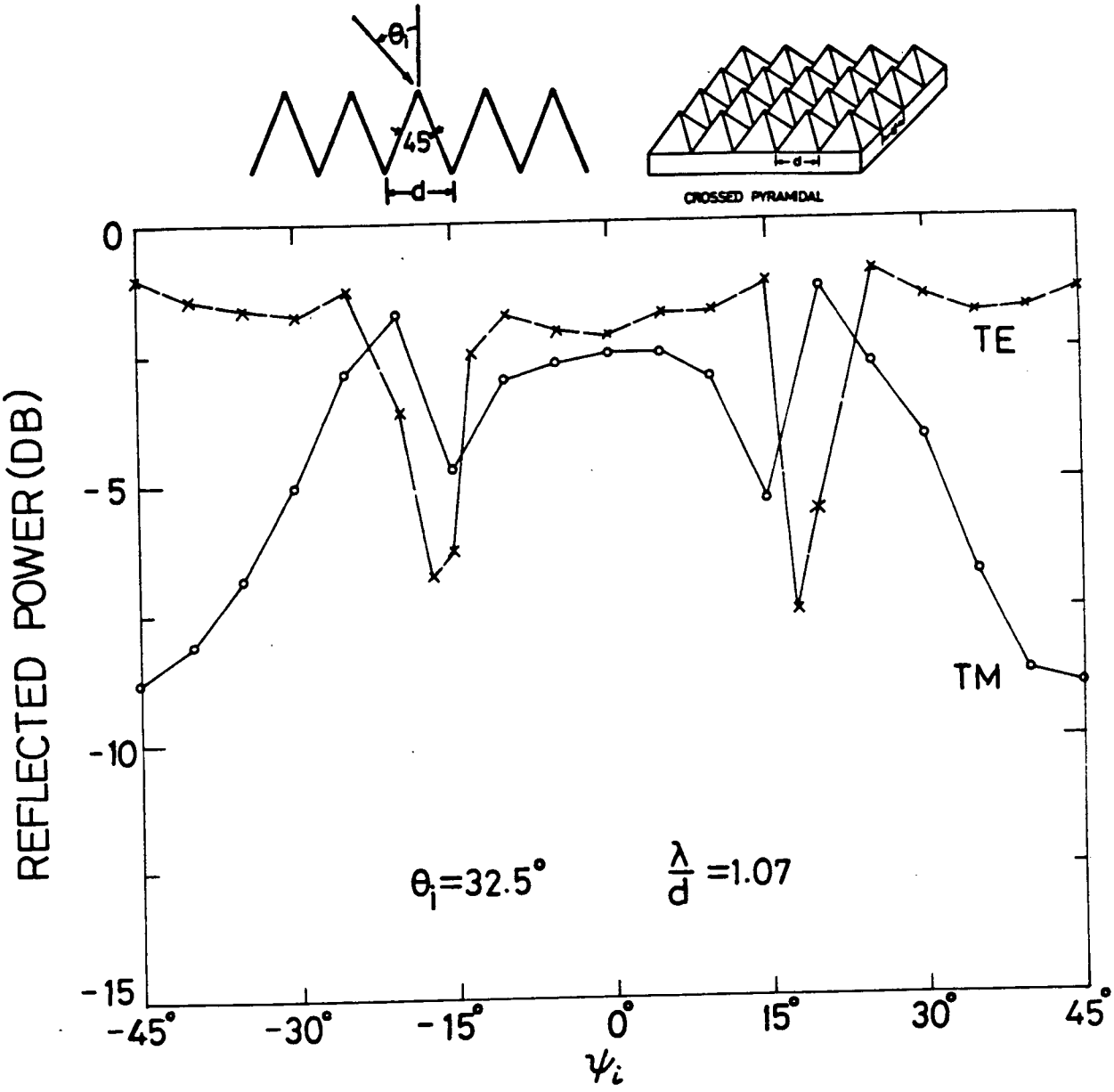

Fig. 4.21. Reflected power vs. angle of rotation for plate A4 at f=35 GHz, θ_i=32.5°

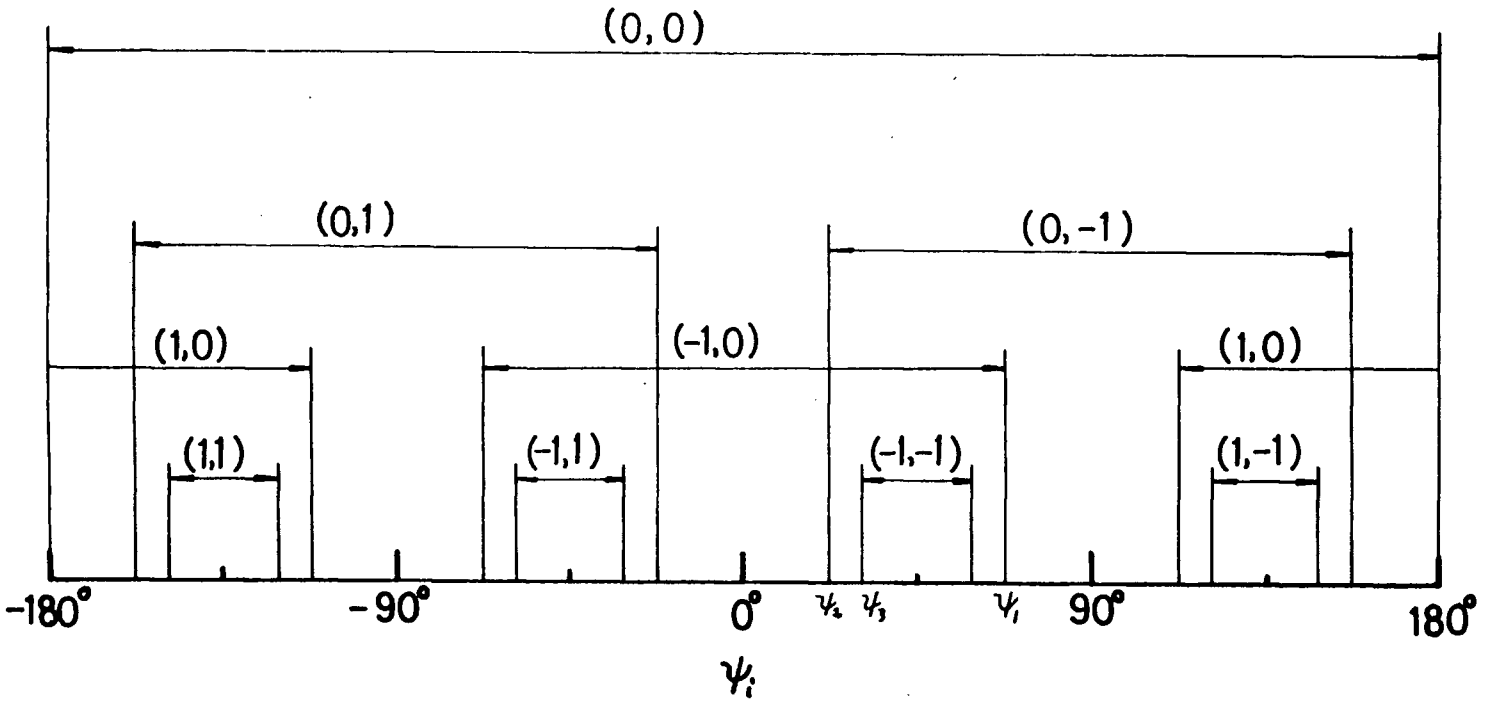

Fig. 4.22. Diagram of azimuthal angular regions in which spectral orders exist for a crossed grating at $\lambda/d=1.07$, $\theta_i=32.5°$

region boundaries: $\psi_1=67.8°$, $\psi_2=22.2°$, $\psi_3=31.5°$

experimental TM curve at about ψ_i=3° in Fig. 4.19, where the appearance of the spectral order (-1,-1) causes a re-distribution of incident power among the three existing orders (0,0),(-1,0) and (-1,-1). Similarly, we attribute the small peak of the experimental TM curve and the dip of the experimental TE curve, both at ψ_i=20°, to the (0,-1) Wood anomaly at ψ_i=21.1° indicated in Fig. 4.20, where a fourth diffracted order appears. In this case, the agreement between theory and experiment is very good for both TM and TE polarizations. There exist four spectral orders around ψ_i=45°, instead of only two orders at ψ_i=0°.

The azimuthal angular response of plate A4 at f=35 GHz and θ_i=32.5° is presented in Fig. 4.21. The general shape of the TE curve is somewhat similar to that at f=37.5 GHz and θ_i=46° shown in Fig. 4.19, while for TM polarization, the reduction in specular reflection becomes much less. The downward peak of TE curve at ψ_i=18° and the upward peak of TM curve at ψ_i=20° are caused by the (0,-1) Wood anomaly which should occur at ψ_i=22.2° according to the results of calculation shown in Fig. 4.22. The experimental discrepancy is due to locating the plate. The effect of the (-1,-1) Wood anomaly which should exist at ψ_i=31.5° is not so evident in the observed curves.

4.5 PLATE A9 ---- INFLUENCE OF THE RATIO λ/d

Plate A9 has the same apex angle of 90° as that of plate B9, but with a different period. Therefore, we group together in Fig. 4.23 and Fig. 4.24 four cases of the experimental results obtained from these two plates in order to investigate the effect of the ratio λ/d on the behavior of crossed gratings. The reflected power curves as a function of incident angle for plate A9, measured at frequencies 37.5 GHz (λ/d=1.00), 35 GHz (λ/d=1.07) and 33 GHz (λ/d=1.14), are presented in Fig. 4.23a, Fig. 4.23b and Fig. 4.24a respectively. The curves at λ/d=1.37 in Fig. 4.24b are for plate B9 and are the same as those in Fig. 4.3b, except that the reduction is expressed in terms of dB here for easy comparison. From these four pairs of curves we can see that the value of the ratio λ/d affects the diffraction efficiency greatly. The behavior of the grating with λ/d=1.00 (see Fig. 4.23a) looks quite different from those with other values of λ/d. At λ/d=1.00, the reduction in specular reflection for both polarizations fluctuates very much as the angle of incidence varies, and the reduction in TE polarized specular reflection is the largest among these four cases and reaches its maximum 13.8 dB at θ_i=8.5°, where 96% of incident energy is scattered to the spectral order (-1,0), noticing that only two spectral orders (0,0) and (-1,0) exist in the full range of θ_i since order (-1,0) is cut off at $\theta_i=\sin^{-1}(\lambda/d-1)=0°$. The maximum reduction for TM polarization occurs at θ_i=32.5° which is close to the Bragg

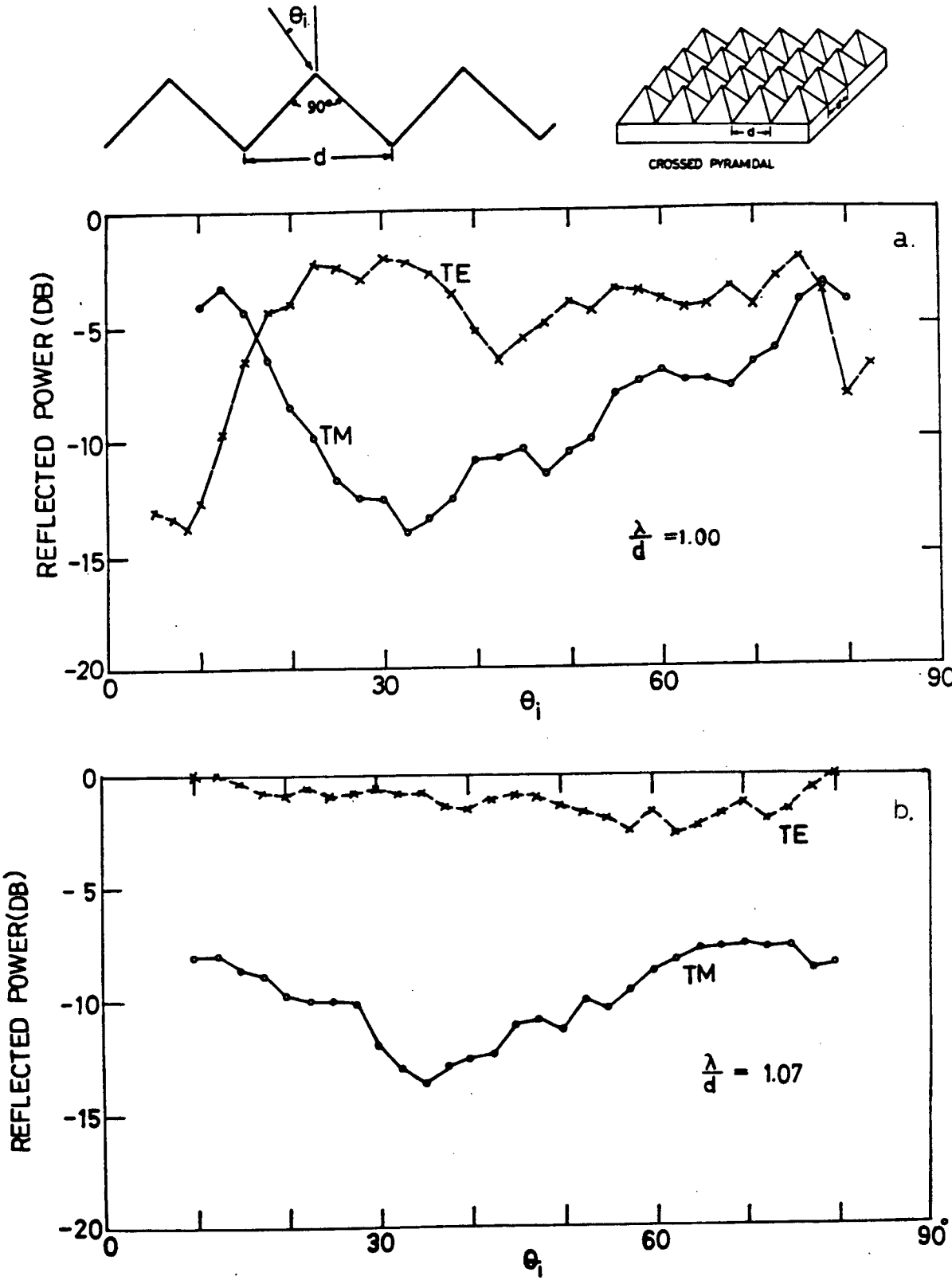

Fig. 4.23. Reflected power vs. angle of incidence for plate A9: a. at f=37.5 GHz (λ/d=1.00) b. at f=35 GHz (λ/d=1.07)

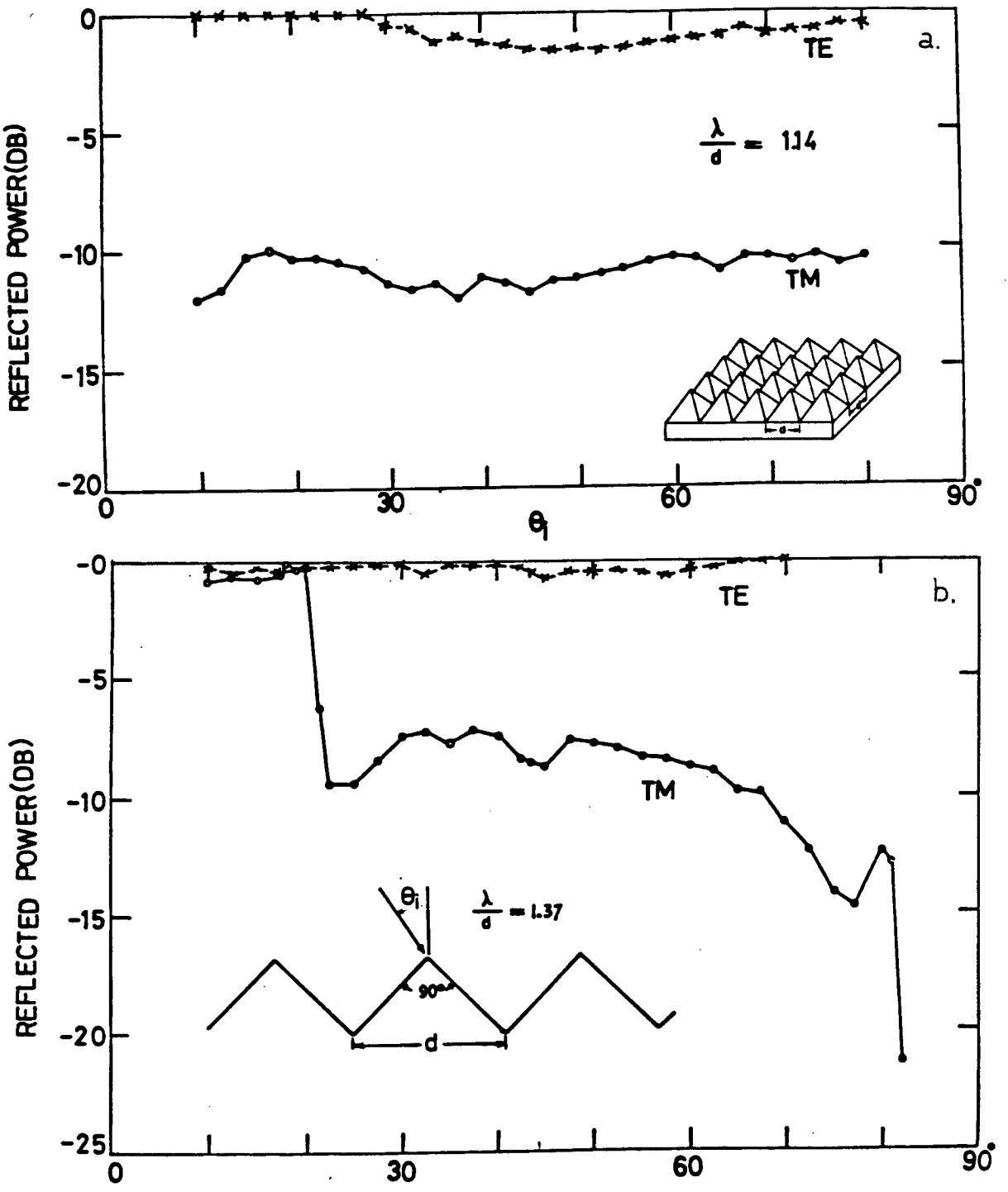

Fig. 4.24. Reflected power vs. angle of incidence for
a. plate A9 at f=33 GHz ($\lambda/d=1.14$)
b. plate B9 at f=35 GHz ($\lambda/d=1.37$)

angle $\theta_i=\sin^{-1}(\lambda/(2d))=30°$. On the contrary, there appears a minimum reduction at $\theta_i=30°$ for TE polarization.

The curves in Fig. 4.23b, Fig. 4.24a and Fig. 4.24b looks somewhat similar, and the behavior of a polarizer is conserved over a wide range of θ_i, where the reduction for TE polarization is small, and that for TM polarization is roughly 10 dB or 90%. From the point of view of a good polarizer, the best operating range is found in Fig. 4.24a to be $10°\leq\theta_i\leq27.5°$, where the surface can scatter 90% of the TM components of an arbitrarily polarized incident wave, while TE polarization is totally reflected. In Fig. 4.24b, the very small reduction for both TM and TE polarizations below 20° is due to the fact that theoretically the (-1,0) spectral order will cease to propagate as long as θ_i is smaller than $\sin^{-1}(\lambda/d-1)=22°$ where the (-1,0) Wood anomaly occurs, and the surface should act as it were a flat metal plane, as discussed in Section 4.2. For $\lambda/d=1.07$ and 1.14, the (-1,0) Wood anomaly should occur at $\theta_i=4°$ and 7.8° respectively, but these two positions are out of our range of convenient measurements. The Bragg angles are 32.3°, 34.6° and 43.4° for the values of λ/d 1.07, 1.14 and 1.38 respectively, their effects are not evident as found in Figures 4.23b, 4.24a and b.

Measured frequency response of plate A9 at $\theta_i=32.5°$ under non-oblique incidence is shown in Fig. 4.25. Within the range 33 GHz$\leq$f$\leq$37.5 GHz, or $1.136\leq\lambda/d\leq1$, the polarizer-like behaviour is still preserved. This is

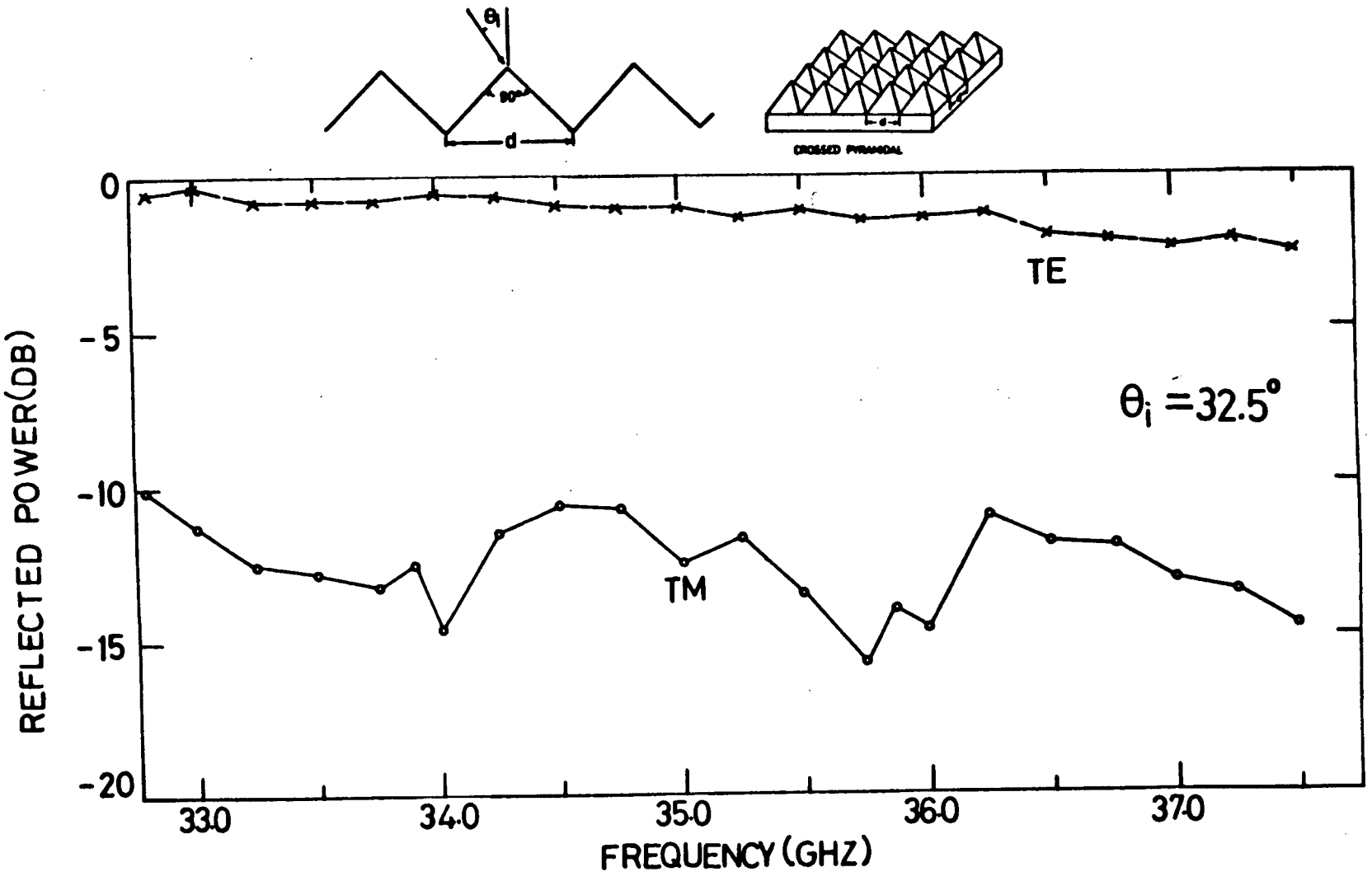

Fig. 4.25. Reflected power vs. frequency for plate A9 at $\theta_i=32.5^\circ$, $\psi_i=0$

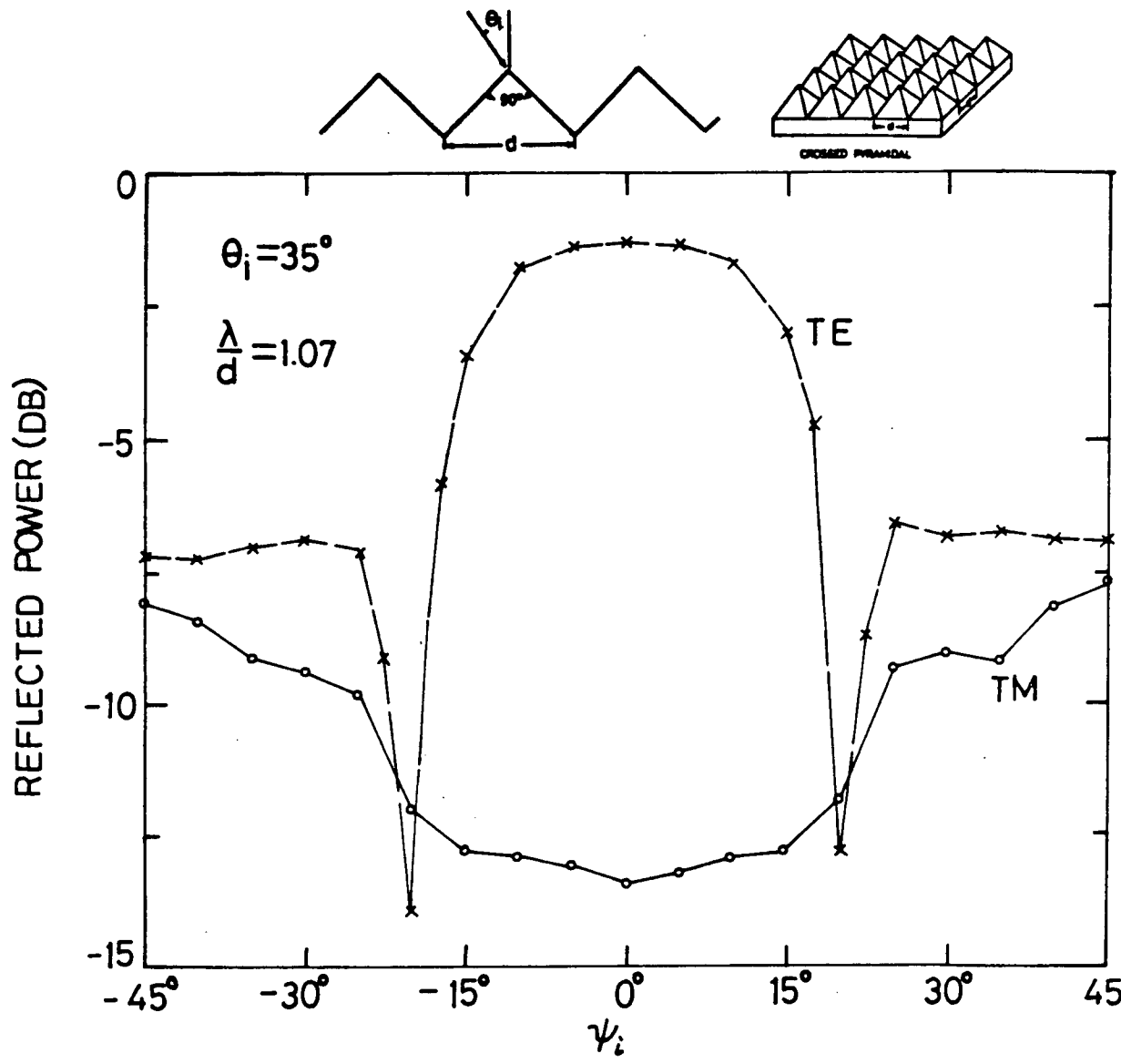

Fig. 4.26. Reflected power vs. angle of rotation for plate A9 at f=35 GHz, θ_i=35°

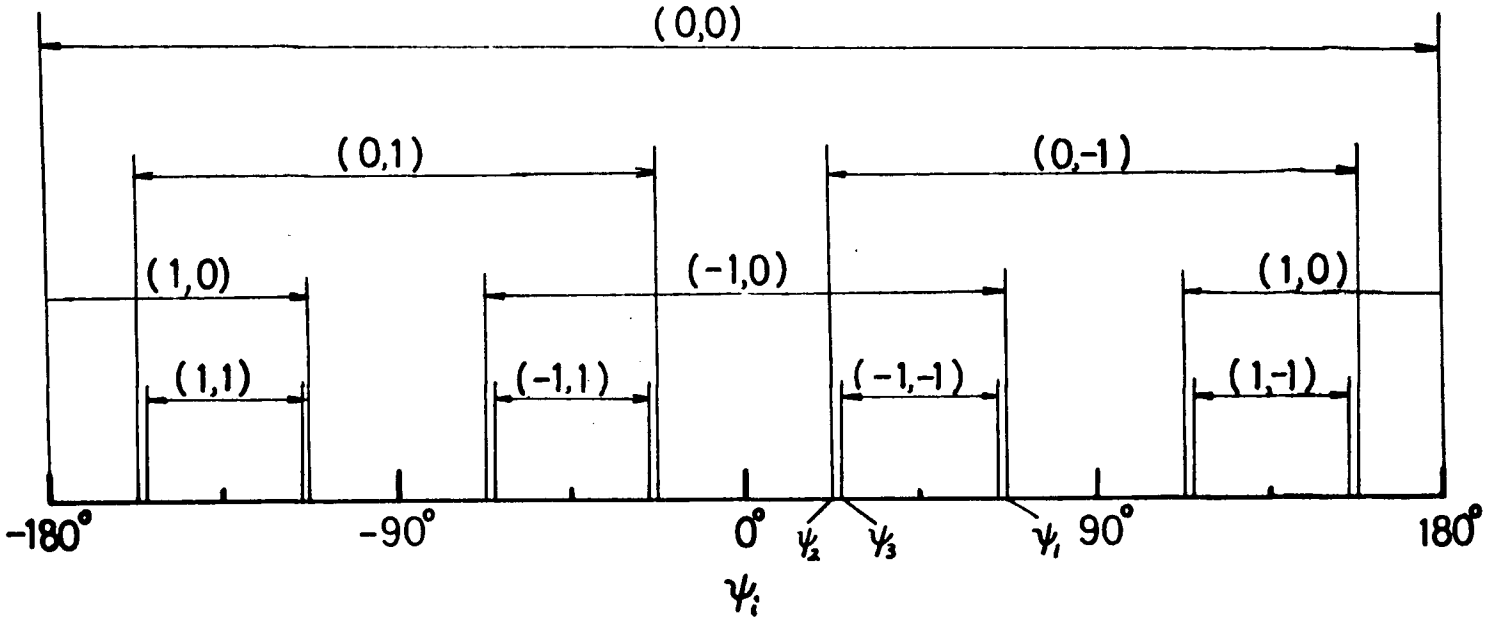

Fig. 4.27. Diagram of azimuthal angular regions in which spectral orders exist for a crossed grating at $\lambda/d=1.07$, $\theta_i=35°$

region boundaries: $\psi_1=67.2°$, $\psi_2=22.8°$, $\psi_3=24°$

consistent with the frequency response of plate B9 in Fig. 4.6, where λ/d varies from 1.46 to 1.28. It seems that the apex angle of 90° determines the polarizer-like behavior of plates A9 and B9. Therefore, the profile of a pyramidal crossed grating has great effect on the general behavior of the grating, while at some values of λ/d, a small change in λ/d may change the behavior of the grating tremendously (for example, from λ/d=1.00 to 1.07 in Fig. 4.23).

The experimental results in Fig. 4.26 display the reflected power as a function of angle of rotation for plate A9 at f=35 GHz and θ_i=35°. The curves are basically symmetrical about ψ_i=0° as before. It is interesting that when ψ_i becomes larger than 10°, the reduction for TE polarization increases rapidly and reaches 12.8 dB or 95% at ψ_i=20°. Then, there appears an abrupt rise in TE curve from 20° to 25°. We attribute this rise to the (0,-1) Wood anomaly which should occur at ψ_i=22.8° according to our calculation (see Fig. 4.27). The appearance of the spectral order (0,-1) at this position causes a re-distribution of incident energy between three orders (0,0), (-1,0) and (0,-1). In Fig. 4.26, the TE curve changes suddenly again at ψ_i=25°. This change is due to the appearance of the order (-1,-1) at ψ_i=24°, as shown in Fig. 4.27, where the (-1,-1) Wood anomaly should exist. Again, we have very good agreement between theoretical predictions and experimental results. For TM polarization, the effect of these two Wood anomalies is not so obvious.

4.6 PLATE B6 ---- INFLUENCE OF APEX ANGLE *a*

Together with plate B9, Plate B6 was designed to check with some earlier numerical results. Fig. 4.28 shows the measured reflected power as a function of angle of incidence for the singly-periodic equivalent of plate B6 at f=35 GHz ($\lambda/d=1.37$) When θ_i is small, there is no reduction in specular reflection for both polarizations, and the surface behaves as a plane conductor. This is because only the n=0 order exists when $\theta_i<\sin^{-1}(\lambda/d-1)=22°$. For angles of incidence greater than this limit value, the reduction for TE polarization remains small, but for TM polarization, there appears a sudden drop between 20° and 25°, which is caused by the n=-1 Wood anomaly occured at $\theta_i=22°$. Also, a minimum relative reflected power of 0.28 is observed at $\theta_i=42.5°$ which is close to the Bragg angle $\theta_i=\sin^{-1}(\lambda/(2d))=43.5°$.

Fig. 4.29 presents the experimental results for the corresponding crossed grating plate B6 under non-oblique incidence. We can see from the figure that the behavior of this doubly-periodic grating is quite different from that of its singly-periodic equivalent. For the incident angle greater than twenty degrees, the reduction in TM polarized specular reflection becomes much larger than that for the classical grating, whereas for TE polarization the reduction gets smaller. It is worth notice that the influence of the Wood anomaly occured at $\theta_i=22°$ is remarkable for TM polarization, instead of for TE polarization in the case of

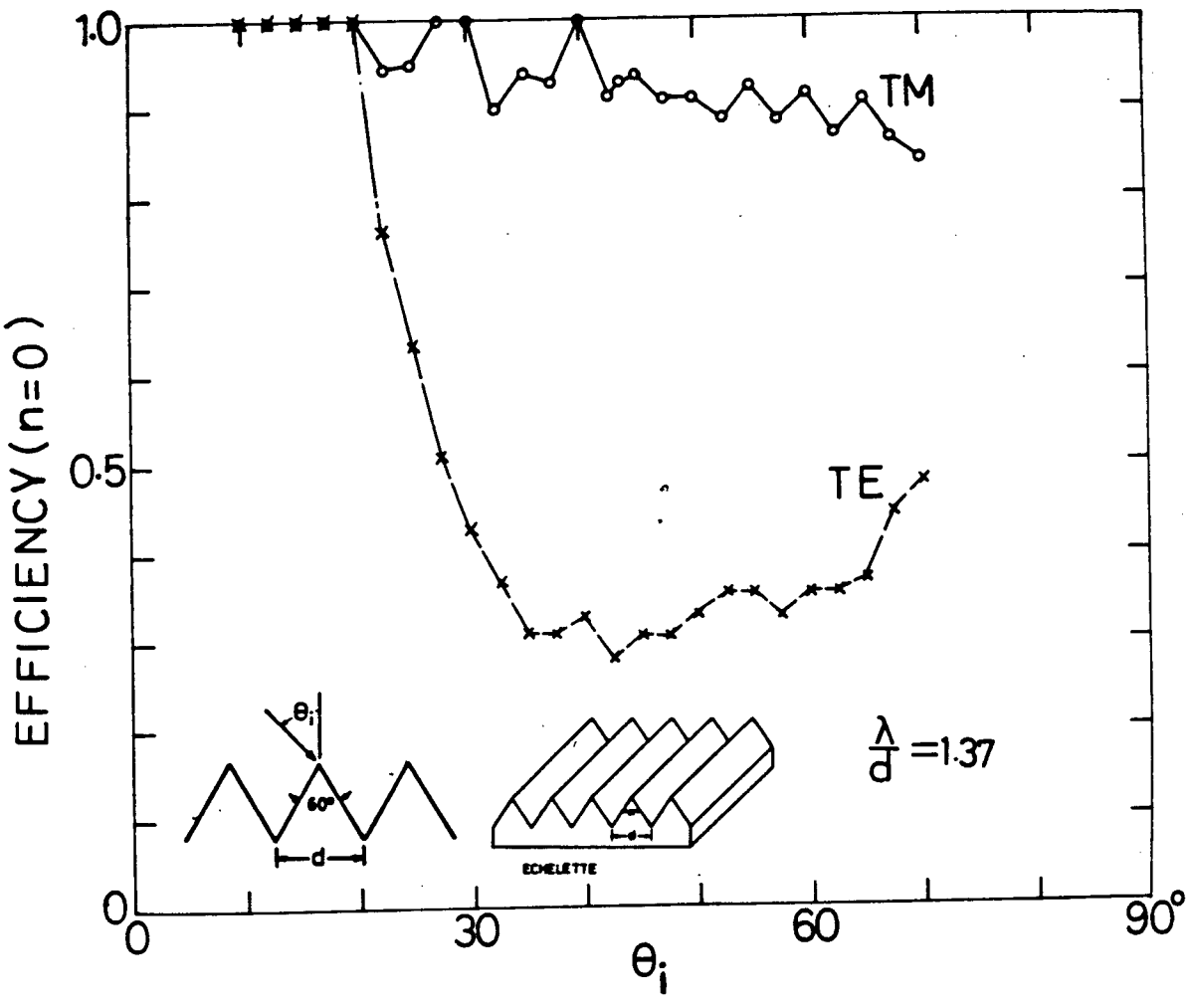

Fig. 4.28. Relative reflected power (or ϵ_0) vs. angle of incidence for the singly periodic equivalent of plate B6 at f=35 GHz, ψ_i=0

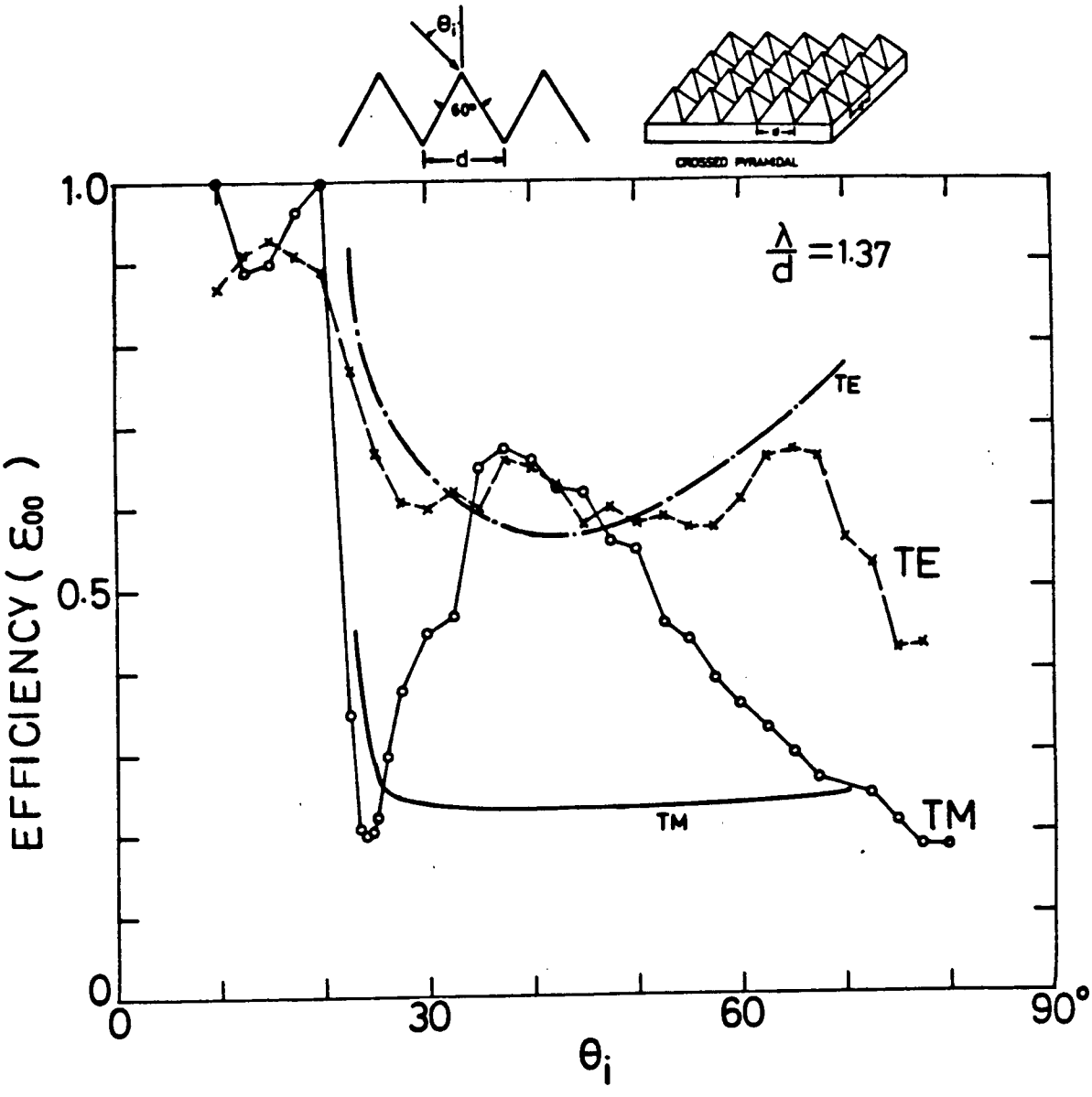

Fig. 4.29. Relative reflected power (or ϵ_{00}) vs. angle of incidence for plate B6 at f=35 GHz, ψ_i=0

its classical grating. No maximum reduction is observed around the Bragg angle (43.5°) Instead, there is a local minimum reduction at 37.5°, around which TE and TM curves overlap roughly. The reduction for both polarizations is still small when the incident angle is less than 20°, since only the specular reflection exists in this range where the relative reflected power should be unity theoretically. The discrepancy is probably due to the experimental errors. Also in Fig. 4.29, for comparison with the experimental results. we display the calculated curves [16] obtained by using the coordinate-transformation method mentioned in Chapter 1. Although the behavior of the two curves in some regions (e.g., in the range $22° \leq \theta_i \leq 62°$ for TE polarization) is similar to each other, the agreement is much less than that found in the case of plate B9. Noticing that plate B6 with apex angle of 60° is more deeply-grooved, the great discrepancy between numerical prediction and experimental results is presumably due to the fact that for deeper grooves the numerical results converge very slowly, or not at all [5].

The measured frequency response for plate B6 at $\theta_i = 43.5°$ under non-oblique incidence is illustrated in Fig. 4.30, where no significant reduction in specular reflection is found.

Fig. 4.31 shows reflected power curves as a function of angle of rotation for plate B6 at f=35 GHz and $\theta_i = 43.5°$. Although the energy properties of the grating are

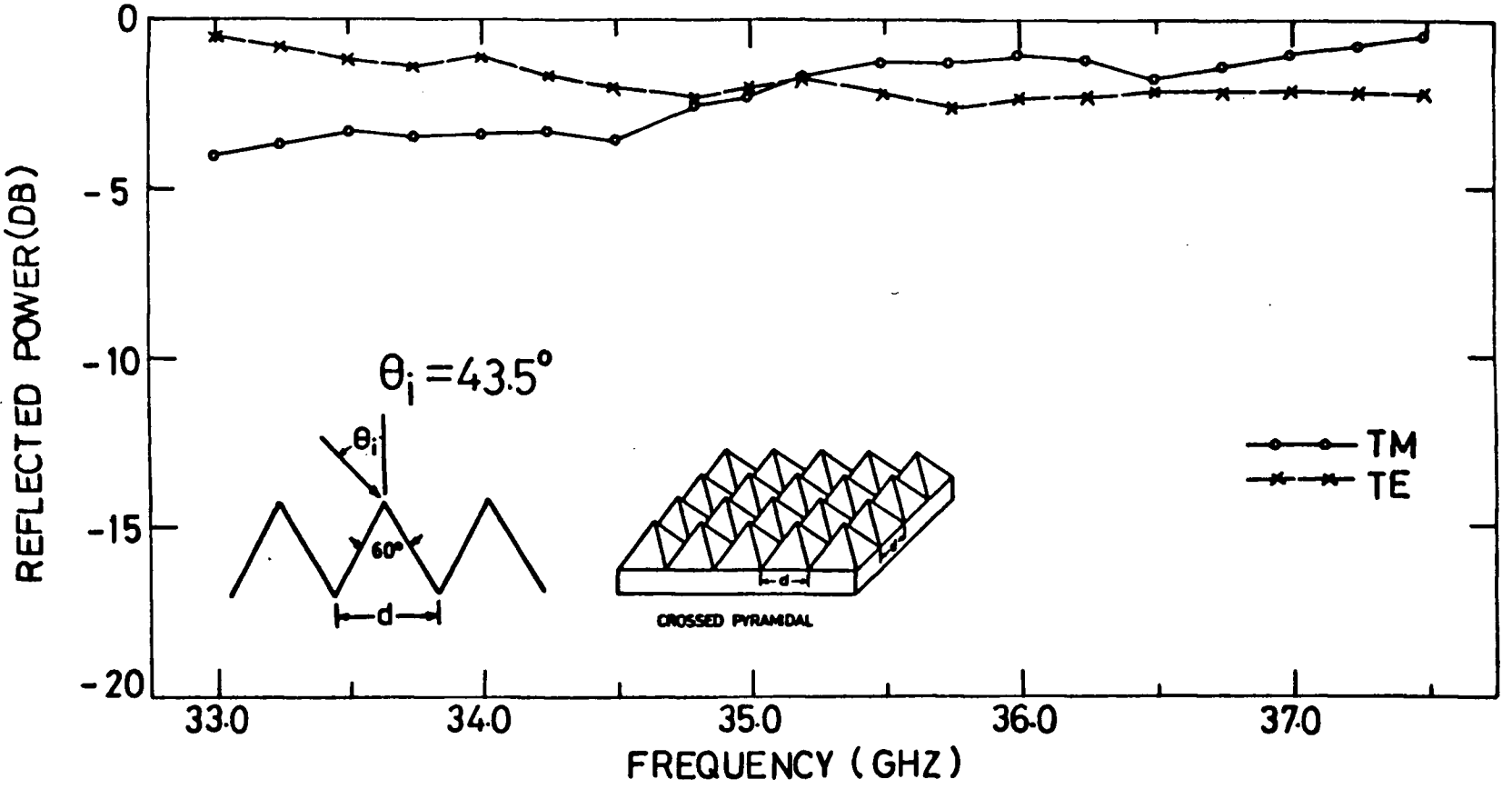

Fig. 4.30. Reflected power vs. frequency for plate B6 at θ_i=43.5°, ψ_i=0

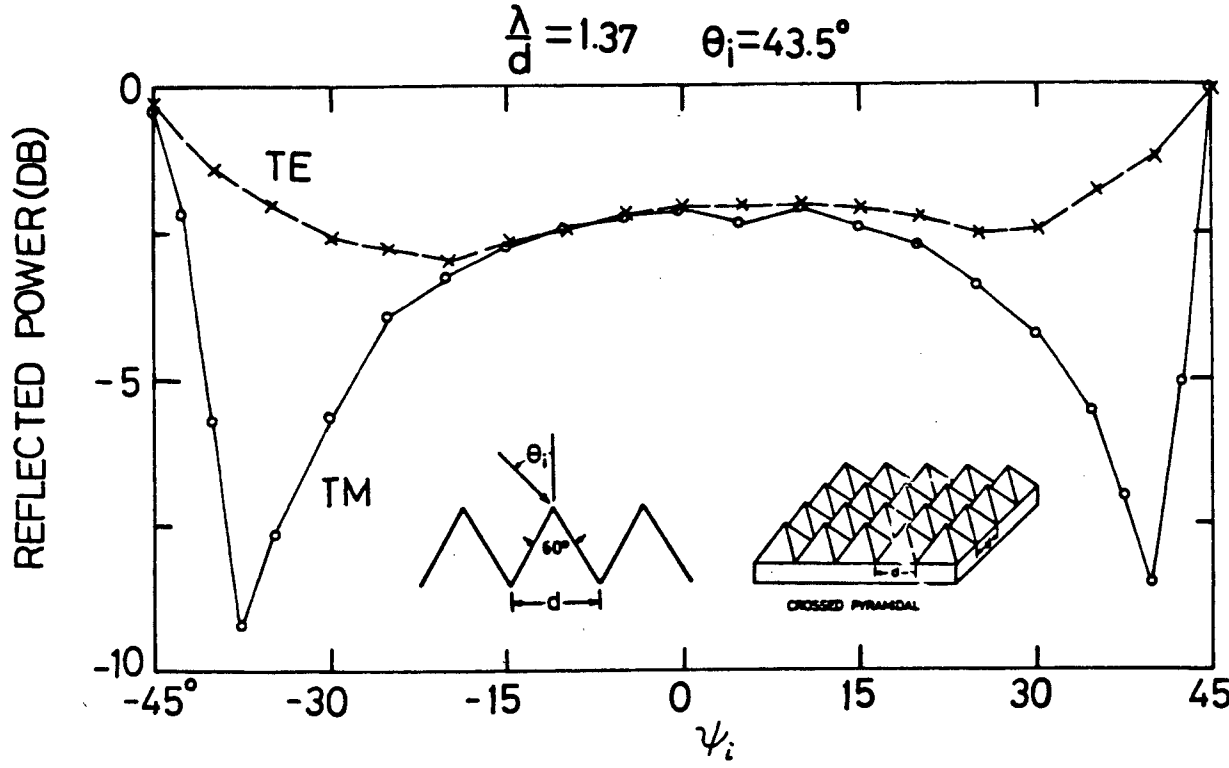

Fig. 4.31. Reflected power vs. angle of rotation for plate B6 at f=35 GHz, θ_i=43.5°

polarization independent around ψ_i=0°, the effects of polarization become apparent as ψ_i gets greater than 15°. The reduction in TE polarized specular reflection becomes smaller and reaches zero at ψ_i=45°, while the reduction in TM polarized specular reflection gets larger , reach a maximum of 8.5 dB at 40°, and then suddenly decreases to zero at ψ_i=45°. Since the incident conditions here (λ/d=1.37 and θ_i=43.5°) are the same as those in Fig. 4.4 for plate B9, we can use the schematic diagram in Fig. 4.5 to explain the above behavior of plate B6. As discussed before for plate B9, the diffracted order (-1,0) is cut off at ψ_i=43.9° according to the calculation, and only specular reflection (the order (0,0)) for both polarizations exists in a very narrow range of ψ_i centered by ψ_i=45°, where the crossed grating should behave like a perfectly conducting flat surface even with such a noticeable roughness. Hence, we attribute the sharp rise of TM polarized reflected power from 40° to 45° in Fig. 4.31 to a sudden total energy transfer from the order (-1,0) to the order (0,0), and the experimental result that no reduction for both polarizations is observed at ψ_i=45° in Fig. 4.31 is exactly what the theory predicts.

The azimuthal angular responses of plate B6 in Fig. 4.31 and plate B9 in Fig. 4.4 give us good examples to look into the influences of the apex angle of pyramidal grating and the ratio λ/d. It seems that the apex angle has an important effect on the general behavior of the grating,

whereas the value of λ/d defines some critical points, for example, the positions of Wood anomalies, where remarkable changes in the shape of the curves often occur. Therefore, both of apex angle α and ratio λ/d determine the properties of the grating at a particular incident condition.

4.7 PLATE A6 ---- A BLAZED CROSSED GRATING SURFACE FOR TE POLARIZATION

Since plate A6 and plate B6 have the same profile with an apex angle of 60°, we collect their experimental curves together in Figures 4.32 and 4.33 to see how the behavior of the grating changes as the value of λ/d varies. Figures 4.32a, 4.32b and 4.33a are from the measurements of plate A6 at frequencies 37.5 GHz (λ/d=1.00), 35 GHz (λ/d=1.07) and 33 GHz (λ/d=1.14), respectively. Fig. 4.33b is for plate B6 and is the same as Fig. 4.29, except that the reduction is expressed in terms of dB here. Again, the experimental results at λ/d=1.00 in Fig. 4.32a looks most interesting. In Fig. 4.32a, although the reduction for both polarization is weak when the incident angle is small, it becomes larger after θ_i is greater than 40°. The reduction in TE polarized specular reflection reaches a maximum of 17.2 dB at θ_i=77.5°, where 98% of the incident energy is diffracted into a single order (-1,0), the direction of which can be determined as $\theta_i(-1,0)$=1.4° and ψ_i=180° by Equations (2.13) and (2.14). In the point of view of elimination of specular reflection, this is the best result for TE polarization

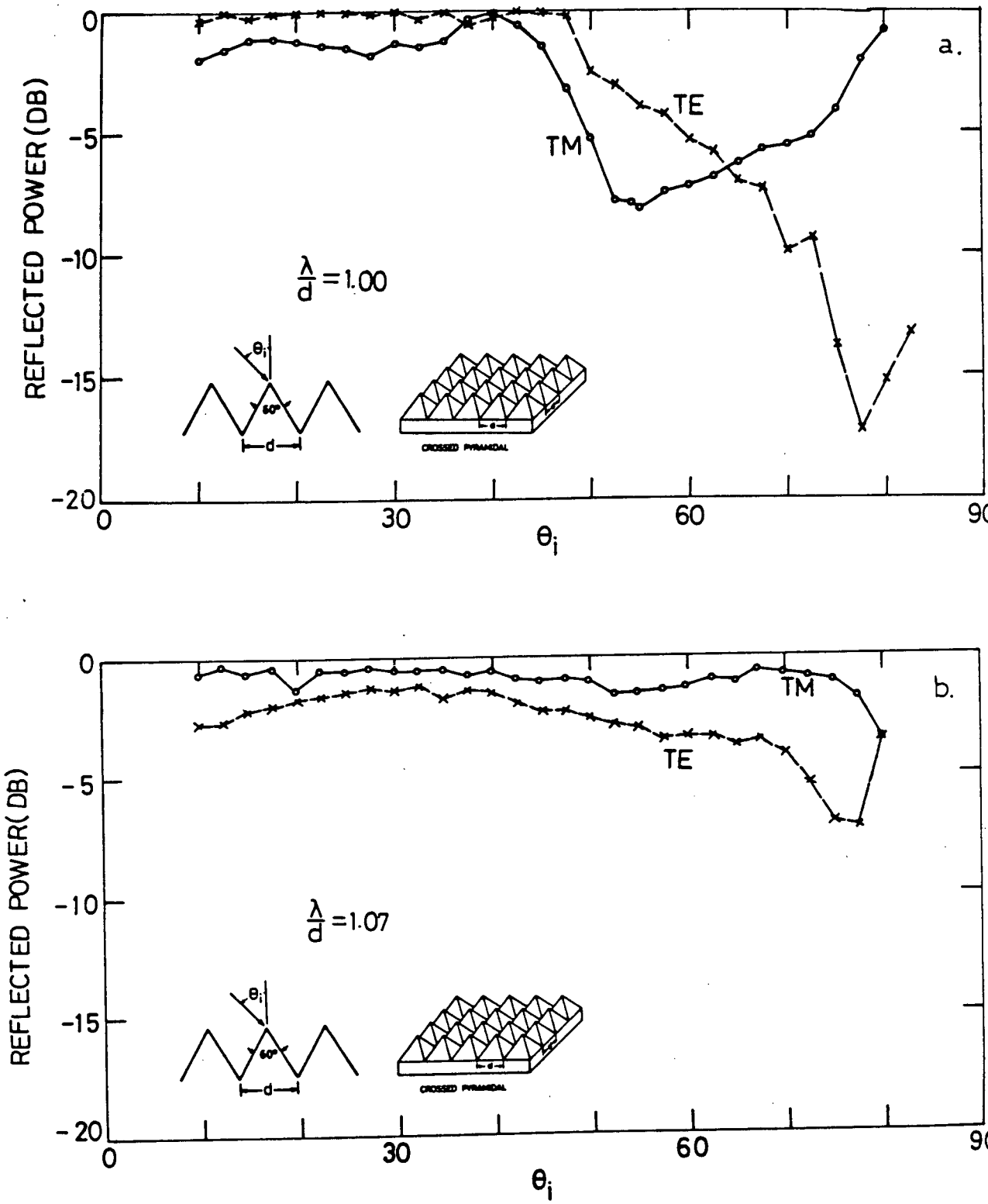

Fig. 4.32. Reflected power vs. angle of incidence for plate A6: a. at f=37.5 GHz (λ/d=1.00) b. at f=35 GHz (λ/d=1.07)

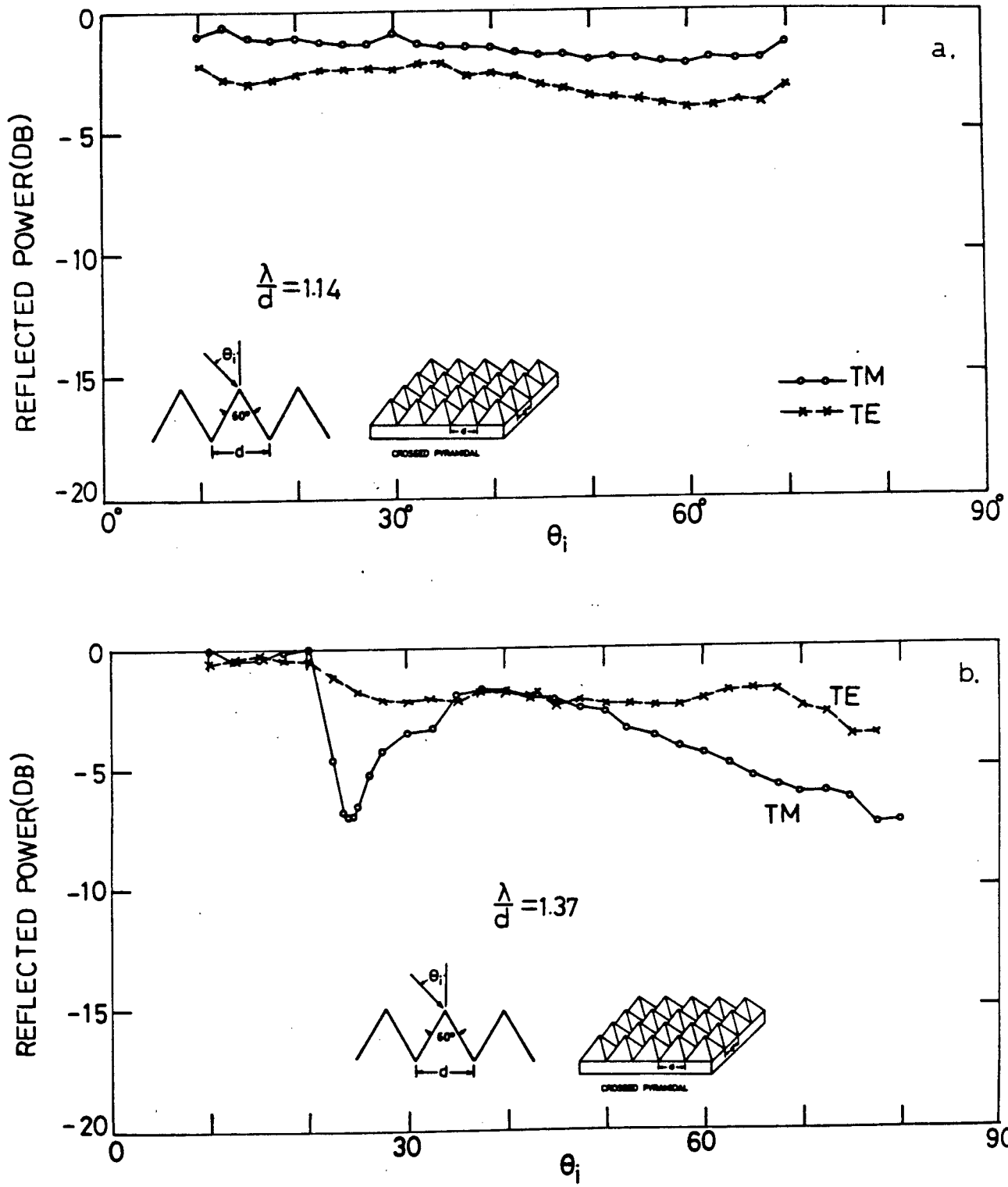

Fig. 4.33. Reflected power vs. angle of incidence
a. for plate A6, at f=33 GHz ($\lambda/d=1.14$)
b. for plate B6, at f=35 GHz ($\lambda/d=1.37$)

which we got from all the crossed grating plates investigated. Also in Fig. 4.32a, the intersection of TM curve with TE curve at θ_i=64° provides an equal reduction of 6.6 dB for both polarizations. At this particular incident angle, plate A6 scatters about 80% of the energy of an arbitrarily polarized incident wave into a single order (-1,0). This is the best performance achieved with regard to equal reduction for both polarizations. The behavior curves of this grating at λ/d=1.07 and λ/d=1.14 are alike as seen in Fig. 4.32b and Fig. 4.33a. In both cases, the reduction in TM polarized specular reflection is always less than that for TE polarization. The behavior of the grating with a apex angle of 60° at λ/d=1.37 has been discussed in last section. The drop of reflected power for TM polarization in Fig. 4.33b is due to the (-1,0) Wood anomaly. The Bragg angles are 30°, 32.3°, 34.6° and 43.4° for λ/d=1.00, 1.07, 1.14 and 1.37 respectively. As observed in Fig. 4.32 and Fig. 4.33, no maximum reduction occurs at the Bragg angle in these four cases.

The reflected power as a function of angle of rotation for plate A6 at f=35 GHz and θ_i=35° is illustrated in Fig. 4.34. In order to analyze the shape of the curves, we can apply the calculated results presented in Fig. 4.27 to this case, because of the same incident conditions here (λ/d=1.07 and θ_i=35°) as those in Fig. 4.26 for plate A9. The most remarkable feature in Fig. 4.34 is a very steep falling down of reflected power for TM polarization from 20° to 22.5°.

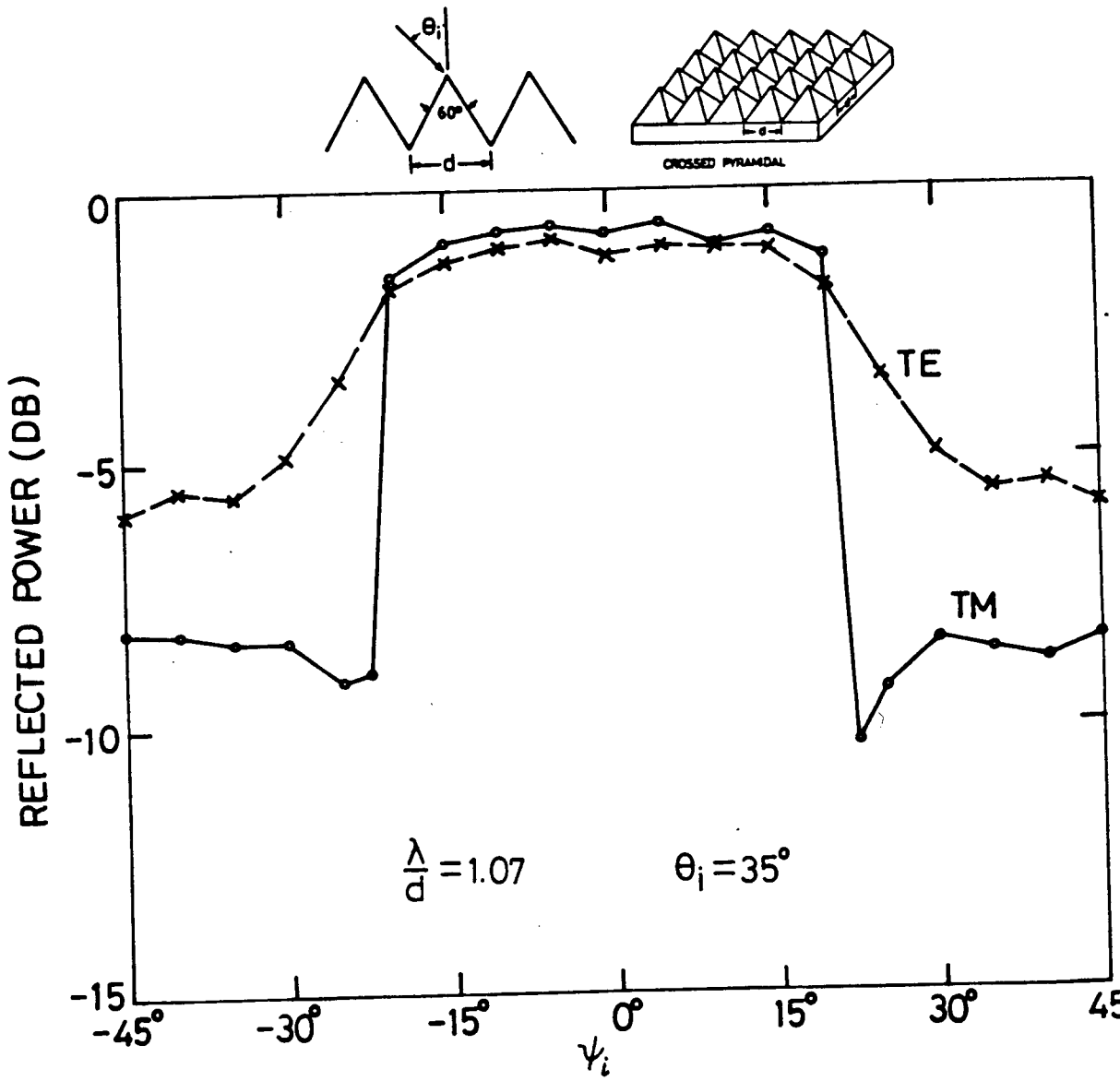

Fig. 4.34. Reflected power vs. angle of rotation for plate A6 at f=35 GHz, θ_i=35°

According to the calculation, this is due to the appearance of the diffracted order (0,-1) at ψ_i=22.8°. where the (0,-1) Wood anomaly occurs. The (-1,-1) Wood anomaly at ψ_i=24°, which is close to the (0,-1) Wood anomaly, causes the TM polarized reflected power to increase somewhat from 22.5° to 30°. For TE polarization, the influence of Wood anomalies is not obvious.

It is interesting to take a comparison between the azimuthal angular behavior of plate A6 and plate A9 having the same period but different apex angle. In the case of plate A6 (see Fig. 4.34), the effect of Wood anomalies is much more apparent for TM polarization than that for TE polarization, whereas in the case of plate A9 (see Fig. 4.26) the reverse is true. In both cases, the positions where Wood anomalies occur are very close to what the theory predicts. From the comparison, we can see again, as we have discussed for plates B6 and B9 in the end of last section, that the profile of the grating (that is, the apex angle for pyramidal grating) affects the general behavior of grating very much, while the grating period (more accurately, the ratio λ/d) determines the positions of Wood anomalies, where great change in grating behavior always happens.

Chapter 5

EXPERIMENTAL RESULTS OF CROSSED GRATINGS WITH HEMISPHERICAL CAVITIES

5.1 INTRODUCTION

This chapter presents the results of the experiments carried out on crossed gratings with hemispherical cavities which are regularly spaced along two orthogonal directions on a conducting plane surface. Fig. 5.1 illustrates the profile of this crossed grating, and gives the dimensions of such two plates investigated. Each surface consisted of 16x16 identical hemispherical cavities which were hollowed on a 208x208 mm aluminium plate with thickness of 20 mm. The crossed gratings have the same period, but different cavity radius. It is worth notice that the period 13 mm is greater than the wavelength within our experimental range (8 mm to 9.09 mm). For example, at f=35 GHz, the ratio λ/d is 0.66. According to the discussion in Section 2.3, in the case of $d>\lambda$, generally more than three diffracted orders are excited. For instance, if either of these two crossed gratings with hemispherical cavities is illuminated normally ($\theta_i=0°$) by a incident plane wave with λ=8.57 mm (f=35 GHz), there will exist as many as nine diffracted orders (see the calculation in the end of Section 2.3). Therefore, blazing to a single spectral order is not possible for these two crossed gratings in our measurements, although elimination of specular reflection is possible. This is quite different

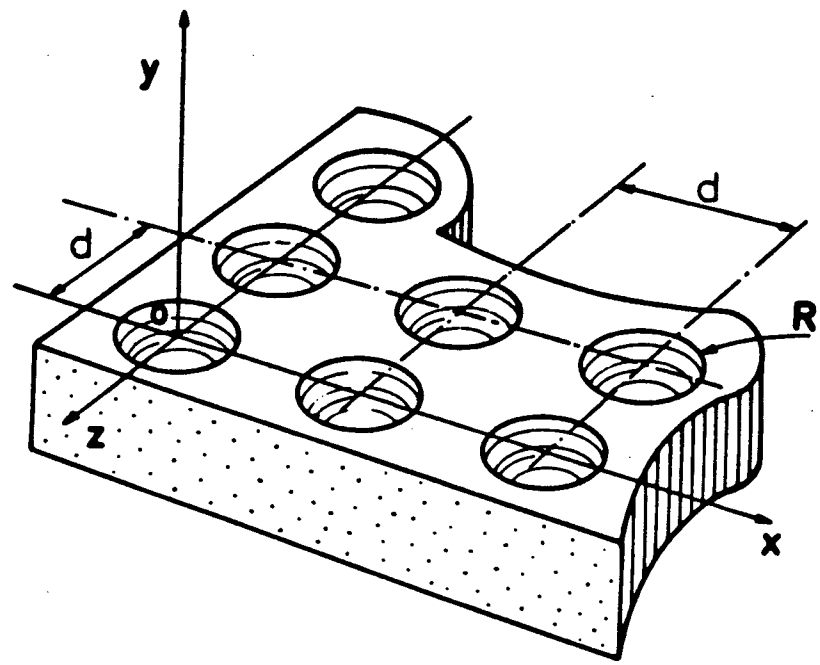

PLATE	DIMENSIONS		HEMISPHERICAL
	d (mm)	R (mm)	CAVITIES
R4	13	4	16x16
R6	13	6	16x16

Fig. 5.1. The profile of a crossed grating with hemispherical cavities, and dimensions for such two plates investigated

from our measurements on the pyramidal gratings. In the latter case, the periods were chosen to be in the range of $\lambda/2<d\leq\lambda$ and hence blazing to a single order (-1,0) is possible.

These two gratings were made by Laboratoire de Radioélectricité, Université de Provence, and were specially designed for comparison with newly work [22] for which some numerical results are available for the simple case of normal incidence. The numerical work for the non-normal incidence case is being performed [56] and our experimental study on this case provides the opportunity for a check on the reliability of the theory. Since these two plates were available in our laboratory for a short period of five days, only limited measurements had been taken.

5.2 PLATE R4

The measure reflected power as a function of θ_i for plate R4 under non-oblique incidence at f=35 GHz ($\lambda/d=0.66$) is presented in Fig. 5.2. It is interesting to see that when the incident angle is less than 30°, the reduction in specular reflection for both polarizations is greater than 5 dB. It was reported [22] that the efficiency for both polarizations in the order (0,0) for a infinite crossed grating of this profile under normal incidence ($\theta_i=0°$) has a value of 0.08 (or -10.8 dB in terms of reduction), which is indicated as Point P in Fig. 5.2. This is the only available numerical result for this grating. We could not take

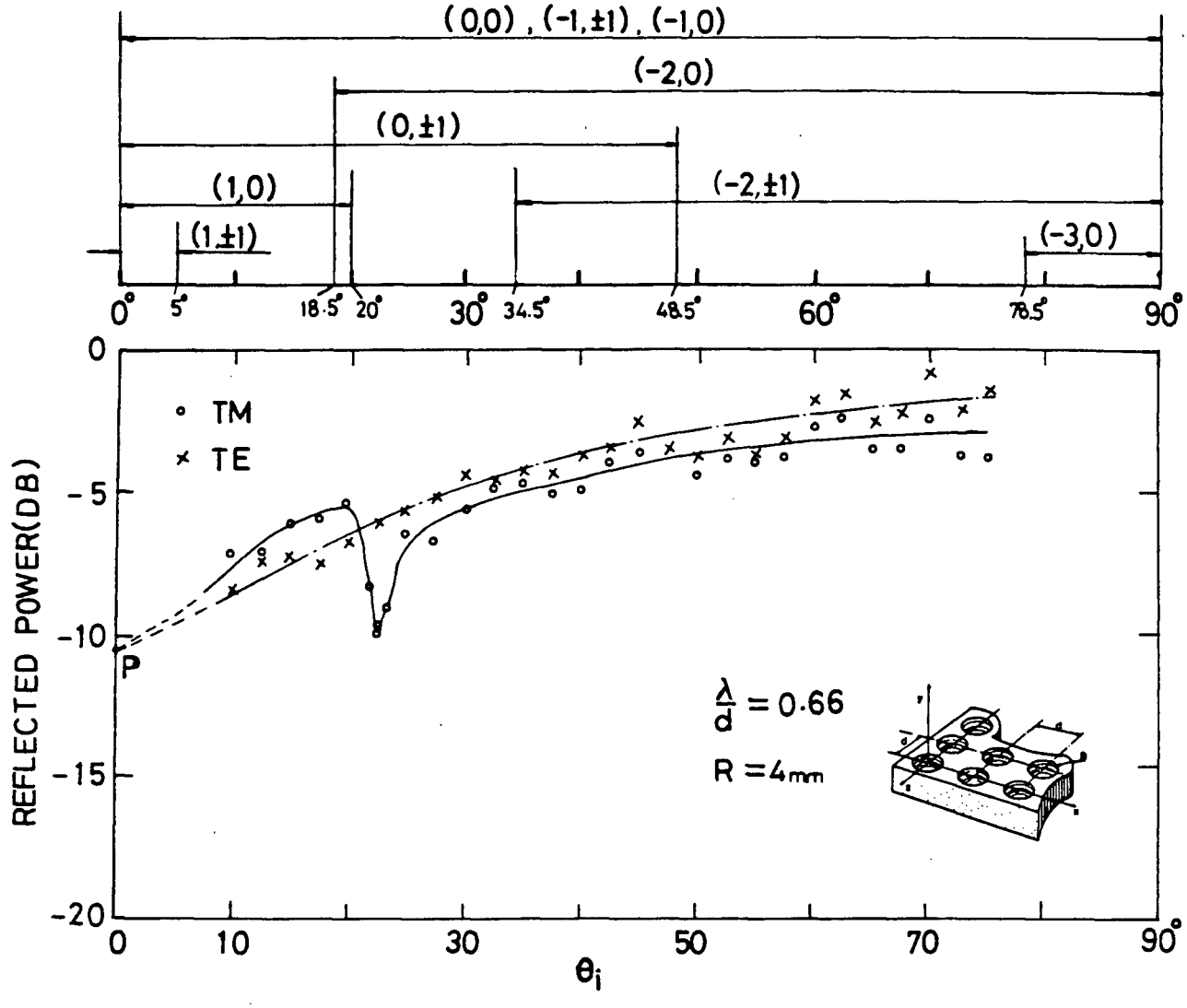

Fig. 5.2. Measured reflected power vs. θ_i for plate R4 at f=35 GHz, ψ_i=0;

and calculated angular regions of ψ_i for all existing diffracted orders (on top)

measurements near normal incidence as mentioned in Chapter 3. However, from Fig. 5.2, we can still observe that this calculated result agrees quite well with the tendency of both TM and TE curves when the incident angle becomes smaller and approaches 0°. This more than 10 dB reduction in specular reflection for normal incidence means that 90% of the incident energy of an arbitrarily polarized plane wave is scattered into the other eight spectral orders and only 10% of that is specularly reflected.

In Fig. 5.2, on top of the experimental data, we also display schematically the results of our calculation by using Rayleigh wavelength equation (2.10), which indicate the regions where various spectral orders can exist. One can see that there are at least seven spectral orders at any position of θ_i. Four Wood anomalies exist within our range of measurement ($10° \leq \theta_i \leq 75°$). The (1,0) Wood anomaly at $\theta_i = 20°$ (calculated value) probably cause the small dip in the TM curve at $\theta_i = 22.5°$. The effects of others are not evident. One will see later that the effects of Wood anomaly on the behavior of these two crossed grating with hemispherical cavities are less apparent, which probably due to the multi-diffracted-order nature when the grating period is greater than the incident wavelength.

Fig. 5.3 shows the experimental results for the same plate at a different frequency 33 GHz ($\lambda/d = 0.70$). A frequency deviation of about 6% from 35 GHz does not change the behavior of the grating very much. The reduction for

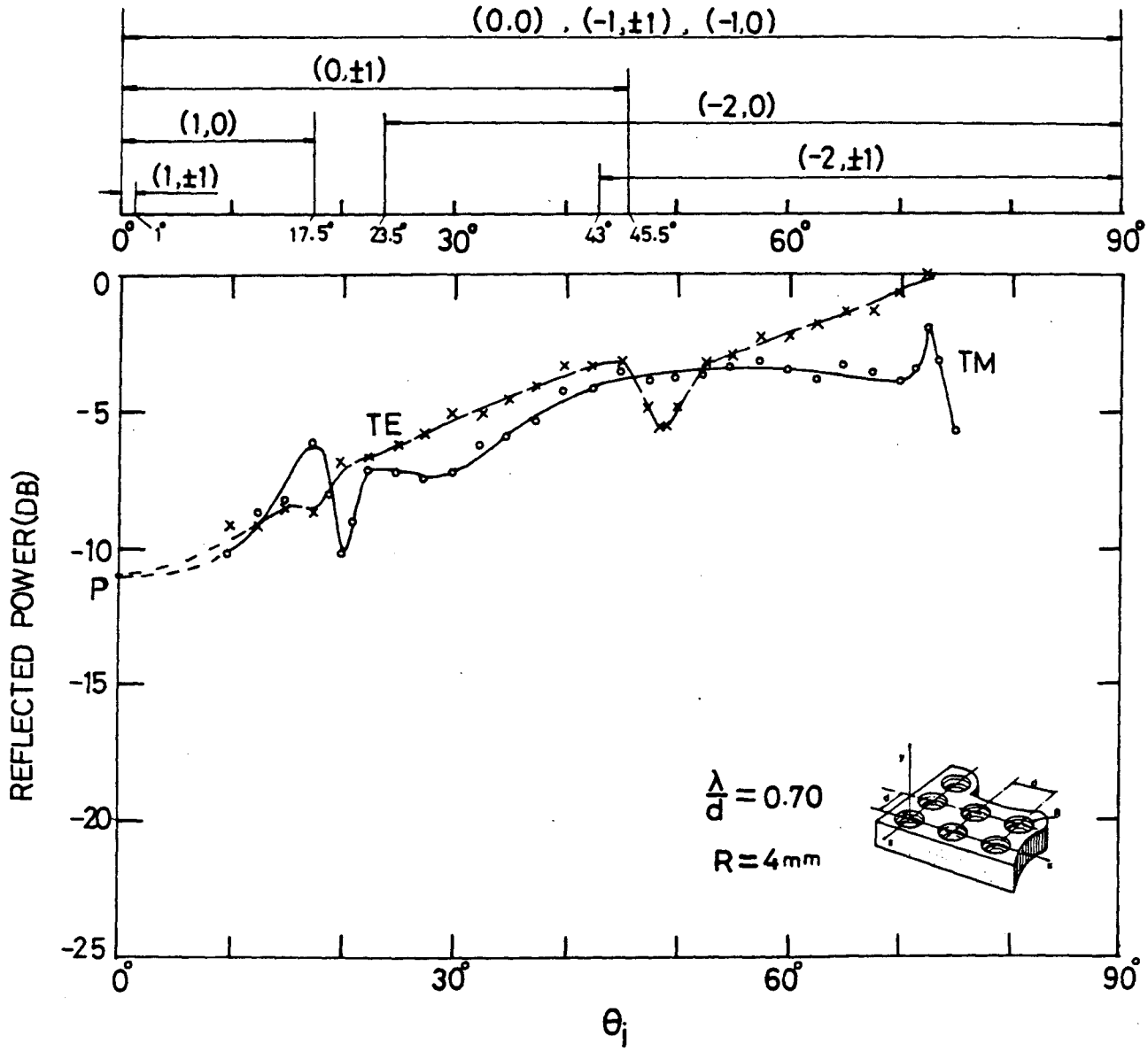

Fig. 5.3 Measured reflected power vs. θ_i for plate R4 at f=33 GHz, ψ_i=0;

and calculated angular regions of ψ_i for all existing diffracted orders (on top)

both polarizations is still greater than 5 dB when θ_i is smaller than 30°, and it also seems that the reduction in specular reflection for both polarizations at θ_i=0° would be more than 10 dB according to the tendency of both TM and TE curves, as seen in Fig. 5.3. This is consistent with the results shown in Fig. 5.2. Small changes in gradient of TE and TM curves are observed in Fig. 5.3, some of which we attribute to the corresponding Wood anomalies, the calculated positions of which are shown on top of the experimental curves. For example, a small peak in experimental TM curve at θ_i=17.5° is probably due to the (1,0) Wood anomaly at the same angle as calculated, and a small change in gradient of TE curve at θ_i=45° corresponds to the disappearance of the spectral orders (0,±1) at θ_i=45.5°.

Fig. 5.4 presents the reflected power as a function of angle of rotation (ψ_i) for plate R4 at f=35 GHz and θ_i=10°. The experimental curves are roughly symmetrical about ψ_i=0°. A remarkable feature of the behavior in this case is that within the full range of ψ_i, the reduction for both polarizations is greater than 5 dB. Again, the diagram showing the calculated angular region of ψ_i for all existing diffracted orders is displaced directly on top of the experimental curves for easy comparison. Only the results in the range of $0° \leq \psi_i \leq 45°$ are shown because of the symmetry of the behavior curves. According to the calculation, seven spectral order exist in the range of $0° \leq \psi_i \leq 45°$ and a 8th

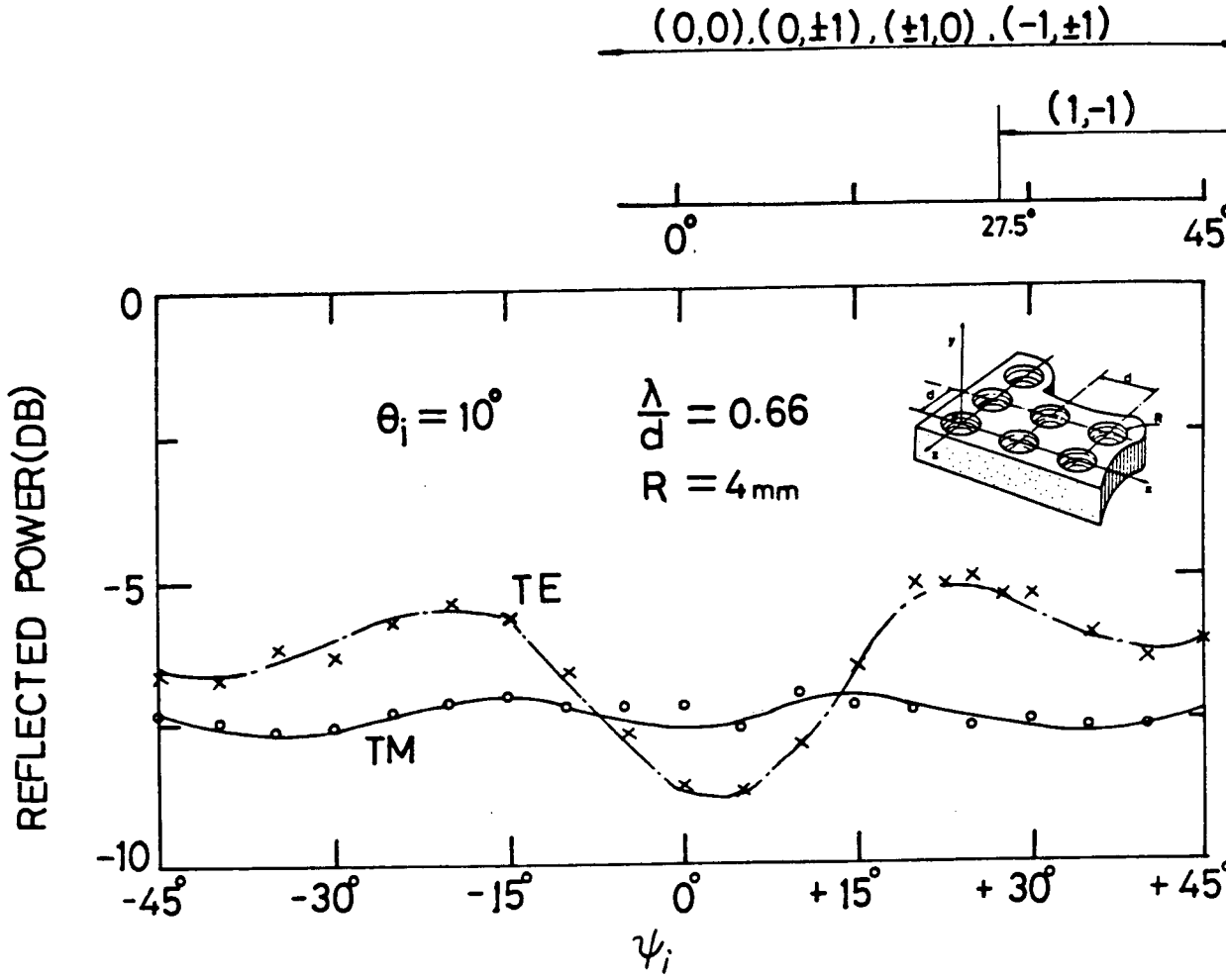

Fig. 5.4. Measured reflected power vs. ψ_i for plate R4 at f=35 GHz, θ_i=10°;

and calculated angular regions of ψ_i for all existing diffracted orders (on top)

order (1,-1) begins to propagate at ψ_i=27.5° which corresponds to a smooth change of the experimental TE curve near this position.

The azimuthal angular responses of plate R4 at the same frequency of 35 GHz, but at a different fixed θ_i of 30° are shown in Fig. 5.5. While the curves here look more complicated than those in Fig. 5.4, they have a common feature that the reduction in specular reflection for both polarizations is about 5 dB or more. Relating this with the fact shown in Fig. 5.2 that the relative reflected power is predicted 8% (or -10.8 dB) for normal incidence (θ_i=0°) and keeps lower than 32% (or -5 dB) when θ_i is smaller than 30° under non-oblique incidence (ψ_i=0°). We can conclude reasonably that this crossed grating will reflect specularly at most 32% (-5 dB) of the incident energy of an arbitrarily polarized plane wave whenever the incident angle θ_i from the normal of the surface plane is less than 30° (ψ_i is arbitrary). This anti-reflection property of plate R4 around normal incidence is of great interest to the proposed application on solar energy absorption where non-tracking collectors are used.

On top of the experimental curves in Fig. 5.5, the calculation results show that four Wood anomalies occur in the range of $0° \leq \psi_i \leq 45°$, which are responsible for the complication of the curves. The (-1,1) Wood anomaly at ψ_i=37.5° accounts for the reduction peak at ψ_i=37° for TM polarization, while the very close (-2,0) and (-2,-1) Wood

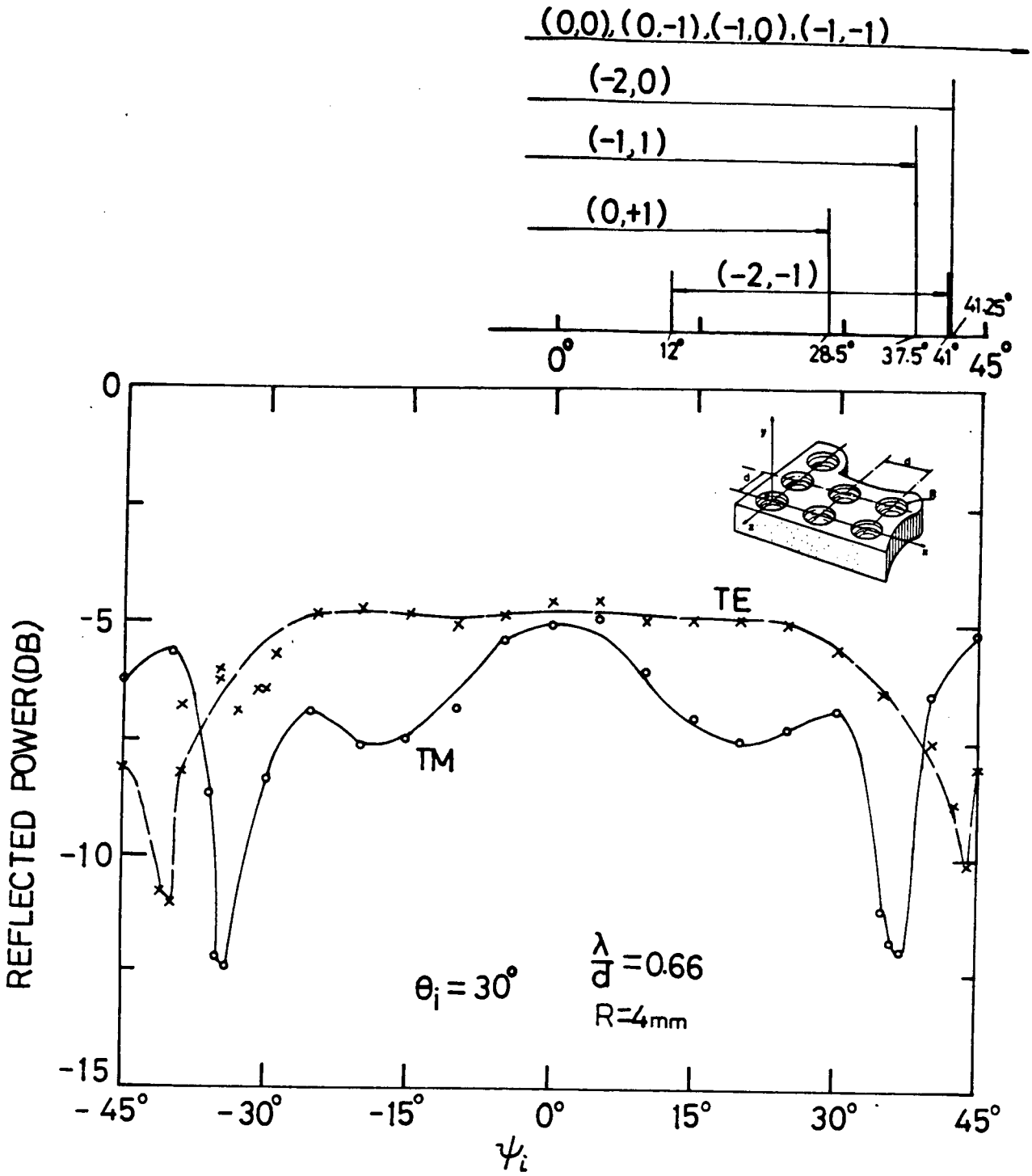

Fig. 5.5. Measured reflected power vs. ψ_i for plate R4 at f=35 GHz, θ_i=30°;

and calculated angular regions of ψ_i for all existing diffracted orders (on top)

anomalies at ψ_i=41° and ψ_i=41.25°, respectively, correspond to the reduction peak at ψ_i=44° for TE polarization. The discrepancy is due to positioning the plate.

5.3 PLATE R6

Plate R6 has the same period as that of plate R4, but a larger cavity radius of 6 mm. In Figures 5.6 and 5.7, we present the variation of reflected power with the incident angle θ_i for plate R6 under non-oblique incidence at f=35 GHz (λ/d=0.66) and f=33 GHz (λ/d=0.70) respectively. The behavior curves in both cases are remarkably different from those for plate R4 in Figures 5.2 and 5.3. Thus, we find experimentally that the cavity depth R affects the shape of the curves greatly.

The only available numerical result for plate R6 is indicated as point P in Fig. 5.6, where the relative reflected power for both polarizations in the case of normal incidence (θ_i=0°) is 0.8 (or -0.97 dB by means of reduction). This value corresponds quite well with the tendency of experimental TE and TM curves shown in Fig. 5.6.

The largest reduction in specular reflection for plates R4 and R6 is 20.1 dB as found at θ_i=76° for TM polarization in Fig. 5.7, where 99% of the incident TM-polarized energy is scattered into other seven spectral orders. This shows that essential elimination of specular reflection for TM polarization can be achieved by using this kind of crossed grating, although the available angular range is very narrow

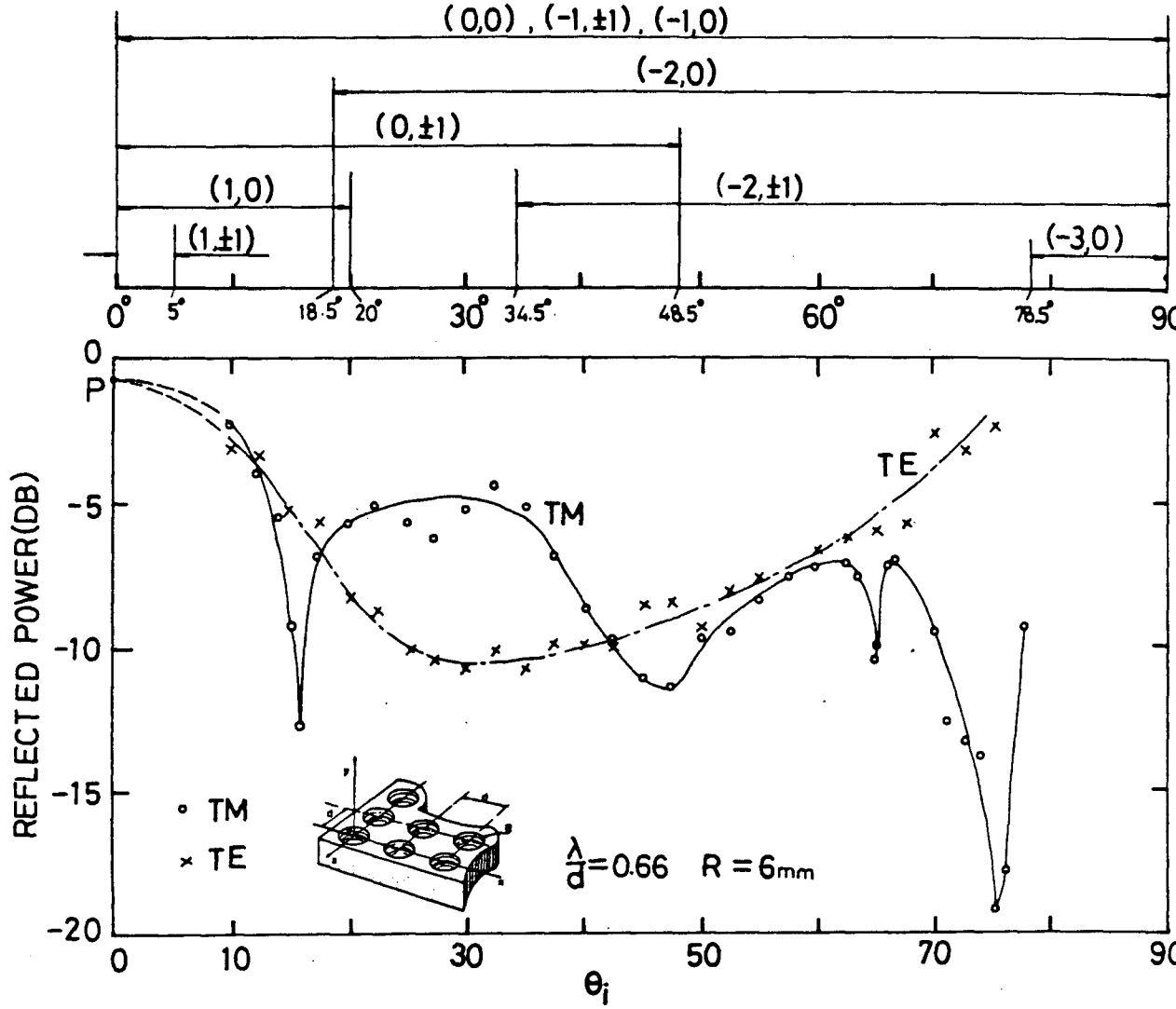

Fig. 5.6. Measured reflected power vs. θ_i for plate R6 at f=35 GHz, ψ_i=0;

and calculated angular regions of ψ_i for all existing diffracted orders (on top)

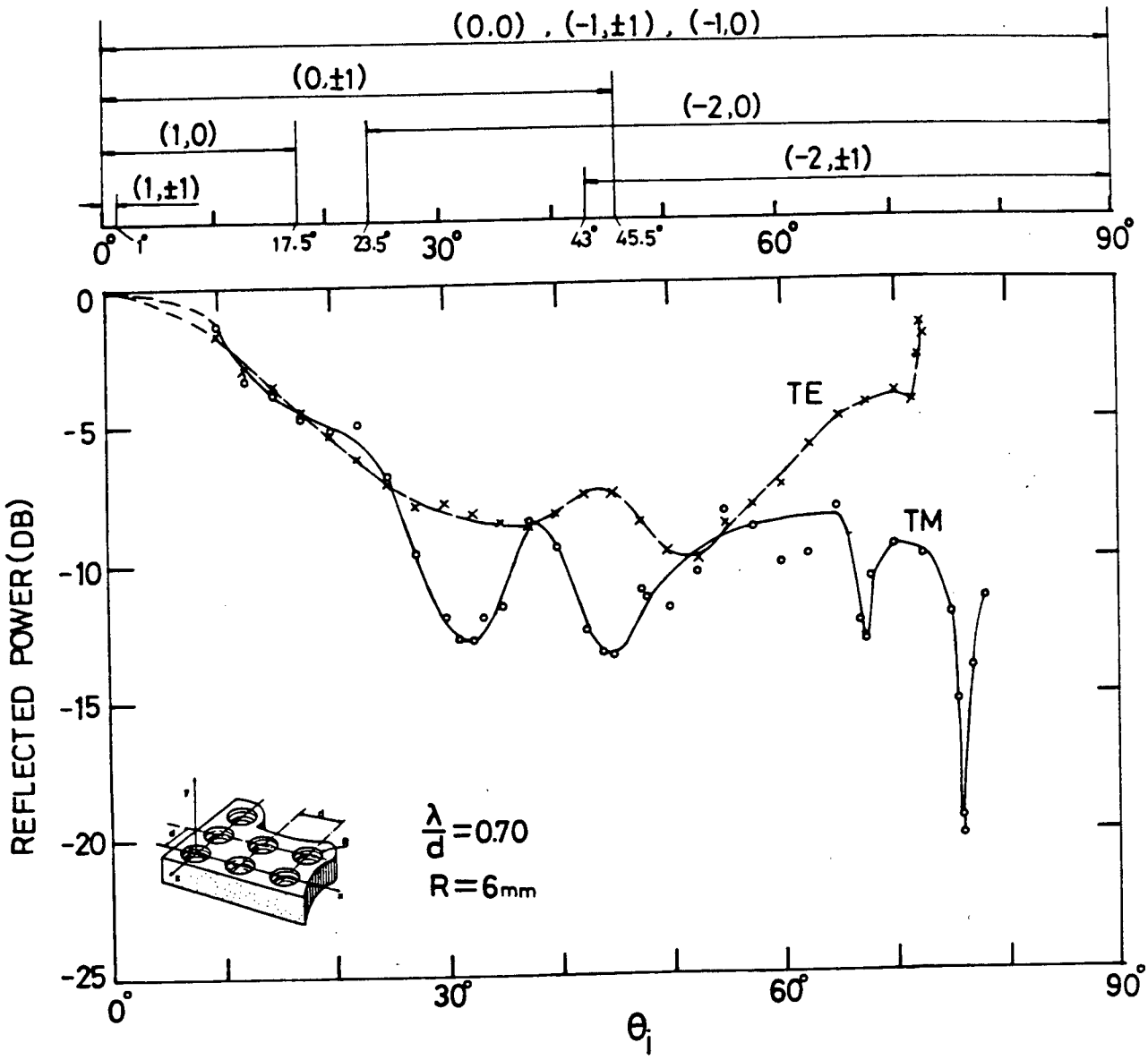

Fig. 5.7. Measured reflected power vs. θ_i for plate R6 at f=33 GHz, $\psi_i=0$;

and calculated angular regions of ψ_i for all existing diffracted orders (on top)

here.

By using the calculated results shown schematically on top of Figures 5.6 and 5.7, we can investigate the effects of Wood anomalies. The (0,±1) and (-2,±1) Wood anomalies can account for the changes of the TM curve at the corresponging positions in Figures 5.6 and 5.7. The influence of the other Wood anomalies are not evident here. The two reduction peaks for TM polarization at θ_i=65° and θ_i=75° in Fig. 5.6 are not caused by Wood anomalies, since two similar peaks can be found at θ_i=67.5° and θ_i=76° in Fig. 5.7 and there is no Wood anomaly at all in that range of θ_i. The Bragg angle effect is not observed either in Fig. 5.6 or in Fig. 5.7 (the Bragg angles are 19.3° for λ/d=0.66 and 20.5° for λ/d=0.70).

Fig. 5.8 shows the measured reflected power as a function of angle of rotation (ψ_i) for plate R6 at f=35 GHz and θ_i=10°. It is observed that the reduction in TE polarized specular reflection is always somewhat greater than that for TM polarization in this case. This is very different from the behavior of plate R4 under the same incident condition, shown in Fig. 5.4. Again, we can see that the cavity depth R has an important influence on the behavior of this kind of crossed gratings.

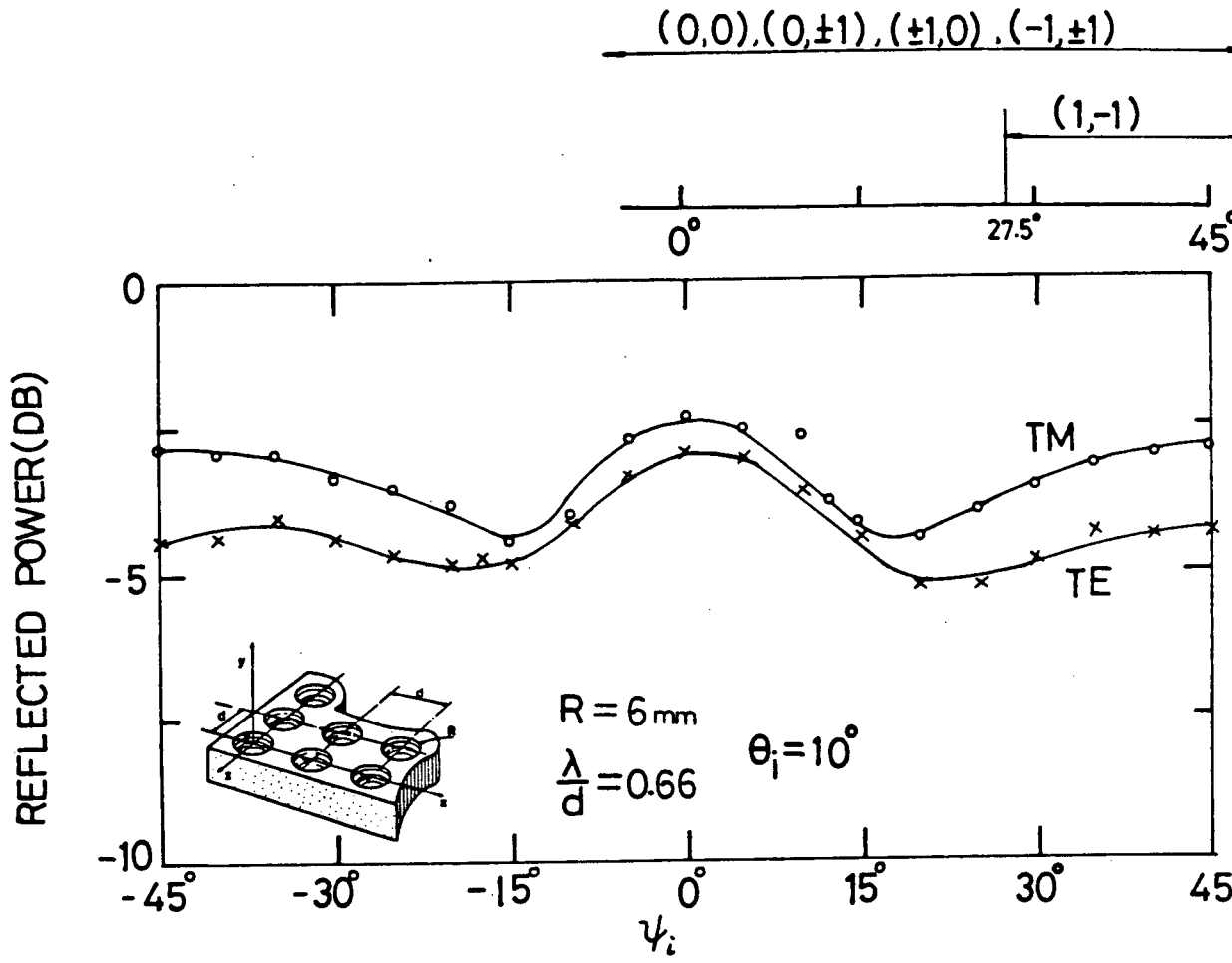

Fig. 5.8. Measured reflected power vs. ψ_i for plate R6 at f=35 GHz, θ_i=10°;

and calculated angular regions of ψ_i for all existing diffracted orders (on top)

Chapter 6

ERROR ANALYSIS

There are mainly two kinds of errors: experimental errors and errors from the non-ideal nature of the surface. Experimental errors occur in positioning the plate, readings, non-plane wave illumination, and site reflections. The surface is non-ideal from the fact that it has finite conductivity, finite size, and milling errors in groove dimensions.

The error in positioning the plate accounts for the shift of symmetry of the measured azimuthal angular response curves with respect to the predicted symmetry about $\psi_i=0$. The non-plane wave illumination has little influence on the performance of grating as shown by Jull and Ebbeson [10]. The site reflections are believed to cause the oscillatory behavior of some of the experimental curves and they are a large source of experimental error.

By using microwave radiation in the range of 35 GHz, all groove dimensions which had been designed in the range of the incident wavelength were large enough to be milled to a sufficient accuracy, and also we can work with near-perfectly conducting models (it was reported [20] that the model of infinite conductivity for metal gratings is very well adapted even when the wavelength exceeds 4 μm). Hence, the effects of finite conductivity, surface roughness and oxide layers which are the largest source of error in the optical region [1], are negligible in this range of

frequency.

It is also believed that the finite size of grating only affects the performance of grating slightly. The measurements on some profiles of singly periodic gratings in the microwave region conducted by Deleuil [1,20] showed that, as soon as the number of corrugations is greater than about twelve, gratings behave as if they were infinitely wide. Further numerical analysis by Jull and Hui [14] shows that for high efficiency diffraction gratings, as the grating size decreases, the diffracted beam broadens but the diffraction efficiency can remain high until the number of corrugations is very small. For instance, Facq's numerical results [7] for TM-polarized scatter from finite near-optimum rectangular-groove surfaces at θ_i=30° show a reduction in diffraction efficiency from 98.8% for an infinite surface to 97.4% for 10 corrugations and 96% for 5 . Therefore very few corrugations are needed for effective reduction of specular reflection. The above conclusion is for singly periodic gratings, but it seems quite reasonable to believe that the situation for crossed gratings is similar to that for classical gratings, and for the nine crossed grating plates investigated experimentally, there must be enough corrugations for grating-like behavior.

It is worth while pointing out that there is another kind of experimental error. In our measurements it had been actually assumed that when the incident wave was TE-polarized (say), the specularly reflected wave would be

still totally TE-polarized. Therefore the orientation of the receiving horn was always the same as that of the transmitting horn when the reflected power was measured. This assumption is true for classical gratings in the case of non-oblique incidence (ψ_i=0°). For crossed gratings, there is still no theoretical analysis on this problem.

In order to investigate the above assumption, we took some measurements on plate C4: by holding both horns vertically-oriented, we measured the power of TE component of the reflected wave when the incident wave is TE-polarized; then by changing the receiving horn from vertical to horizontal, we measured the power of TM component of the reflected wave. The results, presented in Fig. 6.1, show that when the incident wave is TE-polarized, the power of the TM component of the reflected wave is at most 5% (-13 dB) of that of the TE component, either in the case of non-oblique incidence (see Fig. 6.1a) or in the case of oblique incidence (see Fig. 6.1b). One similar measurement was also taken on Plate R4 in the case of θ_i=30°, ψ_i=-15°, and f=35 GHz. The measured relative power of TM component of the reflected wave is 2.2% (-16.5 dB) of that of the TE component when the incident wave is TE-polarized.

From the above sample measurements, it seems reasonable that in general, when the incident wave is TE-polarized, the measured power of TE component of the reflected wave can approximate the total reflected power. It is believed that a

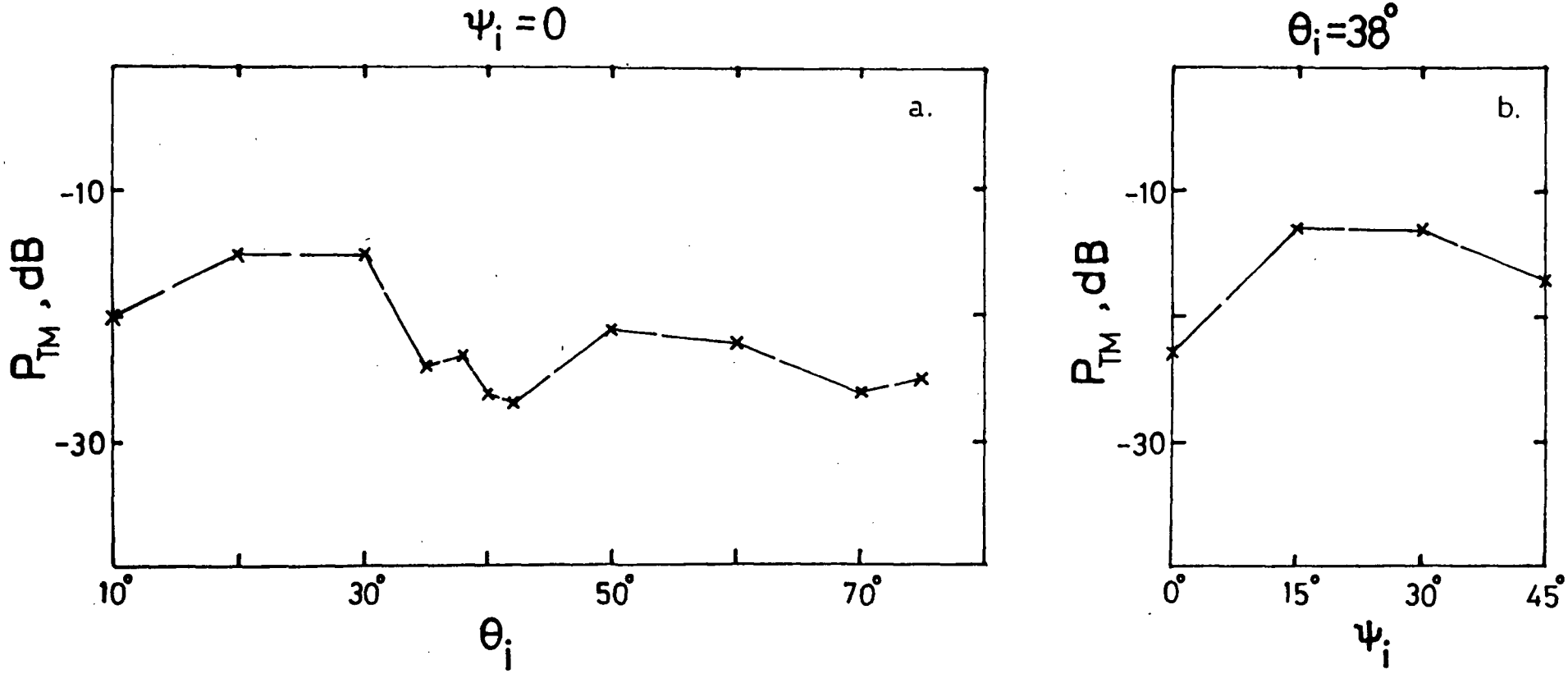

Fig. 6.1. Relative power P_{TM} of TM component of the reflected wave when a TE-polarized wave is incident on plate C4
(that of TE component is 0 dB)

a. non-oblique case ($\psi_i = 0$)
b. oblique case ($\theta_i = 38°$ fixed)

similar approximation is valid for a TM incident wave. In other words, the crossed-polarized reflected power can be neglected when compared with the co-polarized reflected power. Hence, our measurements on reflected power from crossed gratings seem within acceptable accuracy as far as the above problem is concerned.

Chapter 7

CONCLUSIONS

To our knowledge, this work is the first systematic experimental investigation of the scattering of an electromagnetic wave by a conducting pyramidal crossed grating, concentrated on the case of a higher ratio of groove depth to period of grating, for which numerical results are still very difficult to obtain. Some measurements were also taken on the conducting crossed grating with hemispherical cavities. Summarized below are the conclusions drawn:

1. It is demonstrated experimentally for the first time that elimination of specular reflection from a conducting pyramidal surface can be achieved. The best performance is that 99.94% of the power of a TM-polarized incident wave can be scattered into a single spectral order (-1,0) by plate A4. For TE polarization, the best result is a reduction of 98%, achieved by plate A6. The same plate can also diffract at the other incident angle 80% of the energy of an arbitrarily polarized incident wave, and this is the best result from the point of view of equal reduction for both polarizations.

   The above results are less satisfactory if compared with those obtained from the two-dimensional gratings with rectangular grooves [11]. However, the possibilities of obtaining better performances of

pyramidal crossed gratings still exist since our investigation is just the beginning.

2. It is worth noting that very interesting phenomena occur when the incident wavelength is equal to the period of the pyramidal crossed grating, and in this case of $\lambda/d=1$ our three best results just mentioned were obtained. We suggest that further experimental and theoretical investigation for crossed gratings with different profile (for example, crossed gratings with hemispherical cavities) be conducted under the condition of $\lambda/d=1$.
3. For situation in which the angle of incidence is near grazing ($\theta_i>80°$), reduction in TM-polarized specular reflection can be as large as 99.3%, which is obtained by plate B9. This is a desirable property for some applications.
4. The polarizer-like behavior of some pyramidal crossed gratings is observed. The best performance is that 90% of the TM components of an arbitrarily polarized incident wave can be scattered by a pyramidal surface (plate A9), while TE polarization is completely reflected.
5. It is shown experimentally that the product formula linking shallow crossed and classical gratings is not valid for deeply-grooved crossed gratings, and in general the reflection free properties of a singly-periodic surface cannot carry over to its

doubly-periodic equivalent.

6. The Wood anomaly often causes remarkable changes in the shape of behavior curves of grating, the position of which is determined by the values of incident angles (both θ_i and ψ_i), period of grating and incident wavelength (or the ratio λ/d). The experimental points are in good agreement with the theoretical predictions concerning the Wood anomalies.
7. For classical gratings with period in the range $\lambda/2<d\leq\lambda$, the largest reduction in specular reflection in the non-oblique case ($\psi_i=0°$) always occurs at the Bragg angle $\theta_i=\sin^{-1}(\lambda/(2a))$. However, this Bragg angle effect is not evident for crossed gratings.
8. Because of the square-symmetry of the pyramidal grating, it was originally thought that this kind of crossed grating was an interesting profile for the reduction of specular reflection when the direction of incidence is arbitrary. However, our measured azimuthal angular responses have shown that the reduction in specular reflection also depends on the value of ψ_i greatly. It seems that an effective wide range of ψ_i where the specular reflection is eliminated is at least difficult to find, if not impossible.
9. The major parameter of the grating profile (the apex angle α in the case of pyramidal crossed gratings, the cavity depth R in the case of crossed gratings with hemispherical cavities) has an important effect on the

general behavior of grating, and the value of the ratio λ/d defines the critical positions of Wood anomalies. Thus, the grating profile and the ratio λ/d both determine the properties of grating at a particular incident condition.

10. Our experimental results prove indirectly the theoretical prediction that a crossed grating with hemispherical cavities (plate R4) can eliminate 90% of specular reflection for an arbitrarily polarized incident wave in the case of normal incidence, and it is also observed that this plate can still keep cancelling at least 68% of specular reflection when the incident wave is deviated from the normal of surface by an angle as large as 30°. This is very interesting for the study of solar energy captation with a roughened surface.
11. It is demonstrated experimentally that a crossed grating with hemispherical cavities (plate R6) can eliminate 99% of TM polarized specular reflection, though the effective angular range is very narrow.

In general, our experimental results agree with the theoretical predictions, and provide useful information for an understanding of the behavior of these two kinds of crossed gratings. This may assist and give new impetus to further numerical and experimental investigations.

APPENDIX: NUMERICAL RESULTS FOR PERFECTLY CONDUCTING STRIPS OF SIX SYMMETRICAL TRIANGULAR CORRUGATIONS

We obtained from a computer program by Facq [17] numerical results for perfectly conducting strips of six symmetrical triangular corrugations, with the same profiles as those of the classical grating plates investigated experimentally. A comparison between numerical and experimental results is presented in Fig. A.1. After taking into account the effect of the larger size of a experimental grating of 30-39 grooves, which increases the diffraction efficiency, the correspondence between the calculated and measured values is good. There are only two exceptions where the measured value is slightly less than the calculated value.

Also obtained were the calculated power patterns which are exhibited in Figures A.2-A.6. Since a grating is finite there is always a forward-scatter lobe in $90° < \theta < 180°$. In Figures A.5 and A.6 there is also a backscatter lobe but essentially no specular reflection, indicating near total diffraction to the n=-1 spectral order.

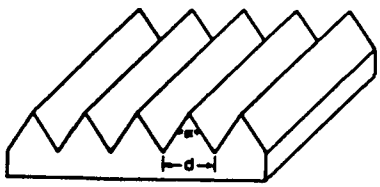

ECHELETTE

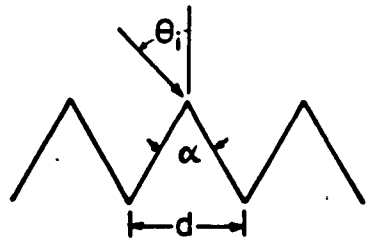

STRIP	d (mm)	α	f (GHz)	θ_i	DIFFRACTION EFFICIENCY ϵ_{-1} NUMERICAL TM	NUMERICAL TE	EXPERIMENTAL TM	EXPERIMENTAL TE
A4	8.00	45°	35	32.4°	.8488	.7281	.975	.620
B6	6.23	60°	35	43.5°	.1962	.6566	.073	.718
B9	6.23	90°	35	43.5°	.9605	.3603	.99998	.553
C4	6.9	44°	35	38.1°	.9526	.9704	.99997	.9611
C4	6.9	44°	33.75	40.0°	.9701	.9489	.9967	.9946

Fig. A.1. Comparison between numerical results for perfectly conducting strips of six symmetrical triangular corrugations and experimental results for the corresponding triangular grating plates of 30-39 grooves with the same profile

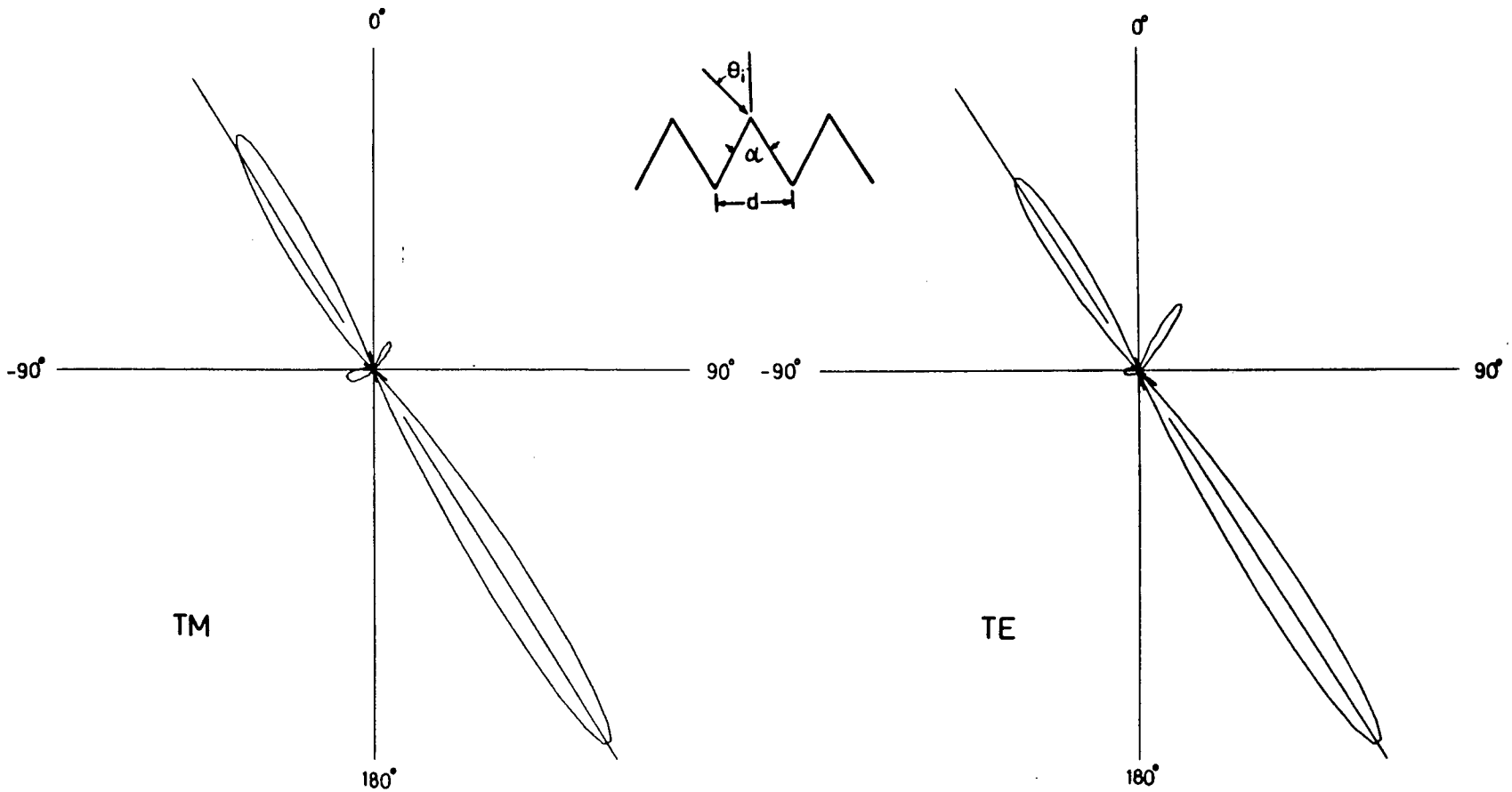

Fig. A.2. Calculated power patterns for strip A4 at θ_i=32.4° and f=35 GHz

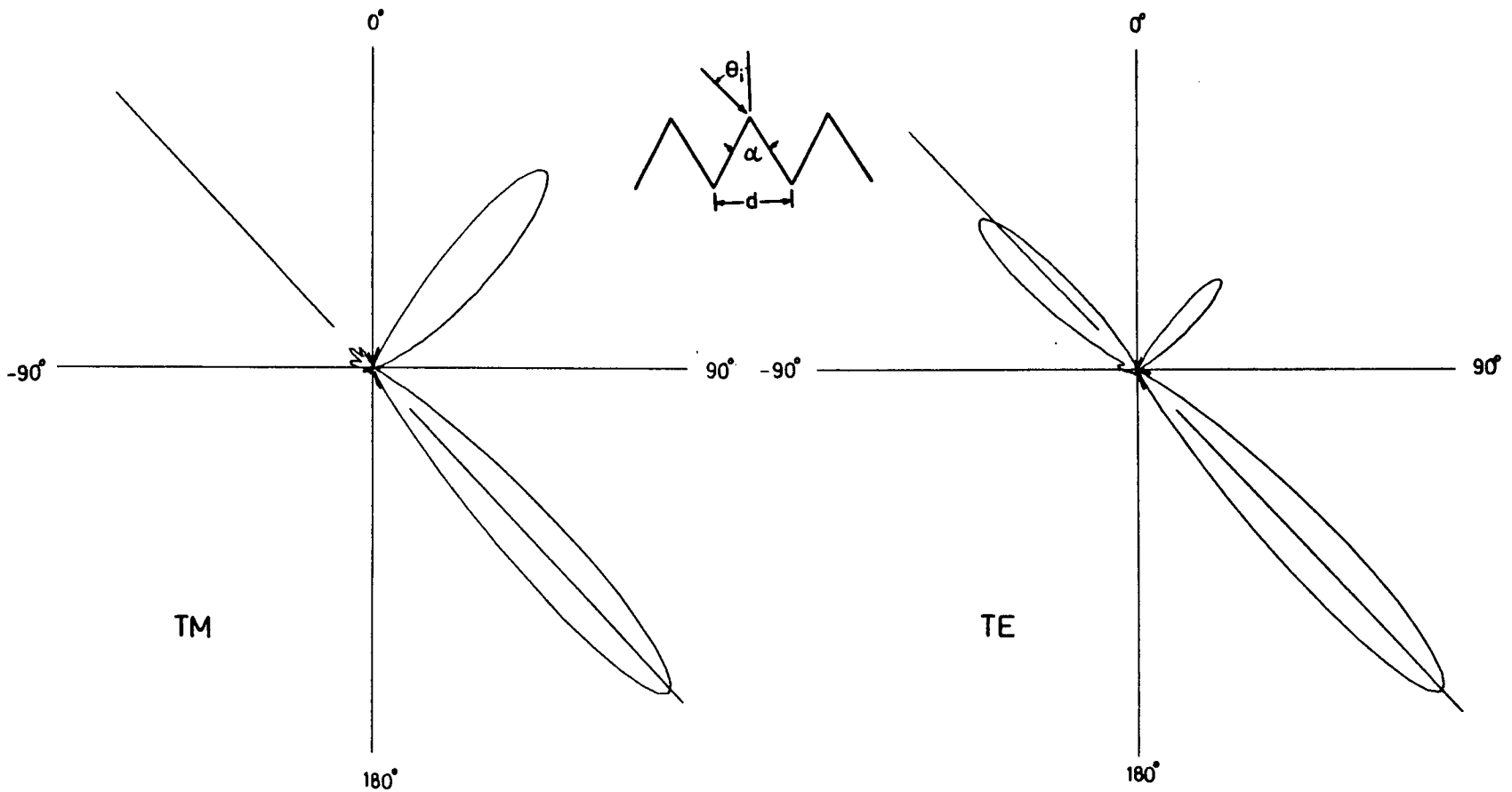

Fig. A.3. Calculated power patterns for strip B6 at θ_i=43.5° and f=35 GHz

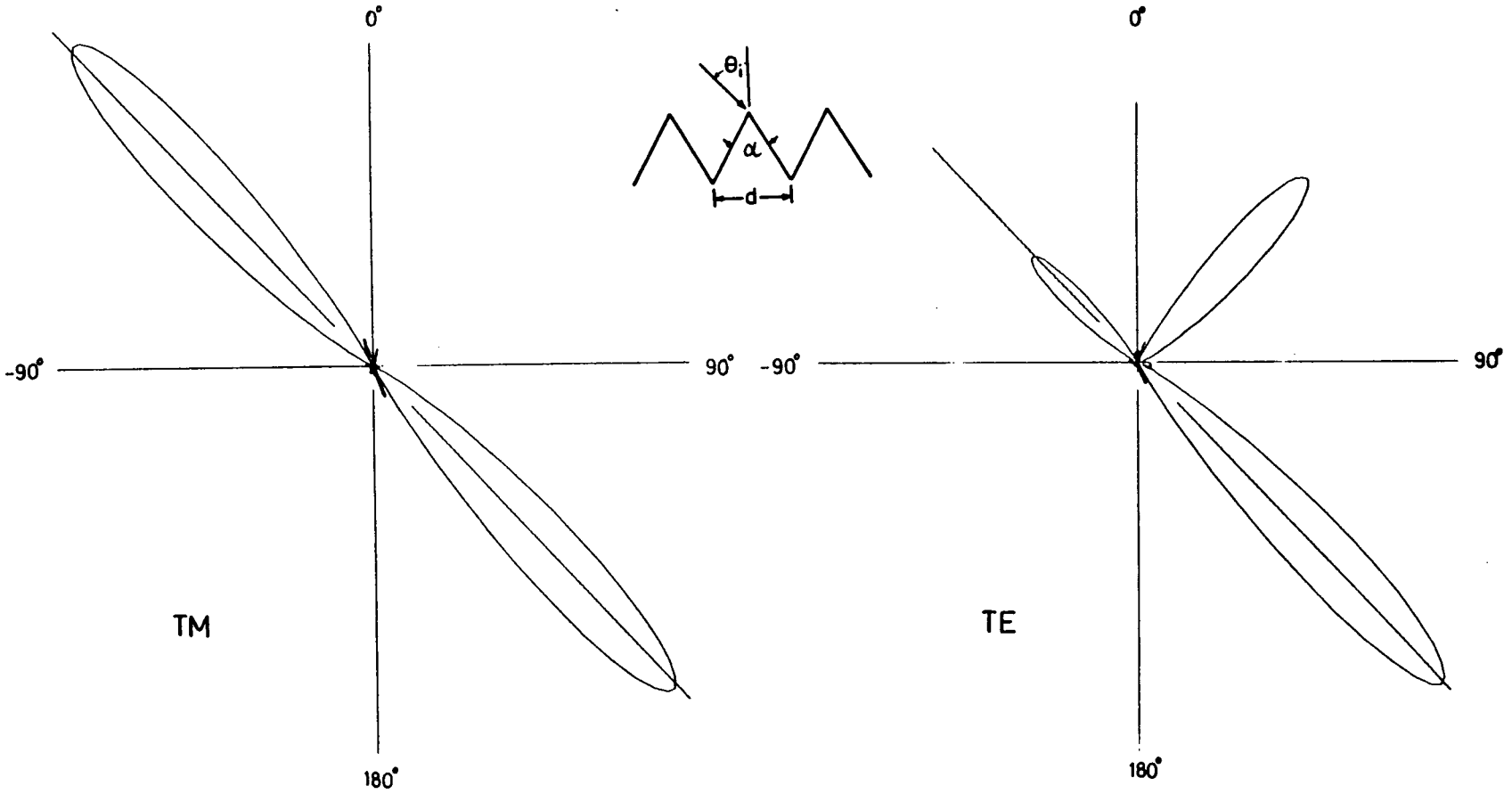

Fig. A.4. Calculated power patterns for strip B9 at θ_i=43.5° and f=35 GHz

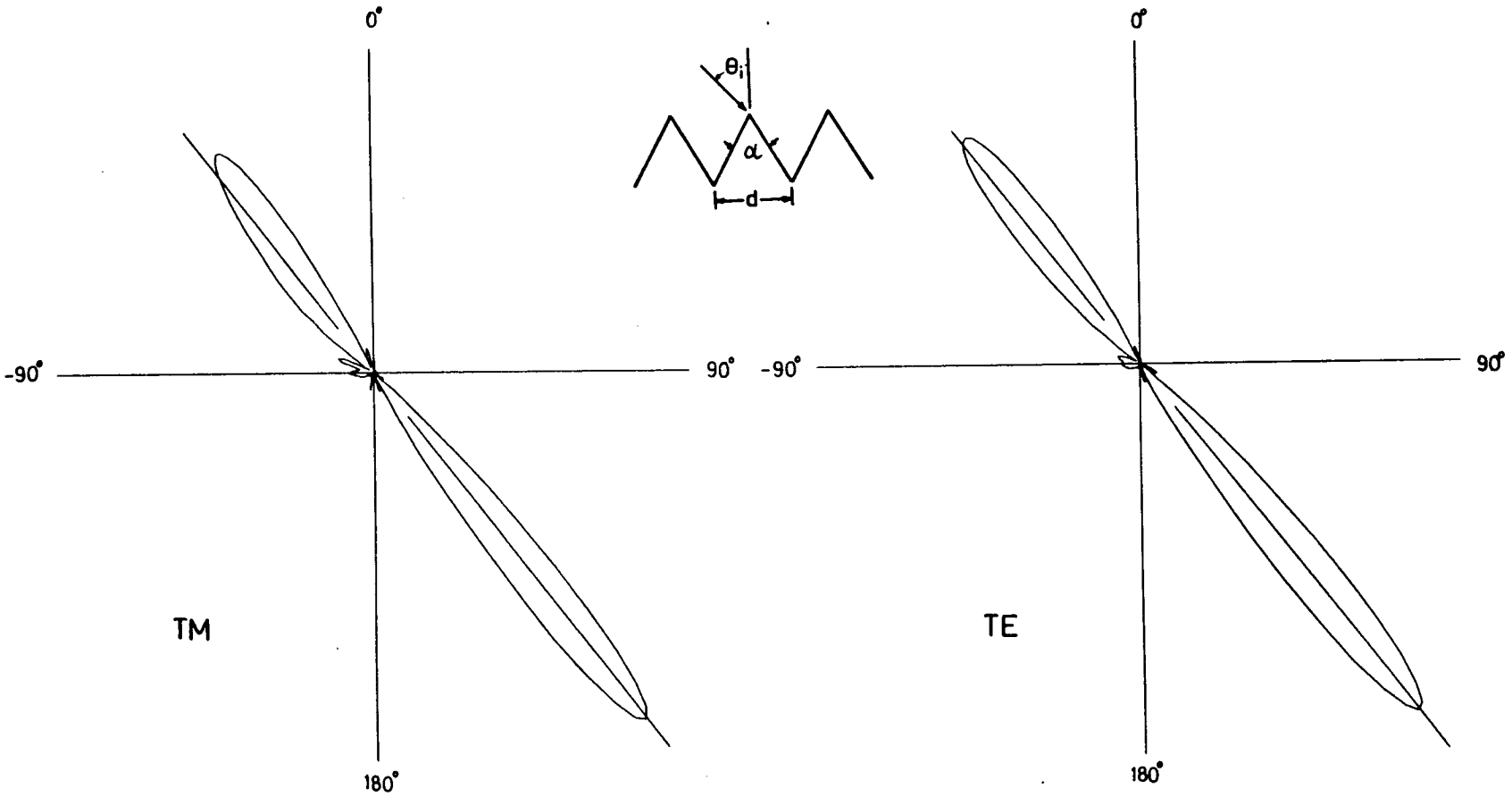

Fig. A.5. Calculated power patterns for strip C4 at θ_i=38.1° and f=35 GHz

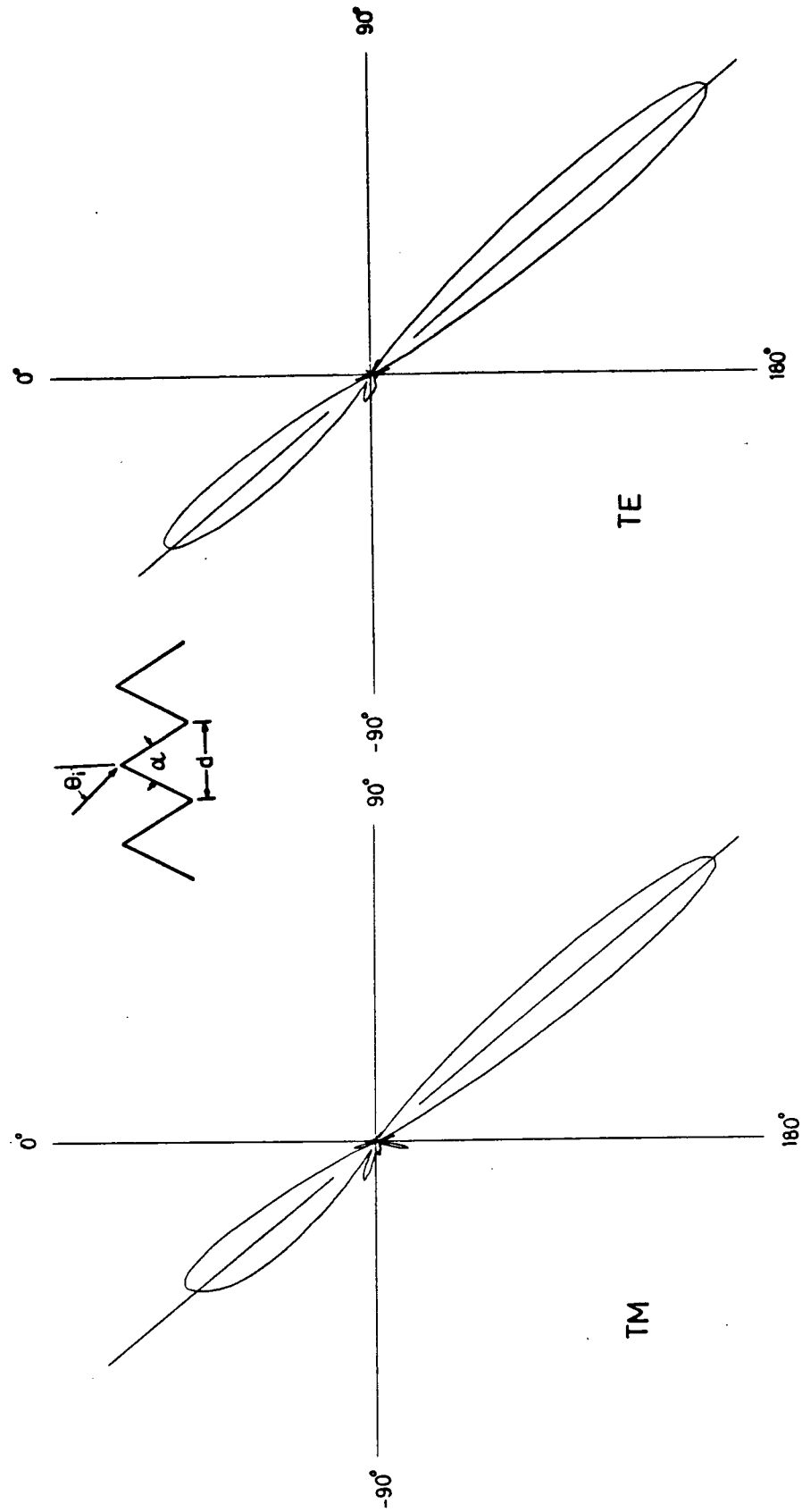

Fig. A.6. Calculated power patterns for strip C4 at θ_i=40.0° and f=33.75 GHz

REFERENCES

[1] P.Bliek and R.Deleuil, "Experimental investigation in microwave range of diffraction by classical and crossed gratings", Proc. SPIE, 240, 263-271, 1980.

[2] L. Cai, E. V. Jull and R. Deleuil, "Scattering by pyramidal reflection gratings", Intern. IEEE AP-S Symposium, Boston, June, 1984.

[3] C-C. Chen, "Transmission of microwaves through perforated flat plates of finite thickness", IEEE Trans. MTT-21,1-6, 1973.

[4] L. S. Cheo, J. Shmoys and A. Hessel, "On simultaneous blazing of triangular groove diffraction gratings", J. Opt. Soc. Am., 67, 1686-1688, 1977.

[5] G. H. Derrick, R. C. McPhedran, D. Maystre and M. Neviére, "Crossed gratings: a theory and its applications", Applied Physics, 18, 39-52, 1979.

[6] G. R. Ebbeson, "The use of fin-corrugated periodic surfaces for the reduction of Interference from large reflecting surfaces", M. A. Sc. Thesis, University of British Columbia, 1974.

[7] P. Facq, "Application des matrices de Toeplitz a la théorie de la diffraction par les structures cylindriques périodiques limitées", D. Sc. Thesis, University of Limoges, 1977.

[8] J. W. Heath, "Scattering by a conducting periodic surface with a rectangular groove profile", M. A. Sc. Thesis, University of British Columbia, 1977.

[9] E. V. Jull, N. C. Beaulieu and D. C. W. Hui, "Perfectly blazed triangular groove reflection gratings", J. Opt. Soc. Am., 1, 180-182, Feb. 1984.

[10] E. V. Jull and G. Ebbeson, "The reduction of interference from large reflecting surfaces", IEEE Trans. AP-25, 656-670, 1977.

[11] E. V. Jull and J. W. Heath, "Conducting surface corrugations for multipath interference suppression", PROC. IEE, 125, 1321-1326, Dec. 1978.

[12] E. V. Jull and J. W. Heath, "Reflection grating polarizers", IEEE Trans. AP-28, 586-588, July 1980.

[13] E. V. Jull, J. W. Heath and G. R. Ebbeson, "Gratings that diffract all incident energy", J. Opt. Soc. Am.,

67, 557-560, April 1977.

[14] E. V. Jull, D. C. W. Hui and P. Facq, "Scattering by dual blazed corrugated conducting strips and large reflection gratings", to be published in J. Opt. Soc. Am., 1985.

[15] J. Y. L. Ma and L. C. Robinson, "Night moth eye window for the millimetre and sub-millimetre wave region", Optica Acta, 30, 1685-1695, 1983.

[16] D. Maystre, R. McPhedran and M. Neviére, Private communication.

[17] D. Maystre and M. Neviére, "Electromagnetic theory of crossed gratings", J. Optics (Paris), 9, 301-306, 1978.

[18] D. Maystre, M. Neviére, and P. Vincent, "On the properties of finitely conducting crossed gratings (some applications)", Proceedings of ICO-11 Conference, Madrid, Spain, 1978.

[19] R. C. McPhedran, G. H. Derrick, M. Neviére and D. Maystre, "Metallic crossed gratings", J. Optics (Paris), 13, 209-218, 1982.

[20] R. Petit, ed., Electromagnetic Theory of Gratings, Springer-Verlag: Berlin, 1980.

[21] E. Toro, "Etude de la diffraction des ondes electromagetiques par un reseau metallique croise forme de cavites hemispheriques", D. Sc. thesis, Université de provence, France, 1983.

[22] E. Toro and R. Deleuil, "Application of a rigorous theory to electromagnetic diffraction from a biperiodic rough surface", submitted for publication, 1984.

[23] P. Vincent, "A finite-difference method for dielectric and conducting crossed gratings", Opt. Commun., 26, 293-296, 1978.

[24] S. J. Wilson and M. C. Hutley, "The optical properties of 'moth eye' antireflection surfaces", Optica Acta, 29, 993-1009, 1982.

[25] A. Wirgin, "Diffraction of light by a perfectly conducting biaxial periodic surface", Opt. Commun., 45, 221-225, April 1983.

[26] A. Wirgin and R. Deleuil, "Theoretical and experimental investigaton of a new type of blazed grating", J. Opt. Soc. Am., 59, 1348-1357, Oct. 1969.